

# Nuclear Medicine

## R · E · V · I · E · W

merged with Problems of Nuclear Medicine

MNiSW: 40 pkt.



See page 66

ISSN 1506–9680

2020, Volume 23, Number 2

Journal of Polish, Serbian, Hungarian, Bulgarian  
and Macedonian Societies of Nuclear Medicine





# Nuclear Medicine

## R · E · V · I · E · W

merged with *Problems of Nuclear Medicine\**

### Editor-in-Chief

G. Kamiński (Warszawa, Poland)

### Deputy Editor-in-Chief

M. Dziuk (Warszawa, Poland)

J. Kunikowska (Warszawa, Poland)

### National Editors

I. Garai (Debrecen, Hungary)

D. Huić (Zagreb, Croatia)

D. Sobic Saranovic (Belgrade, Serbia)

### Board of Editors:

V. Artiko (Belgrade, Serbia)

R.P. Baum (Bad Berka, Germany)

O. Belohlavek (Prague, Czech Republic)

B. Birkenfeld (Szczecin, Poland)

K. Borbély (Budapest, Hungary)

J. Braziewicz (Kielce, Poland)

J. Buscombe (London, United Kingdom)

J.M. Carrill (Santander, Spain)

I. Carrio (Barcelona, Spain)

A. Celler (Vancouver, Canada)

A. Chiti (Rozzano, Italy)

B. Chrapko (Lublin, Poland)

A. Cuocolo (Naples, Italy)

C.S. Cutler (Columbia, United States)

E. Dziuk (Warszawa, Poland)

R. Howman-Giles (Sydney, Australia)

A. Hubalewska-Dydejczyk (Kraków, Poland)

B. Jarząb (Gliwice, Poland)

W. Kloc (Gdańsk, Poland)

W. Knapp (Hannover, Germany)

V.N. Korsunsky (Moscow, Russia)

M. Kostkiewicz (Kraków, Poland)

I. Kozłowicz-Gudzińska (Warszawa, Poland)

O. Kraft (Ostrava, Czech Republic)

L. Królicki (Warszawa, Poland)

J. Kuśmierek (Łódź, Poland)

J. Lepej (Banska Bystrica, Slovak Republic)

A. Lewiński (Łódź, Poland)

T. Maina (Athens, Greece)

B. Małkowski (Bydgoszcz, Poland)

R. Mikołajczak (Otwock-Świerk, Poland)

M. Myslivecek (Olomuc, Czech Republic)

V. Obradović (Belgrade, Serbia)

A.K. Padhy (Singapore)

E. Piperkova (Sofia, Bulgaria)

A. Płachcińska (Łódź, Poland)

Z. Rajkovic (Banja Luka, Bosnia & Herzegovina)

F. Rogowski (Białystok, Poland)

D. Rubello (Rovigo, Italy)

M. Ruchala (Poznań, Poland)

M.M. Saw (Singapore)

A. Signore (Rome, Italy)

H. Sinzinger (Vienna, Austria)

A. Soricelli (Italy)

A. Sowa-Staszczak (Kraków, Poland)

D.A. Stanescu (Bucharest, Romania)

M. Studniarek (Gdańsk, Poland)

A. Syrenicz (Szczecin, Poland)

I. Szilvasi (Budapest, Hungary)

K. Toth (Warszawa, Poland)

J.H. Turner (Fremantle, Australia)

I. Velikyan (Uppsala, Sweden)

M. Vljakovic (Nis, Serbia)

P. Vlcek (Praha, Czech Republic)

The Scientific Committee of the journal is being created and the list of the scientific council members contains the persons who have declared willingness to collaborate.

### Secretary

A. Krajewska (Warszawa, Poland)

### Editorial Office

Wojskowy Instytut Medyczny

ul. Szaserów 128, 04-141 Warszawa

e-mail: nmr@viamedica.pl

### Managing Editor

K. Klimek (Gdańsk, Poland)

\*Following the agreement concluded on 23 February 2011 between the Polish Society of Nuclear Medicine and Via Medica Sp. z o.o. the journal „Nuclear Medicine Review” has merged with „Problemy Medycyny Nuklearnej”, a journal published since 1987.

**Nuclear Medicine Review** (ISSN 1506-9680) is published twice a year by VM Media sp. z o.o., VM Group sp. k., Grupa Via Medica

ul. Świętokrzyska 73, 80-180 Gdańsk, Poland

tel: (+48 58) 320 94 94, fax: (+48 58) 320 94 60; e-mail: redakcja@viamedica.pl, marketing@viamedica.pl

http://www.viamedica.pl

Advertising. For details on media opportunities within this journal please contact the advertising sales department, ul. Świętokrzyska 73, 80-180 Gdańsk, Poland tel: (+48 58) 320 94 52, e-mail: marketing@viamedica.pl

The Editors accept no responsibility for the advertisement contents.

Single issues/advertising inquiries should be addressed to VM Media sp. z o.o., VM Group sp. k., Grupa Via Medica, bank account:

Fortis Bank Polska SA o/Gdańsk 24 1600 1303 0004 1007 1035 9150 — PLN payment;

Fortis Bank Polska SA o/Gdańsk PL 15 1600 1303 0004 1007 1035 9021; SWIFT: PPABPLPK — EUR payment.

Single issues requests should be sent to e-mail: prenumerata@viamedica.pl. Electronic orders option available at: www.nmr.viamedica.pl



© Via Medica 2020

All rights reserved, including translation into foreign languages. No part of this periodical, either text or illustration, may be used in any form whatsoever. It is particularly forbidden for any part of this material to be copied or translated into a mechanical or electronic language and also to be recorded in whatever form, stored in any kind of retrieval system or transmitted, whether in an electronic or mechanical form or with the aid of photocopying, microfilm, recording, scanning or in any other form, without the prior written permission of the publisher. The rights of the publisher are protected by national copyright laws and by international conventions, and their violation will be punishable by penal sanctions.

**Indexation: Crossref, DOAJ (Directory of Open Access Journals), EMBASE, ESCI (Emerging Sources Citation Index), Index Copernicus (100.00), MEDLINE, Polish Medical Bibliography, Ministry of Science and Higher Education (40), Scopus, Ulrich's Periodicals Directory.**

**Editorial policies and author guidelines are published on journal website: [www.journals.viamedica.pl/nuclear\\_medicine\\_review](http://www.journals.viamedica.pl/nuclear_medicine_review)**



19-0213.002.001



# Nuclear Medicine

R · E · V · I · E · W

merged with *Problems of Nuclear Medicine*\*

2020, Volume 23, Number 2

<b>Editorial</b> .....	V
<b>Original articles</b>	
<i>Agata Danilczuk, Anna Nocuń, Beata Chrapko</i> Normal ranges of renal function parameters for <sup>99m</sup> Tc-EC renal scintigraphy .....	53
<i>Andreas Fotopoulos, Petros Petrikis, Ioannis Iakovou, Athanasios Papadopoulos, Sakelariou Konstantinos, Evangelia Gkika, Lampros Lakkas, Christos Touzios, Konstantinos Pappas, Antonios Klaroudas, Argyrios Doumas, Chrissa Sioka</i> The impact of depression and anxiety in prognosis of patients undergoing myocardial perfusion imaging with <sup>99m</sup> Tc tetrofosmin SPECT for evaluation of possible myocardial ischemia .....	58
<i>Beata Ewa Chrapko, Marek Chrapko, Anna Nocuń, Tomasz Zubilewicz, Bogusław Stefaniak, Jakub Mitura, Andrzej Wolski, Piotr Terelecki</i> Patterns of vascular graft infection in 18F-FDG PET/CT .....	63
<i>Maria Henryka Listewnik, Hanna Pivowarska-Bilska, Krzysztof Safranow, Marek Ostrowski, Jacek Iwanowski, Maria Chosia, Bożena Birkenfeld</i> The diagnostic value of dual-phase SPECT/CT scintigraphy based on transport kinetics of <sup>99m</sup> Tc-sestamibi confirmed with histopathological findings in patients with secondary hyperparathyroidism — practical consideration .....	71
<i>Krzysztof Grzegorz Filipczak, Paweł Cichocki, Jacek Kusmierek, Anna Plachcinska</i> Kidney Efficiency Index — quantitative parameter of a dynamic renal scintigraphy. I. Theory and preliminary verification .....	78
<i>Paweł Cichocki, Krzysztof Filipczak, Anna Plachcinska, Jacek Kusmierek</i> Kidney efficiency index quantitative parameter of a dynamic renal scintigraphy. II. usefulness in the diagnosis of obstructive nephropathy .....	84
<i>Ebru Salmanoglu, Ergul Belge Kurutas</i> The levels of oxidative and nitrosative stress in patients who had <sup>99m</sup> Tc-MIBI myocardial perfusion scintigraphy and <sup>99m</sup> Tc-DMSA, <sup>99m</sup> Tc-MAG-3 renal scintigraphy .....	89
<b>Review</b>	
<i>Vincenzo Cuccurullo, Giuseppe Danilo Di Stasio, Giuseppe Lucio Cascini</i> PET/CT in thyroid cancer: the importance of BRAF mutations .....	97
<b>Clinical vignette</b>	
<i>Shirin Shahlaei, Farnaz Nesari Javan, Atena aghaee, Ramin Sadeghi</i> Catheter malposition during a direct radionuclide cystography: case report .....	103
<i>Maria Gazzilli, Domenico Albano, Laura Ardighieri, Francesco Bertagna, Raffaele Giubbini</i> Primary nasal-ethmoid choriocarcinoma detected by 18F-FDG PET/CT: a rare tumor with complete remission .....	105
<i>Fatemeh Farahmandfar, Sara Shakeri, Sadegh Moradian, Shirin Shahlaei, Ramin Sadeghi</i> Primary skeletal muscle lymphoma with unusual soft tissue metastases in the stomach and pancreas detected by 18F-FDG PET/CT .....	108
<i>Salah Nabih Oueriagli, Yassir Benameur, Omar Ait Sahel, Abdelhamid Biyi, Abderrahim Doudouh</i> Unusual 18F-FDG PET-CT finding of paraneoplastic polymyositis in a patient with lung epidermoid carcinoma .....	110
<i>Ali Sellem, Wassim Elajmi, Hatem Hammami</i> Technetium pertechnetate uptake in parathyroid adenoma .....	112





## Dear Sirs and Madams,

It's summer time, holidays but still we have one of the worst crises in the World. Fighting against COVID-19 pandemic became the most important target for everyone. Good luck! Nevertheless, I am happy introducing the second in 2020 issue of "Nuclear Medicine Review". The Polish authors open the chapter "Original articles" with paper *Normal ranges of renal function parameters for <sup>99m</sup>Tc-EC renal scintigraphy*. The second article by Greek investigators concluding that patients who exhibit depression, anxiety, or both, have high rates of myocardial ischemia, and thus are at risk for subsequent cardiological events. The two next papers are from Poland. The first one raised that 18F-FDG PET/CT is a very useful tool for assessment of vascular graft infections. CT findings like gas bubbles, or peri-graft fluid retention were associated with significantly higher glucose metabolism, however, in some cases without anatomic alterations, increased metabolic activity was the only sign of infection. The second one gives us the practical consideration about *The Diagnostic Value of Dual-Phase SPECT/CT Scintigraphy Based on Transport Kinetics of <sup>99m</sup>Tc Sestamibi Confirmed with Histopathological Findings in Patients with*

*Secondary Hyperparathyroidism*. Turkish colleagues — in article titled *The levels of oxidative and nitrosative stress in patients who had <sup>99m</sup>Tc-MIBI myocardial perfusion scintigraphy and <sup>99m</sup>Tc-DMSA, <sup>99m</sup>Tc-MAG-3 renal scintigraphy* — concludes that oxidative and nitrosative balance is impaired due to ionization radiation. These reactive species might stimulate adaptive and protective cellular defense mechanism in irradiated cells soon after exposing to radiation and protect organism from effects of low dose ionizing radiation. And again Polish authors and kidneys: chapter ends an original paper *Kidney Efficiency Index — Quantitative Parameter of a Dynamic Renal Scintigraphy. II. Usefulness in the Diagnosis of Obstructive Nephropathy*.

The Review part consists of the general state of knowledge concerning *PET/CT in thyroid cancer and the importance of BRAF mutations* by Italian authors.

In chapter *Clinical vignette* there are discussed five interesting clinical cases from Iran, Italy, Morocco and Tunisia.

In the end of my letter I would like to wish all of you joyful and healthy vacation!

Yours,

Grzegorz Kamiński



Editor-in-Chief

Nuclear Medicine Review



# Normal ranges of renal function parameters for $^{99m}\text{Tc}$ -EC renal scintigraphy

Agata Danilczuk , Anna Nocun , Beata Chrapko   
 Medical University of Lublin, Poland

[Received 4 V 2020; Accepted 18 VI 2020]

## Abstract

**BACKGROUND:** Dynamic renal scintigraphy remains the recognized method for evaluation of kidney function and perfusion. Although there is an extensive body of knowledge about the use of technetium-99m-mercaptoacetyltriglycine ( $^{99m}\text{Tc}$ -MAG3), much less has been written about renal technetium-99m-ethylenedicycysteine ( $^{99m}\text{Tc}$ -EC) scintigraphy.

The aim of this study was to determine the normal value of renal function parameters in  $^{99m}\text{Tc}$ -EC dynamic renal scintigraphy: Tmax and T1/2. The effects of age, left or right side in the retroperitoneal space, and sex on those parameters were examined.

**MATERIAL AND METHODS:** The research was conducted on 123 patients (F/M: 70/53; aged 2–71; averaging 14.8 years of age) with at least one normal kidney. A total of 194 healthy kidneys were examined, including pediatric kidneys.

**RESULTS:** According to this study, the normal value of Tmax is 2.85 min ( $\pm 1.16$ ) and T1/2 is 8.7 min ( $\pm 3.61$ ). Values calculated for pediatric studies are Tmax is 2.81 ( $\pm 1.16$ ) and T1/2 is 8.63 ( $\pm 3.71$ ).

**CONCLUSIONS:** The normal value of secretory and excretory renal function parameters was calculated. Although the value is slightly lower for children, this is not statistically significant, as globally there are no differences between the kidney-location sides and sexes for any parameter.

**KEY words:** radionuclide imaging; dynamic renal scintigraphy; technetium-99m-ethylenedicycysteine; pediatric renal scintigraphy; renal function; renal function parameters

Nucl Med Rev 2020; 23, 2: 53–57

## Introduction

Dynamic renal scintigraphy is based on physiological processes, is minimally invasive, and repeatable. It allows recognition of various renal abnormalities in an early stage [1, 2]. That is why it remains the gold standard for assessing renal function, despite some shortcomings of this method [3].

The studies examining the dynamic renal scintigraphy performed with the use of the  $^{99m}\text{Tc}$ -ethylenedicycysteine ( $^{99m}\text{Tc}$ -EC) in normal human volunteers revealed that the renal clearance of  $^{99m}\text{Tc}$ -EC is higher than that of  $^{99m}\text{Tc}$ -mercaptoacetyltriglycine ( $^{99m}\text{Tc}$ -MAG3) and more similar to that of 131I-orthoiodohippurate (OIH).  $^{99m}\text{Tc}$ -EC is characterized by faster and more complete renal washout and similar good imaging properties [1, 4, 5].

Dynamic renal scintigraphy includes quantitative estimates of renal perfusion and function. Through the renographic curve shows the change of the radioisotope concentration in renal parenchyma as a function of time [6]. According to the EANM, following the intravenous administration of  $^{99m}\text{Tc}$ -EC, some part (17%) of it is filtered in the glomeruli while a major portion (50%) is secreted in the proximal part of the tubules by organic anion transporters [7]. 70% of the marker is extracted from the body after about 40 minutes and 95% after 1,5 hours following the injection [6]. Three phases can be distinguished in the dynamic renal scintigraphy a vascular phase, a parenchymatous phase (secretory), and an excretory phase with a decline in radioactivity. Three parameters can be obtained from the curve: Tmax, T1/2 and split function (uptake). Tmax is the time to reach the maximum amplitude of the observed activity, and it depends on the transport efficiency of the parenchyma. T1/2 denotes the time when radioactivity in the region of interest is reduced by half. The determination of ROI for both kidneys makes it possible to plot a create renographic curve describing the radioisotope concentration as a function of time (time-activity curves) [8]. The time-activity curve is determined

Correspondence to: Agata Danilczuk  
 Medical University of Lublin, Poland, Aleje Raclawickie 1  
 20–059 Lublin, Poland  
 e-mail: agata@swietlicki.net

after the correction of extra-renal background as recommended by the EANM [9]. The normal state of the split function is considered to range from 45% to 55% of the total uptake for both healthy kidneys [9], although some sources give the range of 42–58% [10].

Up to date, the parameters of dynamic renal scintigraphy with  $^{99m}\text{Tc}$ -EC have only been studied either on small groups of adult volunteers [10, 11] or a small pediatric group [12].

In light of the above, the aim of this study was to evaluate the normal value of renal function parameters in  $^{99m}\text{Tc}$ -EC dynamic renal scintigraphy:  $T_{\text{max}}$  and  $T_{1/2}$ , basing on a larger group of patients with at least one kidney considered as normal. The effects of age left or right side in the retroperitoneal space and sex on those parameters were examined.

## Material and methods

### Patients

All data were collected in the Department of Nuclear Medicine over a period from 6.09.2012 to 13.11.2014 and then analyzed retrospectively. The study was performed on a population of patients referred for diagnostic tests for suspected kidney diseases or dysfunctions. Patients whose scintigraphy did not confirm the disease and patients diagnosed with one dysfunctional and one healthy kidney were included in the study. Due to a large number of tests, we examine not only patients with renal disease, but also a certain number of patients with at least one kidney considered normal in our dynamic renal scintigraphy study. 123 patients (F/M: 70/53; aged 2–71; averaging 14.8 years old) were selected from 259 patients with at least one kidney correct by visual assessment, based on the criteria listed in Table 1. The evaluation was based on 104 patients who were 2–18 years old (F/M: 61/43; aged 2–18; averaging 9.5 years old) and 19 patients above the age of 18 (F/M: 9/10; aged 21–71; averaging 43.8 years old), which does not confirm the suspicion of doctors issuing the referrals.

The total number of kidneys considered normal in the study was 194 (F/M: 113/81; One /two normal kidneys: 52/142; left/right: 104/90; aged 2–71; averaging 14.8 years old). There were 28 kidneys considered normal in the adult population (F/M kidneys: 12/16; left/right: 16/12; aged 21–71; averaging 45.2 years old). There were 166 kidneys considered normal in the pediatric population (F/M: 101/65; left/right: 88/78; aged 2–18; averaging 9.7 years old) that were available for renogram parameters analysis (Fig. 1). The kidneys were divided into 5 groups; 4 pediatric (2–5, 6–9, 10–13 and 14–18 years old) and adults (19–71 years old). The number of kidneys versus patient age is shown in Figure 1.

### Radiopharmaceuticals and imaging

The scintigraphic examination was performed using a dual-head gamma-camera, immediately after the intravenous injection of  $^{99m}\text{Tc}$ -EC prepared using a sterile cold kit (Institute of Isotopes, Budapest, Hungary). The dose range from 18,5MBq to 111MBq, containing 0.3–0.7 mg of the  $^{99m}\text{Tc}$ -EC complex [13]. The amount of radioactivity for infants and children was based on their body weight [14]. Study was performed without furosemide injection, and the patients were asked to void before image acquisition. The  $^{99m}\text{Tc}$ -EC complex was administered intravenously as the acquisition on gamma camera was launched.

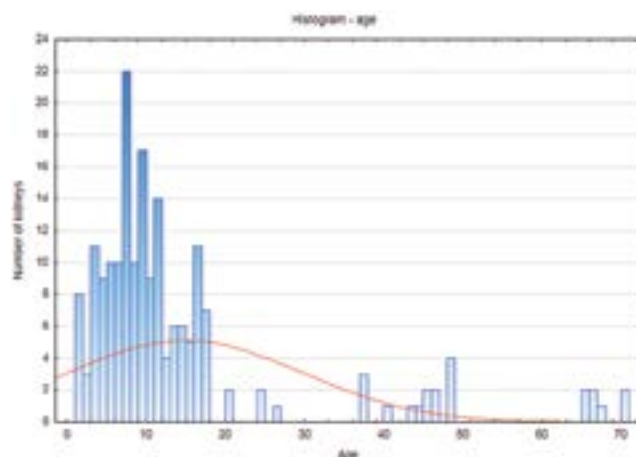


Figure 1. Number of tested healthy kidneys versus the age of patients

Table 1. Criteria for healthy kidney selection

All consecutive kidneys were considered functionally efficient based on the following criteria:

#### Clinical criteria:

- children not younger than 2 years old [9];
- no history of any diseases of the urinary tract or the selected kidney;
- blood levels of urea and creatinine within normal ranges according to the reference values provided by the laboratory;
- in ultrasound, selected kidneys were typically located with normal shapes and sizes;
- no signs of dilated pelvis or calices, cysts, cortical defects, or other morphological abnormalities.

#### Scintigraphic criteria:

- smooth renal outer contour in the parenchymal phase;
- the calyx-pelvis system is not enlarged;
- even distribution of the radioactive substance in the kidney parenchyma;
- a gradual, slow evacuation of the calyx and pelvone system is observed;
- no retention of the radiotracer at the end of the observation;
- renographic curve correct in the visual assessment [6];
- no single kidney;
- no use of furosemide or furosemide administered after the excretory phase.

The study was performed using the Symbia T16 SPECT/CT hybrid gamma camera (Siemens, Erlangen, Germany). The low-energy high-resolution collimator was used. The analyzer window was set at 140 keV. The data were collected on a 128 × 128 matrix. The examination was carried in the posterior-anterior projection, having a kidney in the field of view. In the first minute of the study, the scintigraphy was recorded with a time resolution of 2 seconds (30 projections) and during the remaining 20 minutes with a time resolution of 30 seconds (40 projections). The test time was 21 minutes in total. The percentage uptake of both kidneys (split function) was determined automatically using the method of comparing fields under the time-activity curves after extrarenal background correction [9].

The manual postprocessing and the designation of the regions of interest (ROI) were performed with the use of the dedicated built-in software provided by Syngo (version: SymbianetVA10D) on a generic protocol. The renographic curves were drawn for each

ROI, for both kidneys separately. The drawing of ROI was performed for the entire kidney and the area between the kidneys (blood background) [7].

### Statistics

Peak time (Tmax) was defined as the minutes from the <sup>99m</sup>Tc-EC injection to the point of highest radioactivity over the kidney. Half-clearance time (T1/2) was calculated from the peak time to the point when half of the radioactivity in the kidney disappeared. The split function represented the ratio of one kidney function to the global renal function as a percentage of all measured activity [15].

Statistical analysis was performed using the Statistica 13.1 software (Stat Soft, Poland). All values derived in this study are shown as the mean value ± coefficient interval (95%). The distribution was examined using the Shapiro–Wilk test of normality. Dependencies between the parameters were estimated using the nonparametric Mann-Whitney U test for two independent samples and the Kruskal-Willis test for more than two independent samples. The statistical significance was defined as  $p \leq 0.05$ . Pearson linear correlation coefficients were applied.

### Ethics

Every patient signed an informed consent form. The study protocol and informed consent forms were approved by the

ethics committee of the Bioethical Council, Medical University of Lublin, Poland.

The tests were tolerated well by all patients.

### Results

Mean values, standard deviation (SD) and coefficient interval (CI) of the renographic curve parameters for all kidneys obtained in this study are listed in Table 2. Normal values [here assumed to be the mean value (mean SD)] of Tmax is 2.85 min [0.58 min] and T1/2 is 8.7 min [1.83 min]. The values obtained in the pediatric study are different and age-dependent. They are also given in Table 2. The normal value of Tmax is 2.81 min (0.59 min) and that of T1/2 is 8.63 min (1.86 min).

A comparison of Tmax, T1/2 in different age groups (5 groups: 2–5, 6–9, 10–13, 14–18, 19–71 years) shows that age has no significant effect on both parameters: Tmax ( $p = 0.061$ ) and T1/2 ( $p = 0.386$ ). In the pediatric groups (4 groups: 2–5, 6–9, 10–13 and 14–18 years), too, the differences are insignificant: Tmax ( $p = 0.07$ ) and T1/2 ( $p = 0.192$ ).

The normal values of renographic curve parameters for both sexes and sides are given in Table 3. A comparison of Tmax, T1/2 for female and male patients shows that the sex of the patient does not affect Tmax ( $p = 0.339$ ) and T1/2 ( $p = 0.256$ ). In the case

**Table 2.** Normal values of the renographic curve parameters Tmax, T1/2 depending on the total number of tested kidneys, pediatric study, and age group

	Age group	n	Min [min]	Max [min]	Median [min]	Mean [min]	± SD	conf. interval (95%)	conf. interval (95%)	
								lower	upper	
Tmax	all	194	1.50	4.50	3.00	2.85	0.58	1.16	1.69	4.00
	pediatric	166	1.50	4.50	3.00	2.81	0.59	1.16	1.65	3.97
	2–5 years	31	1.50	4.00	2.50	2.68	0.53	1.09	1.59	3.77
	6–9 years	54	2.00	4.00	2.50	2.68	0.56	1.14	1.54	3.81
	10–13 years	44	2.00	4.00	2.50	2.87	0.60	1.23	1.65	4.10
	14–18 years	37	2.00	4.50	3.00	3.05	0.59	1.21	1.85	4.26
	19–71 years	28	2.00	4.50	3.00	3.06	0.53	1.12	1.94	4.17
T1/2	all	194	5.15	14.90	8.50	8.70	1.83	3.61	5.10	12.32
	pediatric	166	5.15	14.90	8.50	8.63	1.86	3.71	4.90	12.32
	2–5 years	31	5.50	14.90	8.70	8.93	1.98	4.11	4.82	13.04
	6–9 years	54	5.15	12.10	7.70	7.99	1.65	3.34	4.65	11.33
	10–13 years	44	6.10	13.50	8.58	8.98	1.82	3.72	5.27	12.70
	14–18 years	37	5.40	14.10	8.70	8.91	1.93	3.96	4.95	12.87
	19–71 years	28	6.00	12.80	9.24	8.96	1.63	3.40	5.68	12.48

**Table 3.** Comparison of normal values of the renographic curve parameters Tmax, T1/2 for both sexes and sides

	Age group	Female	Male	Left kidney	Right kidney
Mean Tmax [min]	all	2.88	2.80	2.86	2.84
	children (2–18)	2.85	2.75	2.82	2.80
	adults	3.17	2.97	3.03	3.08
Mean T1/2 [min]	all	8.57	8.88	8.74	8.64
	children (2–18)	8.42	8.97	8.66	8.61
	adults	9.82	8.52	9.22	8.89

of children, the differences between Tmax and T1/2 for female and male patients are Tmax ( $p = 0.408$ ) and T1/2 ( $p = 0.075$ ). T1/2 correlates with Tmax ( $p = 0.004$ ). The correlation between these values depending on the age group is ( $r = 0.604$ ) for all kidneys and ( $r = 0.59$ ) for children.

## Discussion

We have developed the standards of dynamic renal scintigraphy parameters for the nuclear medicine department in which the study was conducted. This will facilitate the preliminary assessment of kidney health, which is particularly useful in the study of children. At the same time, to obtain comprehensive results, a more accurate visual assessment of the images is necessary to exclude focal defects in the parenchyma as they may be invisible on the renographic curve. The Tmax and T1/2 parameters were evaluated. The split function ranging from 45% to 55% for each kidney was considered only in the case of patients having both kidneys normal.

Comparing the differences between the obtained calculated parameters one can observe that:

1. The normal value of the secretory function parameter does not significantly depend on age. The changes developing in the kidneys with age are related to all kidney structures. First of all, a reduction in the size and weight of the organ can be observed. The study shows that the size of the glomeruli does not change with age, however, the number of cells in the glomeruli decreases to a significant degree. This may eventually lead to renal function impairment [1]. The scatter plot in Figure 2 shows both parameters tend to slightly increase with age (which demonstrates a slight increase in the parameters for older patients), but the correlation is under the assumed significance level of  $p = 0.05$ . This indicates that there is no need to establish separate norms for adults and children. Only healthy kidneys were taken into consideration, so we do not obtain any information about differences in kidney diseases between adults and children.

2. In terms of the sex, globally, there are no significant differences for any parameters, as can be concluded from Table 3, even though that there are differences in the structure and function of the kidneys depending on the gender [16].
3. Globally, there are no significant differences between the sides.
4. There is a strong positive correlation between the excretory function parameter and the secretory function parameter for normal kidneys.

Compared to Van Nerom first evaluation on healthy volunteers from 1993 [11], calculated times for adults are slightly different (our results are given in Tab. 3). The Tmax mean value [min] for the left and the right kidney is 3.3 and 5.0 (Van Nerom) vs. 3.03 and 3.08. The T1/2 mean value [min] for the left and the right kidney is 6.5; 10.0 (Van Nerom) vs. 9.22; 8.89. The differences might result from the size of the test group; the above-mentioned study was conducted on a group of only six adult male volunteers (averaging 27.5 years old), while the present study was conducted on 27 adults (F/M: 9/10; aged 21–71; averaging 43.8 years old). In a 1997 study examining 4 children with normal kidneys and 15 children with various renal disorders [12], the calculated renal function parameters for normal kidneys were found to be similar for  $^{99m}\text{Tc-EC}$  and  $^{99m}\text{Tc-MAG3}$ . The mean Tmax values (min) were 3.2 and 3.1, respectively, and the mean T1/2 values were 6.3 and 6.4, respectively. Again, the difference might stem from the size of the test group. The differences might also depend on the group selection because in the aforementioned study both normal kidneys and kidneys with various renal disorders were examined.

Compared to the Sohaib data from 2013 [15], the calculated function parameters are much lower. More specifically, the Tmax mean value (min) is 4.6 (Sohaib) vs. 3.06, while the T1/2 mean value [min] is 14.5 (Sohaib) vs. 8.96. Again, the research group is smaller and contains only adult male volunteers (averaging 30 years old). This difference may also result from the fact that all curves were considered correct in the data collecting process. There are also significant differences in the parameters of kidney perfusion that were obtained in the studies conducted with other dynamic renal scintigraphy radiopharmaceuticals such as  $^{99m}\text{Tc-MAG3}$  [15, 17].

International Scientific Committee of Radionuclides in Nephrourology (ISCORN) noted that the final urine flow depends on the hydration state. Dehydration can cause false-positive results and hydration degrees significantly affected renogram pattern and renal parameters [18]. When the ROI was placed over the whole kidney, the parameters that increased statistically significantly in the dehydrated state where Tmax, T1/2 [5, 17, 19]. The quality of dynamic renal imaging can be degraded by a full bladder, the patient should void before image acquisition, to promote drainage, or it can influence renal function parameters [5]. Our study was performed without furosemide injection, and the patients were asked to void before image acquisition.

In this study mean values, standard deviation (SD) and coefficient interval (CI) were used. The use of the standard error of the mean (SEM) should be limited to inferential statistics where the author explicitly wants to inform the reader about the precision of the study and how well the sample truly represents the entire population. In terms of diagrams and figures, too, the use of SD is preferable to the SEM. To determine the standard range for the biological parameter, it is proposed that the coefficient interval

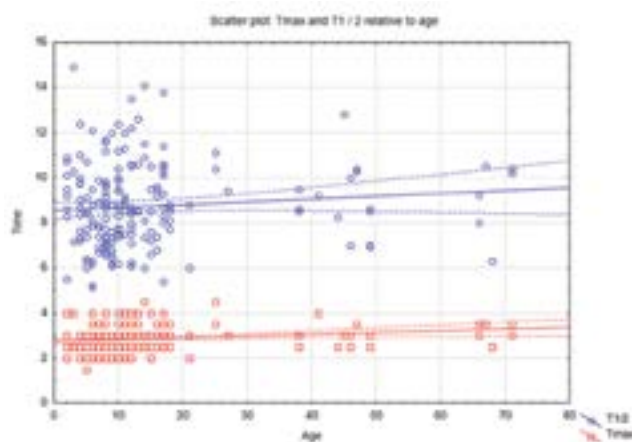


**Figure 2.** Scatter plot of secretion and extraction times (Tmax and T1/2) versus the age of patients in  $^{99m}\text{Tc-EC}$  dynamic renal scintigraphy

(the level of confidence of 95%) should be used to ensure that the deterministic parameter is captured by the interval [20].

A great advantage of this study is that it concerns the problem that has not been widely discussed in the literature and that it was conducted on a larger research group. Although the <sup>99m</sup>Tc-MAG3 dynamic renal scintigraphy has been investigated by many studies, the standards of <sup>99m</sup>Tc-EC dynamic renal scintigraphy have not yet been sufficiently defined. At the same time, it should be noted that the calculated norms for the analyzed parameters may disagree with the standards obtained in other research centers, due to the subjectivity of ROI selection and renographic curve correctness assessment. The results of this study can be a starting point for further research on the establishment of renographic curve parameter norms for patients with particular kidney diseases.

The best cutoff value to separate normal from abnormal values would be obtained by comparing results for normal and diseased populations. In practice, it is often difficult to generalize such a comparison because the degree of abnormality can depend on the selection criteria used to define the disease population. Any value lying outside of the fifth or 95<sup>th</sup> percentile is considered abnormal. Values outside the lower range of normal are likely to represent a processing problem rather than an abnormality of renal function.

## Conclusions

In this study, we proposed the range of normal renal function parameters for <sup>99m</sup>Tc-EC dynamic renal scintigraphy. The study has demonstrated that the normal value of the secretory and excretory function parameter does not depend on age, and that, globally, there are no differences between the sexes and the sides for any parameter.

## Conflicts of interest

There are no conflicts of interest.

## References

- Mititelu R, Bratu O. Radionuclide Imaging. An Update on the Use of Dynamic Renal Scintigraphy. *Medicina Moderna - Modern Medicine*. 2017; 24(4): 199–203, doi: [10.31689/rmm.2017.24.4.199](https://doi.org/10.31689/rmm.2017.24.4.199).
- Taylor AT. Radionuclides in nephrourology, Part 2: pitfalls and diagnostic applications. *J Nucl Med*. 2014; 55(5): 786–798, doi: [10.2967/jnumed.113.133454](https://doi.org/10.2967/jnumed.113.133454), indexed in Pubmed: [24591488](https://pubmed.ncbi.nlm.nih.gov/24591488/).
- Keramida G, James JM, Prescott MC, et al. Pitfalls and Limitations of Radionuclide Renal Imaging in Adults. *Semin Nucl Med*. 2015; 45(5): 428–439, doi: [10.1053/j.semnuclmed.2015.02.008](https://doi.org/10.1053/j.semnuclmed.2015.02.008), indexed in Pubmed: [26278854](https://pubmed.ncbi.nlm.nih.gov/26278854/).
- Moran JK. Technetium-99m-EC and other potential new agents in renal nuclear medicine. *Semin Nucl Med*. 1999; 29(2): 91–101, doi: [10.1016/s0001-2998\(99\)80002-6](https://doi.org/10.1016/s0001-2998(99)80002-6), indexed in Pubmed: [10321823](https://pubmed.ncbi.nlm.nih.gov/10321823/).
- Kabasakal L, Turoğlu HT, Onsel C, et al. Clinical comparison of technetium-99m-EC, technetium-99m-MAG3 and iodine-131-OIH in renal disorders. *J Nucl Med*. 1995; 36(2): 224–228, indexed in Pubmed: [7830118](https://pubmed.ncbi.nlm.nih.gov/7830118/).
- Ell PJ, Gambhir SS. *Nuclear Medicine in Clinical Diagnosis and Treatment*, 3rd ed. AJNR Am J Neuroradiol. 2006; 27: 464–465.
- European Nuclear Medicine Guide. <https://www.nucmed-guide.app/#!/chapter/312> (2.01.2019).
- Taylor AT. Radionuclides in nephrourology, part 1: Radiopharmaceuticals, quality control, and quantitative indices. *J Nucl Med*. 2014; 55(4): 608–615, doi: [10.2967/jnumed.113.133447](https://doi.org/10.2967/jnumed.113.133447), indexed in Pubmed: [24549283](https://pubmed.ncbi.nlm.nih.gov/24549283/).
- Gordon I, Piepsz A, Sixt R. Guidelines for standard and diuretic renogram in children. *Eur J Nucl Med Mol Imaging*. 2011; 38(6): 1175–1188, doi: [10.1007/s00259-011-1811-3](https://doi.org/10.1007/s00259-011-1811-3).
- Kabasakal L, Atay S, Vural VA, et al. Evaluation of technetium-99m-ethylenedicycysteine in renal disorders and determination of extraction ratio. *J Nucl Med*. 1995; 36(8): 1398–1403, indexed in Pubmed: [7629584](https://pubmed.ncbi.nlm.nih.gov/7629584/).
- Van Nerom CG, Bormans GM, De Roo MJ, et al. First experience in healthy volunteers with technetium-99m L,L-ethylenedicycysteine, a new renal imaging agent. *Eur J Nucl Med*. 1993; 20(9): 738–746, doi: [10.1007/BF00180902](https://doi.org/10.1007/BF00180902), indexed in Pubmed: [8223766](https://pubmed.ncbi.nlm.nih.gov/8223766/).
- Kibar M, Noyan A, Anarat A. 99Tcm-N,N-ethylenedicycysteine scintigraphy in children with various renal disorders: a comparative study with 99Tcm-MAG3. *Nucl Med Commun*. 1997; 18(1): 44–52, doi: [10.1097/00006231-199701000-00009](https://doi.org/10.1097/00006231-199701000-00009), indexed in Pubmed: [9061700](https://pubmed.ncbi.nlm.nih.gov/9061700/).
- Lever SZ, Lever JR. Technetium-99m Pharmaceuticals: Preparation and Quality Control in Nuclear Medicine. *J Nucl Med*. 2009; 50(5): 831–831, doi: [10.2967/jnumed.109.062166](https://doi.org/10.2967/jnumed.109.062166).
- Prigent A, Cosgriff P, Gates GF, et al. Consensus report on quality control of quantitative measurements of renal function obtained from the renogram: International Consensus Committee from the Scientific Committee of Radionuclides in Nephrourology. *Semin Nucl Med*. 1999; 29(2): 146–159, doi: [10.1016/s0001-2998\(99\)80005-1](https://doi.org/10.1016/s0001-2998(99)80005-1), indexed in Pubmed: [10321826](https://pubmed.ncbi.nlm.nih.gov/10321826/).
- Sohaib M, Rafique A, Saeed S, et al. A comparison of single plasma sample methods to estimate renal clearance using 99mTc-ethylenedicycysteine and 99mTc-mercaptoacetyltryglycine. *Clin Physiol Funct Imaging*. 2013; 33(5): 353–358, doi: [10.1111/cpf.12034](https://doi.org/10.1111/cpf.12034), indexed in Pubmed: [23701132](https://pubmed.ncbi.nlm.nih.gov/23701132/).
- Sabolić I, Asif AR, Budach WE, et al. Gender differences in kidney function. *Pflugers Arch*. 2007; 455(3): 397–429, doi: [10.1007/s00424-007-0308-1](https://doi.org/10.1007/s00424-007-0308-1), indexed in Pubmed: [17638010](https://pubmed.ncbi.nlm.nih.gov/17638010/).
- Lin WY, Changlai SP, Kao CH. Normal ranges of renal physiological parameters for technetium-99m mercaptoacetyltryglycine and the influence of age and sex using a camera-based method. *Urol Int*. 1998; 60(1): 11–16, doi: [10.1159/000030196](https://doi.org/10.1159/000030196), indexed in Pubmed: [9519415](https://pubmed.ncbi.nlm.nih.gov/9519415/).
- Jung HS, Chung YAn, Kim EN, et al. Influence of hydration status in normal subjects: fractional analysis of parameters of Tc-99m DTPA and Tc-99m MAG3 renography. *Ann Nucl Med*. 2005; 19(1): 1–7, doi: [10.1007/BF02986328](https://doi.org/10.1007/BF02986328), indexed in Pubmed: [15770966](https://pubmed.ncbi.nlm.nih.gov/15770966/).
- Durand E, Blaufox MD, Britton KE, et al. International Scientific Committee of Radionuclides in Nephrourology (ISCORN). International Scientific Committee of Radionuclides in Nephrourology (ISCORN) consensus on renal transit time measurements. *Semin Nucl Med*. 2008; 38(1): 82–102, doi: [10.1053/j.semnuclmed.2007.09.009](https://doi.org/10.1053/j.semnuclmed.2007.09.009), indexed in Pubmed: [18096466](https://pubmed.ncbi.nlm.nih.gov/18096466/).
- Barde MP, Barde PJ. What to use to express the variability of data: Standard deviation or standard error of mean? *Perspect Clin Res*. 2012; 3(3): 113–116, doi: [10.4103/2229-3485.100662](https://doi.org/10.4103/2229-3485.100662), indexed in Pubmed: [23125963](https://pubmed.ncbi.nlm.nih.gov/23125963/).

# The impact of depression and anxiety in prognosis of patients undergoing myocardial perfusion imaging with $^{99m}\text{Tc}$ tetrofosmin SPECT for evaluation of possible myocardial ischemia

Andreas Fotopoulos<sup>1</sup> , Petros Petrikis<sup>2</sup> , Ioannis Iakovou<sup>3</sup> , Athanasios Papadopoulos<sup>4</sup>, Konstantinos Sakelariou<sup>1</sup>, Evangelia Gkika<sup>1</sup>, Lampros Lakkas<sup>5</sup>, Christos Touzios<sup>1</sup>, Konstantinos Pappas<sup>5</sup>, Antonios Klaroudas<sup>1</sup>, Argyrios Doumas<sup>2</sup> , Chrissa Sioka<sup>1</sup> 

<sup>1</sup>Department of Nuclear Medicine, Medical School, University Hospital of Ioannina, Greece, Ioannina, Greece

<sup>2</sup>Department of Psychiatry, Medical School, University Hospital of Ioannina, Ioannina, Greece

<sup>3</sup>2<sup>nd</sup> Nuclear Medicine Laboratory, AHEPA University Hospital, Aristotle University of Thessaloniki, Thessaloniki, Greece

<sup>4</sup>Department of Medical Physics, University Hospital of Ioannina, Greece

<sup>5</sup>Department of Cardiology, University Hospital of Ioannina, Greece

[Received 13 XII 2019; Accepted 22 IV 2020]

## Abstract

**BACKGROUND:** The goal of this study was to evaluate the prevalence of depression and anxiety in patients subjected to myocardial perfusion imaging (MPI) with  $^{99m}\text{Tc}$  tetrofosmin stress-rest single-photon emission computer tomography (SPECT), and their impact on their cardiological events or disease.

**MATERIAL AND METHODS:** Patients referred to the Nuclear Medicine Department for  $^{99m}\text{Tc}$  tetrofosmin myocardial MPI-SPECT were asked to fulfill the Zung Self-Rating Depression Scale (ZDS) and Hamilton anxiety questionnaire (HAQ). Among 213 patients who completed the ZDS and HAQ, 80 patients (59 males and 21 females) were selected for this study because they had no known psychological disease, other disease that could influence psychological status, or use of narcotic drugs. Collected data from MPI and psychological status were subsequently analyzed.

**RESULTS:** Among all 80 patients, 52 patients (65%) had abnormal MPI of whom 28/52 (53.8%) exhibited either depression, anxiety or both, and 28 (35%) patients had normal MPI of whom 10/28 (35.7%) had abnormal psychological status. The higher number of patients with abnormal psychological status in association with abnormal MPI was noted predominantly in patients with previously established coronary artery disease. A correlation was also noted between obesity, cardiac heredity and depression or anxiety in patients with abnormal MPI.

**CONCLUSIONS:** Patients that exhibit depression, anxiety, or both, have high rates of myocardial ischemia, and thus are at risk for subsequent cardiological events.

**KEY words:** myocardial perfusion imaging; myocardial ischemia; depression; anxiety; psychological status; MPI; SPECT

Nucl Med Rev 2020; 23, 2: 58–62

## Introduction

Anxiety and depression are frequently manifested in patients with cardiovascular diseases. Prevalence may vary between

15 and 50%, according to diagnostic criteria used and demographic characteristics of the patients [1]. Depression may be associated with coronary artery disease (CAD) and its consequences such as cardiac arrhythmias, myocardial infarction (MI) and heart failure. Although the exact physiological mechanisms for this association remain unclear, it may be due to hypothalamic – pituitary dysregulation, altered immune function or existence of common unknown risk factors for both medical conditions [2, 3]. Scientific evidence over the last few years reported significant association between anxiety or depression and various organic conditions including cardiac

Correspondence to: Andreas Fotopoulos  
Department of Nuclear Medicine, Medical School,  
University Hospital of Ioannina, Greece, Ioannina, Greece  
e-mail: professor.fotopoulos@yahoo.com

diseases [1, 4]. Furthermore, patients with cardiac diseases and depression tend to exhibit poor risk factor control resulting into further deterioration of their cardiac disease and prognosis [1]. Anxiety has been also linked to increased mortality in patients with CAD but this association was reported less strong than that of depression [5]. It is interesting that anxiety seems to improve in patients that have detailed imaging studies concerning their disease and good communication with their physician about the status of their medical condition [6].

Myocardial perfusion imaging (MPI) SPECT may be used to assess the myocardial condition either in patients with known MI, or post either percutaneous transluminal coronary angioplasty (PTCA) or coronary artery bypass grafting (CABG) [7], or with silent myocardial ischemia due to non-specific cardiac complaints [8–10]. The MPI grading may be able to provide an excellent tool to monitor response to treatment, follow-up status and long term prognosis [11, 12].

Women overall appear to display more nonspecific cardiac complaints than men. However, these symptoms by themselves have unknown clinical significance not necessarily linked to myocardial ischemia in the absence of other relative clinical manifestations [10]. However, MPI may be able to identify myocardial ischemia in elderly women with angina or in asymptomatic women with concomitant diabetes mellitus or hypertension [13]. Female patients with CAD demonstrate positive MPI [14] with sensitivity of 87.16% and specificity of 97% [15]. In such cases, a summed stress score (SSS)  $\geq 14$  denoted an increased risk for cardiac events and an SSS  $\geq 22$  for subsequent significant cardiac events such as acute MI and cardiac death [16].

In the present retrospective study, we evaluated the rate of myocardial ischemia in patients who were subjected to MPI with <sup>99m</sup>Tc-TF-SPECT, due to non-specific cardiac complaints of various types, or in patients that had known myocardial disease for follow up after CABG or PTCA. Furthermore, in all patients we evaluated the association of anxiety and/or depression with the known cardiovascular risk factors such as age, smoking, obesity, diabetes mellitus (DM), arterial hypertension, dyslipidemia and cardiac heredity.

## Material and methods

### Patients

In the present study there were 80 patients, 59 men and 21 women, that had MPI either for non-specific cardiac symptoms (workup to rule out CAD), or patients with known CAD and previous PTCA or/and CABG for follow up of their myocardial status. Cardiac risk factors were noted in each patient's medical history (obesity, smoking, arterial hypertension, diabetes mellitus, dyslipidemia, and cardiac heredity). Patients were considered as smokers when smoking habits were active or stopped during the last 3 months. Females under anti-hypertensive drugs or with systolic blood pressure (BP)  $\geq 140$  mm Hg or diastolic BP  $\geq 90$  mm Hg were noted as having hypertension as risk factor. Diabetes mellitus as risk factor was noted in females under antidiabetic medication and fasting glucose  $> 126$  mg/dL. Finally, dyslipidemia was considered in patients receiving therapy with statins or exhibiting fasting cholesterol level  $> 220$  mg/dL.

### SPECT MPI

All study participants had been subjected to <sup>99m</sup>Tc-TF-SPECT before and after stress using a 1-day imaging protocol according to published guidelines [17]. Stress protocol was consisted either of a dynamic exercise (Bruce protocol treadmill exercise test) or a pharmacological test with either dipyridamole or dobutamine. The electrocardiography was continuously monitored during stress. All patients were first injected with 8 mCi Tc-99m tetrofosmin after stress or 20 mCi at rest followed by acquisition of images 40 minutes later via a 90°-angled dual-head camera, employing a collimator with 64 stops and 25 s per projection over a 180° arc. Reconstruction of images was consisted of filter back projection without attenuation correction [18].

MPI was visually evaluated by two nuclear medicine specialists, using a 17 scoring each segment on a scale of 0 to 4 according to the severity of the myocardial perfusion deficit [18]. Thus, score 0 was designated when there was no decreased myocardial activity, score 1 with mildly decreased activity, score 2 for moderate decreased activity, score 3 for severely decreased activity and score 4 for absent tracer activity. All individuals scores at rest and stress were combined and produced the summed rest score (SRS) and summed stress score (SSS). The difference of the two scores (S-RSS) was also calculated and evaluated. A summed difference score (SDS) was obtained by subtracting the rest score from the stress score; in the presence of a reversible defect (or ischemia) the score was positive. Myocardial ischemia (MIS) was graded as mild when SSS was 4 to 8, moderate from 9 to 13, and severe when SSS over 13 [19].

### Evaluation of psychological status

Patients who were subjected to <sup>99m</sup>Tc-TF-SPECT- MPI in the Department of Nuclear Medicine were asked to fulfill the Zung Self-Rating Depression Scale (ZDS) and Hamilton anxiety questionnaire (HAQ). The ZDS consists of 20 items that quantify the depressive symptoms of a patient. Each item is scored on a range from 1 to 4. Total score lower than 50 is considered as normal, between 50 and 59 as mild depression, between 60 to 69 as moderate depression, while score over 70 as severe depression [20]. The HAQ consists of 14 items and is widely used to assess both psychic and somatic anxiety. Each item is scored on a range of 0 (not present) to 4 (severe anxiety), with a total score ranging from 0 to 56 [21].

Among the patients who agreed to participate to the study, those with known disease such as cancer, multiple sclerosis, chronic kidney disease or any other condition that could influence psychological status were excluded from the study. Furthermore, those with known psychological disease, use of narcotic drugs were also excluded. ZDS and HAQ results were evaluated by a psychiatrist.

### Statistical analysis

The evaluation of the myocardial perfusion studies were analyzed utilizing the statistical software SPSS version 20 for windows (SPSS, Chicago, IL). Several groups of patients were developed based on the gender, the degree of abnormality and their correlation with the specific characteristics of depression, anxiety, obesity, cardiac heredity, smoking and hypertension.

Baseline characteristics were described using, median and frequencies for categorical variables. For the verification of correlation

**Table 1.** Characteristics of the patients [mean value  $\pm$  standard deviation (min-max)]

Characteristics	All 80 patients	Male 59 patients	Females 21 patients
Diagnostic MPI	45/80 (56%)	28/45 (62%)	17/45 (38%)
PTCA & CABG MPI	31/80 (39%)	27/31 (87%)	4/31 (13%)
Mean age [years]	66.69 $\pm$ 11.61	66.72 $\pm$ 11.15	66.57 $\pm$ 13.10
Myocardial infarction	20/80 (25%)	17/80 (85%)	3/80 (15%)
Smoking	25/80 (11%)	19/25 (76%)	6/25 (24%)
Hypertension	59/80 (74%)	43/59 (73%)	16/59 (27%)
Diabetes mellitus	35/80 (44%)	28/35 (80%)	7/35 (20%)
Hyperlipidemia	54/80 (67%)	42/54 (78%)	12/54 (22%)
Obesity	26/80 (33%)	20/26 (77%)	6/26 (23%)
Heart heredity	27/80 (34%)	20/27 (74%)	7/27 (26%)

MPI — myocardial perfusion imaging; PTCA — percutaneous transluminal coronary angioplasty; CABG — coronary artery bypass grafting

"N-1" Chi-squared test has been utilized to determine the significant difference between the means of two groups, which may be related in certain features. The alpha of 0.05 was used as the cutoff for significance and thus if the p-value was less than 0.05, the difference of the two groups was significant. Additionally, a Spearman's rho methodology applied for the identification of the correlation among the different characteristics and features. A Spearman's rank-order correlation between the groups of features provides a degree of correlation regarding the level of the  $r_s$  score. Thus,  $r_s$  of 0.2 to 0.39 describe as weak correlation and 0.4 to 0.59 as moderate correlation, respectively.

## Results

The patients' age, medical history of myocardial infarction and cardiac risk factors are shown in Table 1. Abnormal MPI was found in 52 of 80 patients (65%), and normal MPI in 28/80 (35%) patients. Among all study participants with abnormal MPI 53.8% exhibited depression, anxiety or combination of both (Tab. 2). However, patients with normal MPI demonstrated lower rate of psychological abnormalities at 35.7%. Statistical analysis did not reveal any statistical significance possibly due to the small number of patients studied; however, a statistical trend was noted ( $p = 0.1244$ ). Patients that had previously established CAG and had abnormal MPI performed for follow-up after PTCA or CABG had significantly higher rates of depression or anxiety (57.1%) compared to those that had normal MPI (28.6%). However, such a difference was less pronounced in patients that were undergoing MPI as an initial evaluation of myocardial status for suspected CAD (Tab. 2).

Furthermore, evaluation of the results according to sex demonstrated that men had much higher percentage of abnormal MPI (47/59, 80%) compared to women (5/21, 24%)  $p < 0.0001$  (Tab. 3). In addition, our results suggested that women had a higher rate of anxiety than men; however, due to the small numbers of female patients it was not able to document it statistically, even though a trend of statistical significance was noted,  $p = 0.1363$ .

In addition, a Spearman's rank-order correlation was run to determine the relationship between the depression and anxiety with several cardiologic risk factors. In patients with abnormal MPI, depression and anxiety found to have a moderate correlation

**Table 2.** Rates of abnormal MPI, depression, anxiety, or both in patients subjected to myocardial scintigraphy either for diagnostic reasons or after cardiologic intervention (follow-up)

Psychological status	MPI (+) 52/80 (65%)	MPI (-) 28/80 (35%)	p
<b>All patients that had MPI (N = 80)</b>			
Depression	10/52 (19.2%)	3/28 (10.7%)	0.3284
Anxiety	13/52 (23.1%)	4/28 (14.3%)	0.3512
Both	5/52 (9.6%)	3/28 (10.7%)	0.8764
Total	28/52 (53.8)	10/28 (35.7%)	0.1244 *
<b>MPI performed for diagnostic reasons (N = 45)</b>			
Depression	3/24 (12.5%)	2/21 (9.5%)	0.7520
Anxiety	6/24 (25%)	3/21 (14.3%)	0.3761
Both	3/24 (12.5%)	4/21 (19%)	0.5526
Total	12/24 (50%)	9/21 (42.9%)	0.7471
<b>MPI performed after cardiologic intervention (PTCA, CABG or both) (N = 35)</b>			
Depression	7/28 (25%)	1/7 (14.3%)	0.5523
Anxiety	7/28 (25%)	1/7 (14.3%)	0.5523
Both	2/28 (7.1%)	0/7 (0.0%)	0.4743
Total	16/28 (57.1%)	2/7 (28.6%)	0.1835 *

MPI (-) — Normal myocardial perfusion imaging; MPI (+) — Abnormal myocardial perfusion imaging; PTCA — Percutaneous transluminal coronary angioplasty; CABG — Coronary artery bypass grafting; \* — a trend of statistical significance

**Table 3.** Patients with abnormal MPI and depression, anxiety, or both

Sex	No	MPI (+)	Depression	Anxiety	Both
Male	59	47/59 (80%)	9/47 (19%)	11/47 (23%)	4/47 (9%)
		$p < 0.0001^{**}$	$p = 0.921$	$p = 0.1363^*$	$p = 0.5631$
Female	21	5/21 (24%)	1/5 (20%)	2/5 (40%)	1/21 (5%)
Total	80	52/80 (65%)	10/52 (19%)	13/52 (25%)	5/52 (8%)

MPI — Myocardial perfusion imaging; MPI(+) — Abnormal myocardial perfusion imaging; PTCA — Percutaneous transluminal coronary angioplasty; CABG — Coronary artery bypass grafting; p\* — trend of statistical significance; p\*\* — statistical significance

( $r_s = 0.411$ ,  $p = 0.001$ ) and weak correlation ( $r_s = 0.369$ ,  $p = 0.001$ ), retrospectively, with obesity. On the other hand, in normal MPI group, the obesity was only correlated weakly with the anxiety ( $r_s = 0.351$ ,  $p = 0.001$ ). Another feature that appears correlation with the MPI patient's condition is the cardiac heredity. Thus, weak correlation ( $r_s = 0.231$ ,  $p = 0.001$ ) appeared for abnormal MPI patients between the cardiac heredity and the depression.

## Discussion

Depression and anxiety are frequently observed in patients with cardiovascular disease and linked with increased morbidity and poor prognosis. Apart from a possible direct effect on several cardiovascular risk factors such as blood pressure, they lead the patient into neglecting the physician-directed therapeutic interventions and further deterioration of their cardiovascular status [22, 23].

In the present study, 80 patients were subjected to MPI in order to assess their myocardial status either as an initial evaluation of possible CAD or as a follow-up of known CAD. Among all patients examined, 52 patients (65%) had abnormal MPI and 28 (35%) normal examination. In the group with the abnormal

MPI, 53% exhibited depression (19.2%), anxiety (23.1%) or both (9.6%). In contrast only 35.7% ( $p = 0.1244$ /indicating a trend of statistical significance) of patients with negative MPI exhibited any psychological abnormality (depression 10.7%, anxiety 14.3%, both 10.7%) (Tab. 2). This trend towards statistical significance of increased frequency of psychological abnormalities in patients with positive MPI, but not definite statistical significance, may be due to the relative small number of patients. It suggests though that psychological abnormalities may predispose to the development of CAD, independently of the other well established risk factors. Interestingly, in our study, these differences were more pronounced in the group of patients with known CAD, undergoing the MPI for follow up rather than the group that test for diagnostic purposes, supporting the same conclusion. Definitely, larger studies are needed to verify these findings. A prospective cross-sectional study of 314 patients presented with chest pain showed a significant association between degree of depression and CAD in female patients [24]. Similar results of female predominance of depressive symptoms as well as higher incidence of anxiety and CAD were reported in a Chinese study [25]. Another large study in 514 German CAD patients, evaluated by the Mini International Neuropsychiatric Interview and the Global Assessment of Functioning (GAF) scale demonstrated comorbidity of depression with CAD and treatment of the depression resulted in improvement of this condition [26]. Interestingly, patients undergoing CABG operation, depression and anxiety were increased after the operation compared to the pre-operative period [27].

Evaluation of our results according to sex, demonstrated predominance of men rather than women as having abnormal MPI and thus CAD (Tab. 3). In addition, although our findings suggested that women had a higher rate of anxiety than men, the numbers of female patients were too small to establish any significance; however, with caution we noted a trend of statistical significance. A previous study in patients undergoing MPI for assessing myocardial status in patients with known or unknown CAD was consisted with our findings showing high level of anxiety mostly in women prior to the examination [28]. Other studies in women reported positive MPI findings in 32% [29], and a sensitivity of 91% and specificity of 70% when SSS was  $> 8$  [30]. In general, patients with anxiety disorders or co-existence of anxiety/depression are associated with increased prevalence of coronary heart disease [31]. Although in some studies depression seems to be the most important factor associated with CAD [32, 32], other studies indicate anxiety as the predominant psychological factor contributing to CAD [31]. Nevertheless, co-existence of both psychological factors appears to have added validity towards this regard. A study on 118 men without history of psychological disturbances demonstrated that after CABG, 16–39.8% of them developed depression and 27.1% anxiety independent of CAD severity [33]. However, female patients demonstrate further reduced quality of life after a cardiac event compared to men. This quality of life refers to appearance anxiety, depression and low self-esteem among other things and may last for over one year [34]. In another study, the reported rates of CAD in female veterans' patients were 4.16%, reaching up to 36% when patients were smokers. Furthermore, those with depression had 60% higher chance of CAD [35].

The mechanisms that the described psychological parameters contribute to the development of CAD are not very well

defined and could be multi sequential. Some investigators suggest that somatic-vegetative features of depression may be linked at an early stage to the development of coronary artery disease [36]. In our study, obesity and cardiac heredity were also associated with depression and anxiety. Previous studies have described an association between hypertension and anxiety, and both depression and anxiety have been linked to diabetes mellitus [37] and hypercholesterolemia [38].

## Conclusions

In conclusion, our results showed that patients with myocardial dysfunction, as evident by abnormal MPI, have increased frequency of coexisting depression, anxiety or both, suggesting that these factors may be contributing risk factors. In addition, both males and females were at higher risk for CAD if depression and anxiety were combined with obesity or cardiac heredity. Further larger studies are needed to verify these findings.

## References

- Herrmann-Lingen C. [Anxiety and depression in cardiology patients: how to diagnose, how to treat?]. *Herz*. 2001; 26(5): 326–334, doi: [10.1007/s00059-001-2300-4](https://doi.org/10.1007/s00059-001-2300-4), indexed in Pubmed: [11556160](https://pubmed.ncbi.nlm.nih.gov/11556160/).
- Christoph M, Christoph A, Dannemann S, et al. Mental symptoms in patients with cardiac symptoms and normal coronary arteries. *Open Heart*. 2014; 1(1): e000093, doi: [10.1136/openhrt-2014-000093](https://doi.org/10.1136/openhrt-2014-000093), indexed in Pubmed: [25436115](https://pubmed.ncbi.nlm.nih.gov/25436115/).
- Hung MY, Mao CT, Hung MJ, et al. Coronary Artery Spasm as Related to Anxiety and Depression: A Nationwide Population-Based Study. *Psychosom Med*. 2019; 81(3): 237–245, doi: [10.1097/PSY.0000000000000666](https://doi.org/10.1097/PSY.0000000000000666), indexed in Pubmed: [30652987](https://pubmed.ncbi.nlm.nih.gov/30652987/).
- Ekici B, Ercan EA, Cehreli S, et al. The effect of emotional status and health-related quality of life on the severity of coronary artery disease. *Kardiol Pol*. 2014; 72(7): 617–623, doi: [10.5603/KPa.2014.0023](https://doi.org/10.5603/KPa.2014.0023), indexed in Pubmed: [24526556](https://pubmed.ncbi.nlm.nih.gov/24526556/).
- Celano CM, Millstein RA, Bedoya CA, et al. Association between anxiety and mortality in patients with coronary artery disease: A meta-analysis. *Am Heart J*. 2015; 170(6): 1105–1115, doi: [10.1016/j.ahj.2015.09.013](https://doi.org/10.1016/j.ahj.2015.09.013), indexed in Pubmed: [26678632](https://pubmed.ncbi.nlm.nih.gov/26678632/).
- Chyun DA, Katten DM, Melkus GD, et al. The impact of screening for asymptomatic myocardial ischemia in individuals with type 2 diabetes. *J Cardiovasc Nurs*. 2006; 21(2): E1–E7, indexed in Pubmed: [16601520](https://pubmed.ncbi.nlm.nih.gov/16601520/).
- Kotsalou I, Georgoulas P, Karydas I, et al. A rare case of myocardial infarction and ischemia in a cannabis-addicted patient. *Clin Nucl Med*. 2007; 32(2): 130–131, doi: [10.1097/01.rlu.0000252218.04088.ff](https://doi.org/10.1097/01.rlu.0000252218.04088.ff), indexed in Pubmed: [17242569](https://pubmed.ncbi.nlm.nih.gov/17242569/).
- Giannopoulos S, Markoula S, Sioka C, et al. Detecting Myocardial Ischemia With Technetium-Tetrofosmin Myocardial Perfusion Imaging in Ischemic Stroke. *Neurohospitalist*. 2017; 7(4): 164–168, doi: [10.1177/1941874417704752](https://doi.org/10.1177/1941874417704752), indexed in Pubmed: [28974994](https://pubmed.ncbi.nlm.nih.gov/28974994/).
- Sioka C, Exarchopoulos T, Tasiou I, et al. Myocardial perfusion imaging with (99 m)Tc-tetrofosmin SPECT in breast cancer patients that received postoperative radiotherapy: a case-control study. *Radiat Oncol*. 2011; 6: 151, doi: [10.1186/1748-717X-6-151](https://doi.org/10.1186/1748-717X-6-151), indexed in Pubmed: [22067743](https://pubmed.ncbi.nlm.nih.gov/22067743/).
- D'Antono B, Dupuis G, Arsenault A, et al. Silent ischemia: Silent after all? *Canadian Journal of Cardiology*. 2008; 24(4): 285–291, doi: [10.1016/s0828-282x\(08\)70178-8](https://doi.org/10.1016/s0828-282x(08)70178-8).
- Koh AS, Lye WK, Chia SY, et al. Long-Term Prognostic Value of Appropriate Myocardial Perfusion Imaging. *Am J Cardiol*. 2017; 119(12): 1957–1962, doi: [10.1016/j.amjcard.2017.03.026](https://doi.org/10.1016/j.amjcard.2017.03.026), indexed in Pubmed: [28456317](https://pubmed.ncbi.nlm.nih.gov/28456317/).

12. Smit JM, Hermans MP, Dimitriu-Leen AC, et al. Long-term prognostic value of single-photon emission computed tomography myocardial perfusion imaging after primary PCI for STEMI. *Eur Heart J Cardiovasc Imaging*. 2018; 19(11): 1287–1293, doi: [10.1093/ehjci/jex332](https://doi.org/10.1093/ehjci/jex332), indexed in Pubmed: [29315366](https://pubmed.ncbi.nlm.nih.gov/29315366/).
13. Lee SuJ, Lee KH, Park SM, et al. Myocardial perfusion defects and coronary risk factors in symptomatic and asymptomatic elderly women. *Int J Cardiovasc Imaging*. 2008; 24(3): 277–281, doi: [10.1007/s10554-007-9258-0](https://doi.org/10.1007/s10554-007-9258-0), indexed in Pubmed: [17786583](https://pubmed.ncbi.nlm.nih.gov/17786583/).
14. Pérez Iruela JA, Pastor Fructuoso P, Lumbreras Vega L, et al. [Diagnostic value of myocardial perfusion scintigraphy with (99m)Tc-tetrofosmin in women with suspected ischemic heart disease]. *Med Clin (Barc)*. 2009; 133(9): 330–332, doi: [10.1016/j.medcli.2009.01.042](https://doi.org/10.1016/j.medcli.2009.01.042), indexed in Pubmed: [19523653](https://pubmed.ncbi.nlm.nih.gov/19523653/).
15. Zhang WC, Tian YQ, Yang MF, et al. Stress myocardial perfusion single photon emission computed tomography imaging in the detection of coronary artery disease in woman. *Zhonghua Yi Xue Za Zhi*. 2007; 87(37): 2623–2626, indexed in Pubmed: [18162150](https://pubmed.ncbi.nlm.nih.gov/18162150/).
16. America YG, Bax JJ, Boersma E, et al. The additive prognostic value of perfusion and functional data assessed by quantitative gated SPECT in women. *J Nucl Cardiol*. 2009; 16(1): 10–19, doi: [10.1007/s12350-008-9012-6](https://doi.org/10.1007/s12350-008-9012-6), indexed in Pubmed: [19152124](https://pubmed.ncbi.nlm.nih.gov/19152124/).
17. Arumugam P, Harbinson M, Reyes E, et al. Procedure guidelines for radionuclide myocardial perfusion imaging with single-photon emission computed tomography. *Nucl Med Commun*. 2013; 34(8): 813–826, doi: [10.1097/MNM.0b013e32836171eb](https://doi.org/10.1097/MNM.0b013e32836171eb), indexed in Pubmed: [23719150](https://pubmed.ncbi.nlm.nih.gov/23719150/).
18. Fotopoulos A, Papadimitropoulos K, Papadopoulos A, et al. Myocardial ischemia in female patients with rheumatoid arthritis assessed with single photon emission tomography-myocardial perfusion imaging. *Nucl Med Rev Cent East Eur*. 2019; 22(1): 8–13, doi: [10.5603/NMR.2019.0001](https://doi.org/10.5603/NMR.2019.0001), indexed in Pubmed: [31482536](https://pubmed.ncbi.nlm.nih.gov/31482536/).
19. Belardinelli R, Cianci G, Gigli M, et al. Effects of trimetazidine on myocardial perfusion and left ventricular systolic function in type 2 diabetic patients with ischemic cardiomyopathy. *J Cardiovasc Pharmacol*. 2008; 51(6): 611–615, doi: [10.1097/FJC.0b013e31817bdd66](https://doi.org/10.1097/FJC.0b013e31817bdd66), indexed in Pubmed: [18574390](https://pubmed.ncbi.nlm.nih.gov/18574390/).
20. ZUNG WW. A SELF-RATING DEPRESSION SCALE. *Arch Gen Psychiatry*. 1965; 12: 63–70, doi: [10.1001/archpsyc.1965.01720310065008](https://doi.org/10.1001/archpsyc.1965.01720310065008), indexed in Pubmed: [14221692](https://pubmed.ncbi.nlm.nih.gov/14221692/).
21. HAMILTON M. The assessment of anxiety states by rating. *Br J Med Psychol*. 1959; 32(1): 50–55, doi: [10.1111/j.2044-8341.1959.tb00467.x](https://doi.org/10.1111/j.2044-8341.1959.tb00467.x), indexed in Pubmed: [13638508](https://pubmed.ncbi.nlm.nih.gov/13638508/).
22. Jha MK, Qamar A, Vaduganathan M, et al. Screening and Management of Depression in Patients With Cardiovascular Disease: JACC State-of-the-Art Review. *J Am Coll Cardiol*. 2019; 73(14): 1827–1845, doi: [10.1016/j.jacc.2019.01.041](https://doi.org/10.1016/j.jacc.2019.01.041), indexed in Pubmed: [30975301](https://pubmed.ncbi.nlm.nih.gov/30975301/).
23. Watkins LL, Blumenthal JA, Davidson JRT, et al. Phobic anxiety, depression, and risk of ventricular arrhythmias in patients with coronary heart disease. *Psychosom Med*. 2006; 68(5): 651–656, doi: [10.1097/01.psy.0000228342.53606.b3](https://doi.org/10.1097/01.psy.0000228342.53606.b3), indexed in Pubmed: [17012517](https://pubmed.ncbi.nlm.nih.gov/17012517/).
24. Vural M, Satiroglu O, Akbas B, et al. Coronary artery disease in association with depression or anxiety among patients undergoing angiography to investigate chest pain. *Tex Heart Inst J*. 2009; 36(1): 17–23, indexed in Pubmed: [19436781](https://pubmed.ncbi.nlm.nih.gov/19436781/).
25. Deng BY, Cui JG, Li CJ, et al. [Psychological status in 1083 hospitalized patients with coronary artery disease]. *Zhonghua Xin Xue Guan Bing Za Zhi*. 2010; 38(8): 702–705, indexed in Pubmed: [21055136](https://pubmed.ncbi.nlm.nih.gov/21055136/).
26. Westermair AL, Schaich A, Willenborg B, et al. Utilization of Mental Health Care, Treatment Patterns, and Course of Psychosocial Functioning in Northern German Coronary Artery Disease Patients with Depressive and/or Anxiety Disorders. *Front Psychiatry*. 2018; 9: 75, doi: [10.3389/fpsy.2018.00075](https://doi.org/10.3389/fpsy.2018.00075), indexed in Pubmed: [29593584](https://pubmed.ncbi.nlm.nih.gov/29593584/).
27. Açikel ME. Evaluation of Depression and Anxiety in Coronary Artery Bypass Surgery Patients: A Prospective Clinical Study. *Braz J Cardiovasc Surg*. 2019; 34(4): 389–395, doi: [10.21470/1678-9741-2018-0426](https://doi.org/10.21470/1678-9741-2018-0426), indexed in Pubmed: [31364347](https://pubmed.ncbi.nlm.nih.gov/31364347/).
28. Tamam MO, Bagcioglu E, Mulazimoglu M, et al. Evaluation of anxiety and depression in patients prior to myocardial perfusion scintigraphy. *Int J Psychiatry Clin Pract*. 2012; 16(2): 93–97, doi: [10.3109/13651501.2011.631017](https://doi.org/10.3109/13651501.2011.631017), indexed in Pubmed: [22136214](https://pubmed.ncbi.nlm.nih.gov/22136214/).
29. Mehta R, Ward RP, Chandra S, et al. American College of Cardiology Foundation, American Society of Nuclear Cardiology. Evaluation of the American College of Cardiology Foundation/American Society of Nuclear Cardiology appropriateness criteria for SPECT myocardial perfusion imaging. *J Nucl Cardiol*. 2008; 15(3): 337–344, doi: [10.1016/j.nuclcard.2007.10.010](https://doi.org/10.1016/j.nuclcard.2007.10.010), indexed in Pubmed: [18513640](https://pubmed.ncbi.nlm.nih.gov/18513640/).
30. Amanullah A, Berman D, Hachamovitch R, et al. Identification of Severe or Extensive Coronary Artery Disease in Women by Adenosine Technetium-99m Sestamibi SPECT. *The American Journal of Cardiology*. 1997; 80(2): 132–137, doi: [10.1016/s0002-9149\(97\)00306-8](https://doi.org/10.1016/s0002-9149(97)00306-8).
31. Vogelzangs N, Seldenrijk A, Beekman ATF, et al. Cardiovascular disease in persons with depressive and anxiety disorders. *J Affect Disord*. 2010; 125(1-3): 241–248, doi: [10.1016/j.jad.2010.02.112](https://doi.org/10.1016/j.jad.2010.02.112), indexed in Pubmed: [20223521](https://pubmed.ncbi.nlm.nih.gov/20223521/).
32. Versteeg H, Hoogwegt MT, Hansen TB, et al. Depression, not anxiety, is independently associated with 5-year hospitalizations and mortality in patients with ischemic heart disease. *J Psychosom Res*. 2013; 75(6): 518–525, doi: [10.1016/j.jpsychores.2013.10.005](https://doi.org/10.1016/j.jpsychores.2013.10.005), indexed in Pubmed: [24290040](https://pubmed.ncbi.nlm.nih.gov/24290040/).
33. Valentini M, Spezzaferri R, Brambilla G, et al. [Complexity of observable psychological distress after surgical myocardial revascularization in male subjects]. *Ital Heart J Suppl*. 2005; 6(6): 375–381, indexed in Pubmed: [16013430](https://pubmed.ncbi.nlm.nih.gov/16013430/).
34. Westin L, Carlsson R, Erhardt L, et al. Differences in quality of life in men and women with ischemic heart disease. A prospective controlled study. *Scand Cardiovasc J*. 1999; 33(3): 160–165, doi: [10.1080/14017439950141795](https://doi.org/10.1080/14017439950141795), indexed in Pubmed: [10399804](https://pubmed.ncbi.nlm.nih.gov/10399804/).
35. Gerber MR, King MW, Iverson KM, et al. Association Between Mental Health Burden and Coronary Artery Disease in U.S. Women Veterans Over 45: A National Cross-Sectional Study. *J Womens Health (Larchmt)*. 2018; 27(3): 238–244, doi: [10.1089/jwh.2017.6328](https://doi.org/10.1089/jwh.2017.6328), indexed in Pubmed: [28981382](https://pubmed.ncbi.nlm.nih.gov/28981382/).
36. Stewart JC, Janicki DL, Muldoon MF, et al. Negative emotions and 3-year progression of subclinical atherosclerosis. *Arch Gen Psychiatry*. 2007; 64(2): 225–233, doi: [10.1001/archpsyc.64.2.225](https://doi.org/10.1001/archpsyc.64.2.225), indexed in Pubmed: [17283290](https://pubmed.ncbi.nlm.nih.gov/17283290/).
37. Tajfard M, Ghayour Mobarhan M, Rahimi HR, et al. Anxiety, depression, coronary artery disease and diabetes mellitus; an association study in ghaem hospital, iran. *Iran Red Crescent Med J*. 2014; 16(9): e14589, doi: [10.5812/ircmj.14589](https://doi.org/10.5812/ircmj.14589), indexed in Pubmed: [25593715](https://pubmed.ncbi.nlm.nih.gov/25593715/).
38. Vural M, Satiroğlu O, Akbaş B, et al. Association between depression and anxiety symptoms and major atherosclerosis risk factors in patients with chest pain. *Tohoku J Exp Med*. 2007; 212(2): 169–175, doi: [10.1620/tjem.212.169](https://doi.org/10.1620/tjem.212.169), indexed in Pubmed: [17548961](https://pubmed.ncbi.nlm.nih.gov/17548961/).

# Patterns of vascular graft infection in 18F-FDG PET/CT

Beata E. Chrapko , Marek Chrapko , Anna Nocuń , Tomasz Zubilewicz , Bogusław Stefaniak, Jakub Mitura, Andrzej Wolski , Piotr Terelecki 

Chair and Department of Nuclear Medicine, Medical University of Lublin, Lublin, Poland

[Received 3 V 2020; Accepted 22 V 2020]

## Abstract

**BACKGROUND:** 18F-FDG PET/CT has become an important tool in diagnosis of prosthetic vascular graft infections (PVGI). The aim of the study was to identify the patterns of vascular graft infection in 18F-FDG PET/CT.

**MATERIAL AND METHODS:** The study was performed in 24 patients with vascular graft infection, in 17 patients implanted in an open surgery mode and in 7 patients by endovascular aortic repair (EVAR). Vascular prostheses were evaluated by two visual scales and semi-quantitative analysis with maximum standardized uptake values (SUV max).

**RESULTS:** In the 3-point scale: 23 patients were in grade 1 and one patient was in grade 2. In the 5-point scale: 19 patients were in grade 5 with the highest activity in the focal area, 4 patients were in grade 4 and one patient in grade 3. The visual evaluation of 18F-FDG PET/CT study revealed that peri-graft high metabolic activity was associated with occurrence of morphological abnormalities ( $n = 21$ ) like gas bubbles and peri-graft fluid retention or without abnormal CT findings ( $n = 3$ ). The presence of the gas bubbles was linked to higher uptake of 18F-FDG ( $p < 0.01$ , SUVmax  $11.81 \pm 4.35$  vs  $7.36 \pm 2.80$ , 15 vs 9 pts). In EVAR procedure, the highest metabolic activity was greater than in classical prosthesis (SUVmax 21.5 vs 13).

**CONCLUSIONS:** 18F-FDG PET/CT is a very useful tool for assessment of vascular graft infections. CT findings like gas bubbles, or peri-graft fluid retention were associated with significantly higher glucose metabolism; however, in some cases without anatomic alterations, increased metabolic activity was the only sign of infection.

**KEY words:** fluorodeoxyglucose; PET/CT scan; vascular graft infections

Nucl Med Rev 2020; 23, 2: 63–70

## Introduction

The incidence of prosthetic vascular graft infections (PVGI) is ranging between 1 and 6%, depending on the location of the vascular graft — in intra-abdominal prostheses, the overall risk of infections is around 1%, but considerably increases to 6% when the graft is anastomosed to a femoral artery [1–3]. In 20–75% of cases PVGI may lead to the death, while in 50% it may result in morbidity such as loss of a limb [1, 4]. Regarding the onset of PVGI, there are early and late infections. The early PVGI starts at the time of surgery, when causative organisms infect the graft and may appear up to 4 months after surgery, whereas the more common type — the late one, occurs at least 4 months after the implantation of prosthesis. In the early infections the clinical manifestations of PVGI can be acute, whereas in the late one, may be more subtle. The clinical presentation of the PVGI also depends on the location

of the graft. In deeply fashioned grafts, pathology can be faint and difficult to diagnose. In cases of shallow grafts, for example in an extremity, the manifestations are often overt [4].

There are three groups of predisposing risk factor: patient-related, procedure-related and pathogen-related. The patient-related aspects, among others, include: obesity, diabetes, immunodeficiency, infection at the time of graft placement, and prolonged preoperative hospital stay [5, 6]. The procedure-related factors connected with surgery are: prolonged, emergency or “redo” vascular surgery, bowel injury, groin incision, wound infections, postoperative hematoma, seroma, pseudoaneurysm or wound-bed bleeding [5–7]. The causative pathogens are *Staphylococcus aureus* and *Pseudomonas aeruginosa* in 80% of cases, which produce a very strong biofilm, and when they adhere to the graft, infections can easily develop along the prosthesis and adjacent tissue. The pathogens also release destructive endotoxins, which can cause anastomotic dehiscence [6]. Synthetic vascular graft prostheses are made of either polyester (Dacron®) or polytetrafluoroethylene (PTFE), both of which are also used in endovascular and open mode surgery. The incidence of PVGI is comparable in both materials [7].

The right diagnosis of PVGI is crucial, but there is no clear consensus of diagnostics criteria. The imaging of PVGI is still

Correspondence to: Anna Nocuń  
 Chair and Department of Nuclear Medicine, Medical University of Lublin,  
 8c Jaczewskiego St, 20–954 Lublin, Poland  
 e-mail: ampolak@o2.pl

challenging, because false-positive tests may lead to unnecessary surgery, whereas false-negative are associated with under-treatment and in consequence with high morbidity [4]. Routine tests in PVGI include: clinical, biochemical, microbiological and imaging studies. Laboratory analysis in prosthesis infection commonly reveal elevated white blood cell (WBC) count, increased C-reactive protein (CRP) serum level and increased sedimentation rate. Microbiological assessment is based on skin, wound, blood or graft surrounding tissue culture. An ultrasound scan can easily detect peri-graft fluid. In contrast enhanced computed tomographic angiography (CECT), which is considered as the test of choice, the manifestation of infection is peri-graft ectopic gas, fluid and soft tissue enhancement and formation of the pseudoaneurysm. In advanced PVGI the detection rate in CECT is close 100%. Morphologic abnormalities are often nonspecific in vascular graft infection, therefore the use of metabolic study increases. The positron emission tomography/computed tomography (PET/CT) with use of 18F-fluoro-2-deoxy-D-glucose (18F-FDG) has become an important method of diagnosing inflammation and infection. In early and low-grade PVGI, the utility of 18F-FDG PET/CT is increased. There are different grades of focal pattern of 18F-FDG uptake.

In the recommendation of Management of Aortic Graft Infection Collaboration (MAGIC) there are three main categories of diagnosis of graft infection: clinical/surgical, radiological and laboratory [8]. Diagnostic criteria were ranked as either "major" or "minor" within each category. As it is recommended in MAGIC, Aortic Graft Infection (AGI) is suspected if one isolated major criterion or two of minor criteria from different categories are present. AGI is confirmed if there is one major plus any other criterion (major or minor) from another category. The major clinical/surgical criteria include presence of pus, open wound, fistula development, graft insertion in infected site. The laboratory major criteria are pathogens recovered from explanted graft or intra-operative or from percutaneous aspirate of peri-graft fluid. The serum levels of inflammatory markers like erythrocyte sedimentation rate (ESR), CRP or WBC belong to the minor criteria in laboratory categories in MAGIC. Major radiological criteria on CT scan are peri-graft fluid more than 3 months or peri-graft gas more than 7 week after prosthesis insertion or increased peri-graft gas in serial imaging. Increased metabolic activity on 18F-FDG PET/CT belongs to minor radiological criteria of infections. In our opinion however, there is much more potential value in non-invasive examination like 18F-FDG PET/CT. There are a number of questions and concerns regarding the diagnosis of vascular prosthesis infections by 18F-FDG PET/CT, but the most important issue is finding the pattern of infection.

The aim of the study was to identify the pattern of aortic vascular graft infection in patients with high probability of infective process by us of 18F-FDG PET/CT.

## Material and methods

### Patients

The study was performed in 24 consecutive patients who attended Department of Nuclear Medicine University Hospital in Lublin, between March 2013 and October 2018, with vascular graft infection. Clinical material consisted of 21 male and 3 female patients, mean age 65 (35–84) years. Strong clinical suspicion

**Table 1.** Description of the study material

Patient's details	n	Localization of prosthesis	
		Thoracic aortic graft	Abdominal aortic graft
All	24	4	20
Age	24	48.8 years	60.3 years
Male	21	4	17
Female	3	0	3
EVAR	7	1	6
Open mode	17	3	14
Coexistence of femoral-popliteal	4	0	4
Diabetes mellitus	3	0	3
Smoking	17	3	14

EVAR — endovascular aortic repair

of vascular graft infection was the start point of diagnosis. The definition of vascular prosthesis infection is graft colonization by pathological bacterial strains. According to mentioned above MAGIC criteria [8], the surgical manifestations were: fistula development, infected pseudoaneurysm, erythema, warmth, swelling purulent discharge and pain. Than the laboratory tests, bacterial culture and radiological signs of infection like: peri-graft air, persistent fluid or abscess was noticed in these patients. The main reason of vascular prosthesis implantation was aneurysm of the aorta (19 patients) and Leriche's syndrome (5 patients). In general, there were 4 patients with a thoracic aorta graft (TAG) and 20 patients with an abdominal aorta graft (AAG). In 7 patients endovascular aortic repair (EVAR) was performed: in one patient in the thoracic aorta and in 6 patients in the abdominal aorta. In 17 patients an open surgery mode was applied. In 4 patients the femoro-popliteal graft coexisted (in patients with classical abdominal prostheses). 18F-FDG PET/CT were performed from 12 months to 15 years after vascular graft implantation with the exception of one patient, when 18F-FDG PET/CT was performed 1 month after Bentall de Bono procedure, because of rapid progress of infection symptoms. There were 3 patients with diabetes mellitus in the group of stent-grafts patients. The blood serum inflammatory markers were: CRP mean 80.5 mg/L (range 9–300) and WBC mean 13.4 (range 7–38) K/mL. Baseline study population is presented in Table 1.

### 18F-FDG PET/CT imaging

Patients were prepared for the study with 24 hours of low carbohydrate diet, and fast for at least 6 hours prior to the examination. The interval between insulin and 18F-FDG administration was more than 6 hours. Blood glucose level was measured just before injection and the mean value was 104.7 mg/dL, range was 78–140 mg/dL. One hour before imaging, the subjects were injected with 3.5 MBq of 18F-FDG per kilogram of body weight, mean activity 241.5 MBq, range 198–334 MBq. During the uptake phase, patients were waiting in a quiet, dimly lit room. Patients were scanned in supine position, with arms overhead. 18F-FDG PET/CT scans were obtained from the vertex of skull to the mid-thigh level using 18F-FDG PET/CT system Biograph mCT S(64)-4R (Siemens, Erlangen, Germany).

PET data were collected in a three-dimensional mode, in the caudocranial direction with 2.5 minutes per bed position, and reconstructed with applied absorption and scatter correction. The reconstruction method was the following: True X+ time-of-flight (TOF) and ultra-high-resolution PET technology, 2 iterations, 21 subsets, Gaussian filter full width at half maximum 2.0 mm, image size 200 × 200 (matrix), zoom 1.0 and slice 3 mm. CT was performed prior to PET, without contrast enhancement, using the following parameters: voltage 120 kV, tube current 50, 150 or 200 mAs, pitch 0.8, and slice thickness 3 mm.

### Image analysis

All 18F-FDG PET/CT studies were independently assessed by a consensus of two experienced nuclear medicine physicians. Images were evaluated visually and semiquantitatively on a dedicated workstation equipped with fusion software (Syngo Via VA30A, Siemens, Erlangen, Germany), which displays PET, CT, and PET/CT fused images.

Vascular prostheses were evaluated visually, with two visual scales applied [9, 10]. The first one, a three-point scale, with 18F-FDG uptake patterns scored as follows: 1. focal dominant area of 18F-FDG uptake; 2. inhomogeneous or patched and 3. diffused or homogenous [9]. According to published recommendation, the first two were recognized as PVGI [9]. Second visual scale was also utilized. It was a 5-point scale described by Sah et al. [10] where 18F-FDG uptake patterns and CT information were taken into account. In this scale grade 1, 18F-FDG uptake in vascular graft was normal as in background activity; grade 2, mild increased but diffused along the graft; grade 3, focal, but mild uptake or strongly diffused; grade 4, focal and intense (and diffused 18F-FDG uptake along the graft); grade 5, focal and intense 18F-FDG uptake plus fluid collections or abscess formation [10]. According to this scale, "mild" increase of 18F-FDG uptake means less than twice the blood pool activity in the ascending aorta, whereas "strong" means more than twice the blood pool activity in the ascending aorta. Similarly as described by Sah et al., in this work, in score 1 and 2 images were considered as negative, whereas in score 3, 4 and 5 as positive for graft infection.

Metabolic activity assessed by 18F-FDG uptake in of the vascular graft was also evaluated by semi-quantitative analysis by use of maximum standardized uptake values (SUV max). The SUV max was calculated as the ratio of decay-corrected activity per cubic centimeter of tissue to the injected dosage divided by body weight.

For the semi-quantitative evaluation of the SUV max value, the region of interest (ROI) was placed in the focal area of the most intense 18F-FDG uptake. The background region, for background SUV max evaluation, was placed in the ascending aorta in case of abdominal prosthesis, and in abdominal aorta in case of thoracic one.

There was also visual assessment of non-contrast enhanced CT performed during the 18F-FDG PET/CT examination. The CT findings in the vascular graft location were: gas bubbles, peri-graft fluid retention, thickening of the graft wall, adjacent blurred fat, soft tissue swelling, fistula and pseudoaneurysms.

In the final diagnosis of PVGI the MAGIC criteria of clinical, radiological and laboratory tests were taken into account.

### Statistical analysis

All calculations were expressed as mean ± standard deviation (SD), as well as minimal and maximal values. Differences between study groups were assessed with the U-Mann-Whitney test; p value < 0.05 was considered to indicate statistical significance. Data were evaluated using the statistical package Statistica, version 7.

### Ethics

The study was approved by the Bioethical Council, Medical University of Lublin, Poland. Informed consent was obtained from all participants. No side effects were observed after the radionuclide procedure.

### Results

The analysis of vascular prostheses according to the both applied visual scales [9, 10] provided very similar results. In the 3-point scale: 23 patients were in grade 1 and one patient was in grade 2. In the 5-point scale: 19 patients were in grade 5 with the highest activity in the focal area, 4 patients were in grade 4 and one patient in grade 3. The first two points in 3-point scale and 3 last points in 5-point scale were recognized as PVGI.

The visual assessment revealed that peri-graft high metabolic, focal activity was associated with occurrence of gas bubbles, peri-graft fluid retention, thickening of the graft wall, adjacent blurred fat, soft tissue swelling, fistula and pseudoaneurysm (Fig. 1). In 3 cases (12.5%) increased focal 18F-FDG uptake in the infected grafts was found without morphological abnormalities (Fig. 2). The peri-graft fluid retention was observed in 16 patients, peri-graft gas in 15 patients, thickening around the graft wall, adjacent blurred fat and soft tissue swelling in 16 patients, fistula in 13 patients, pseudoaneurysm in 15 patients and metabolically active lymph nodes in the area of PVGI in 10 patients. The triad of CT sign as pseudoaneurysms, soft tissue swelling and peri-graft fluid deposition were seen in 15 patients.

The synthetic vascular graft prostheses were made of either polyester or PTFE, which are both used in endovascular and in open mode surgery. The highest metabolic activity, which was seen in the area of infection, was expressed by SUV max. In infected stent-grafts the metabolic activity came to SUV max 21.5, whereas in infected classical prosthesis was lower and came to SUV max 13. Only in one patient stent-graft was inserted in the thoracic aorta, and in 6 patients in the abdominal aorta. So because of the overall highest metabolic activity in the stent-graft generally, higher SUV max were observed in the abdominal prosthesis than in the thoracic one (21.5 vs. 12.5). The metabolic activities expressed by SUVs in the infection area are presented in Table 2.

There were statistically significant differences ( $p < 0.01$ ) between mean SUV max in the infected area of stent-grafts compared to classical prostheses (SUV max  $14.4 \pm 5.1$  vs  $8.39 \pm 2.56$ ; 7 vs 17 pts). This difference was less distinctive after background correction ( $p < 0.02$ ; SUV max  $7.38 \pm 4.07$  vs  $3.94 \pm 1.31$ ) (Tab. 3). The adjacent blurred fat and soft tissue swelling were combined with higher glucose metabolism compared to prostheses without these signs on CT scans ( $p < 0.005$ , SUV max  $11.79 \pm 4.08$  vs  $6.84 \pm 2.90$ , 16 vs 8 pts), with similar p value after background

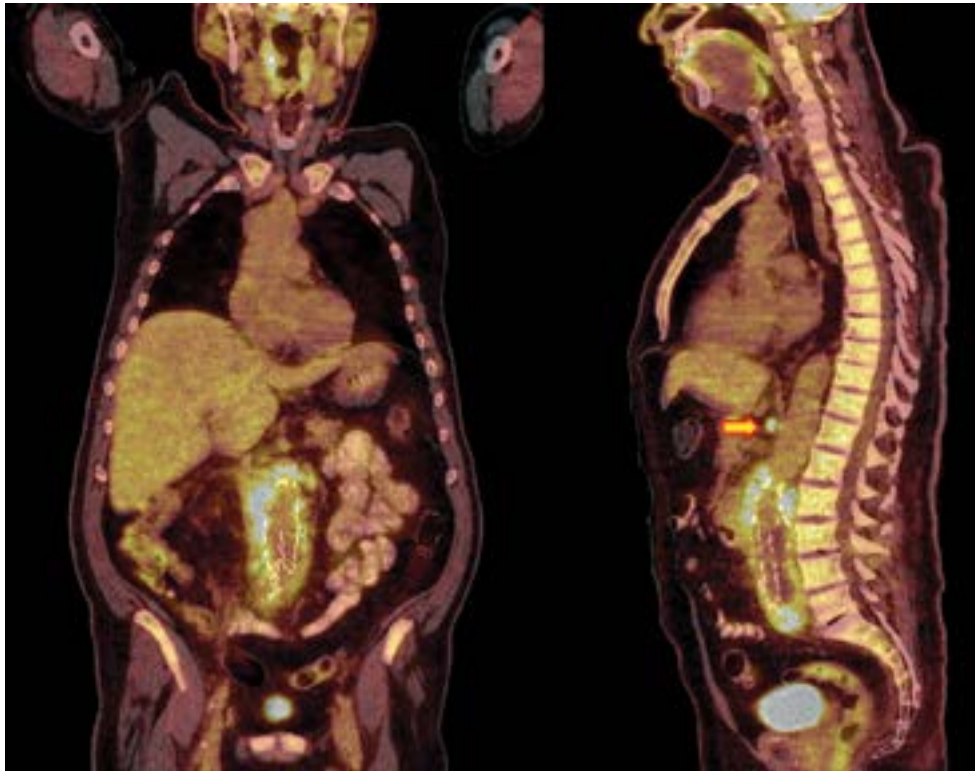


**Figure 1.** Increased 18F-FDG uptake associated with irregular peri-graft soft tissue swelling and fluid retention around infected aortic stentgraft, demonstrated on coronal and sagittal projections of 18F-FDG PET/CT. Infection in the paraaortic lymph node with high radiopharmaceutical activity (arrow)

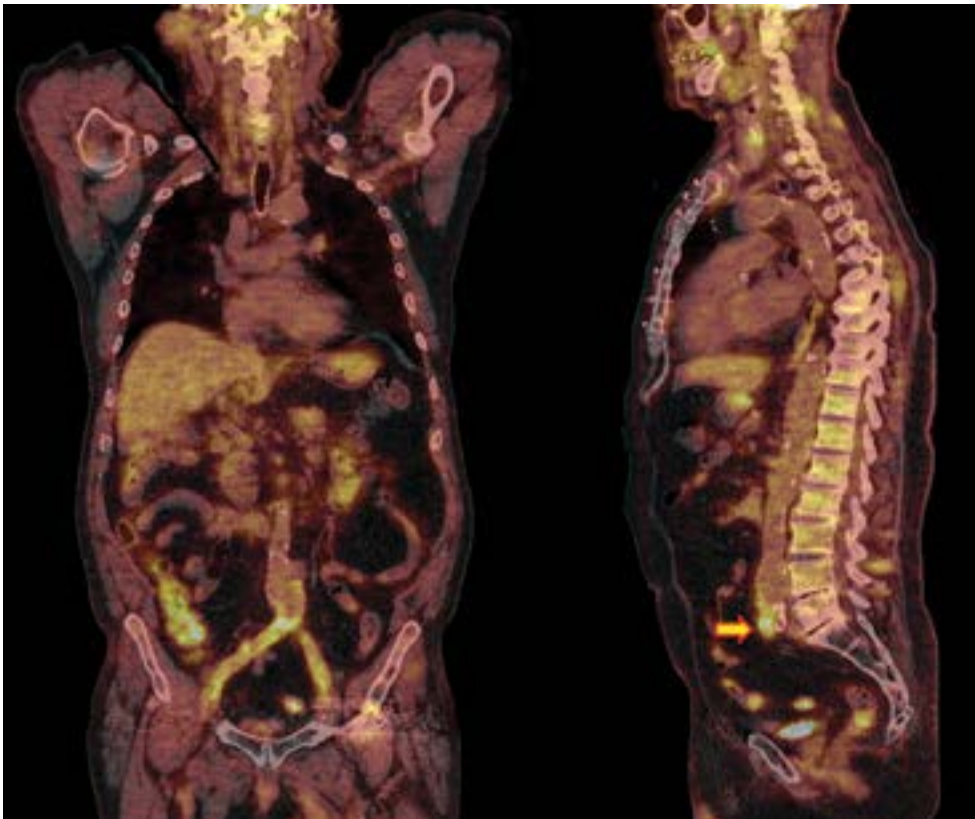


**Figure 2.** Focal 18F-FDG uptake (arrow) in infected classical prosthesis displayed on coronal and sagittal projections of 18F-FDG PET/CT

**Table 2.** SUV max in the area of suspected of infection

Prosthesis	n	SUV max in area suspected of infection		
		median	MAX	MIN
All	24	9.0	21.5	4.2
EVAR	7	8.3	13.0	4.2
Open mode	17	14.4	21.5	4.8
Abdominal	20	9.3	12.5	4.8
Thoracic	4	10.2	21.5	4.2

EVAR — endovascular aortic repair

correction ( $5.83 \pm 3.12$  vs  $3.22 \pm 1.39$ ). The presence of the gas bubbles in adjacent tissue of prosthesis was linked to high uptake of 18F-FDG ( $p < 0.01$ , SUV max  $11.81 \pm 4.35$  vs  $7.36 \pm 2.80$ , 15 vs 9 pts) as well as the peri-graft fluid retention, thickening of the peri-graft wall ( $p < 0.05$ , SUV max  $5.61 \pm 3.21$  vs  $3.62 \pm 1.68$ , 16 vs. 8 pts). Findings are presented in Table 4. Table 5 contains correlation between visual grading scales and CT findings.

Microbiological findings were based on vascular graft, blood, wound, skin and fistula bacterial cultures. The culture were positive from prosthesis (*Proteus mirabilis*, *Staphylococcus aureus*, *Enterococcus faecalis*, *Clostridium difficile*), from fistula (*Proteus mirabilis*, *Staphylococcus aureus*, *Klebsiella pneumonia*, *Escherichia coli*),

from blood (*Escherichia coli*, *Enterobacter cloacae*, *Streptococcus zoepidermicus*), in one patient *Candida albicans* were detected in urine. Some cultures were not conclusive (physiological skin culture or no bacterial growth). But in all patients, further clinical observation confirmed infections of PVG.

In the follow-up of the studied group, 3 patients died in the course of infection: one patient with stent-graft of the ascending aorta in course of an esophageal fistula and two patients with aorto-bi-iliac stent-grafts. There was one patient who lost a lower limb. In 4 patients surgical treatment of infected vascular graft was not performed because of general bad condition and instability of the patients. In those patients antibiotic therapy was continued. In the rest of our patients surgical replacement of prosthesis was performed.

## Discussion

Removal of the infected prosthesis, and replacement with another device to revascularization by anatomical or uninfected extra-anatomical route is an essential vascular graft infection treatment, beyond antibiotic therapy [11]. There is 18–30% mortality rate after surgical explantation of infected aortic prosthesis whereas leaving the prosthesis at the site of infection, despite prolonged antimicrobial treatment, results in 100% mortality over the course of 2 years [10, 12, 13]. The distinction

**Table 3.** Statistically significant differences between SUVs in the stent-grafts compared to classical prostheses

SUVmax	Type of prosthesis	Mean (SD)	p
Without background correction	Stent-grafts	14.40 (SD = 5.01) n = 7 pts	p < 0.01
	classical prostheses	8.39 (SD = 2.64) n = 17 pts	
With background correction	Stent-grafts	7.38 (SD = 4.07) n = 7 pts	p < 0.02
	classical prostheses	3.94 (SD = 1.30) n = 17 pts	

**Table 4.** Statistically significant differences between SUVs in the prosthesis with and without anatomic alterations on CT scans

SUVmax	CT finding	Mean (SD)	p
Without background correction	Gas bubbles	yes 11.81 (SD = 4.35) n = 15 pts	p < 0.01
		no 7.36 (SD = 2.80) n = 9 pts	
With background correction	Gas bubbles	yes 5.76 (SD = 3.23) n = 15 pts	p < 0.01
		no 3.58 (SD = 1.24) n = 9 pts	
With background correction	Peri-graft fluid retention	yes 5.61 (SD = 3.21) n = 16 pts	p < 0.05
		no 3.62 (SD = 1.68) n = 8 pts	
Without background correction	Soft tissue swelling	yes 11.79 (SD = 4.08) n = 16 pts	p < 0.005
		no 6.84 (SD = 2.90) n = 8 pts	
With background correction	Soft tissue swelling	yes 5.80 (SD = 3.02) n = 16 pts	p < 0.005
		no 3.23 (SD = 1.39) n = 8 pts	

**Table 5.** Correlation between CT findings and visual grading scales

*	**	n	Gas bubbles	Thrombus	Fluid	Infiltration	Fistula	Pseudo-aneurysm	Active lymph nodes
3-point scale	5-point scale								
2	3	1	0	0	0	0	0	1	0
1	4	4	0	2	1	1	2	4	2
	5	19	15	9	15	15	11	10	8

\*Three-point scale 1) focal (one dominant area of uptake), 2) inhomogeneous or patched uptake, and 3) diffuse or homogenous uptake; \*\*Five-point scale 1), normal background activity; 2), mildly increased, but diffuse FDG uptake along the graft (mild uptake: less than twice the blood pool activity in the ascending aorta; strong uptake: more than twice the blood pool activity in the ascending aorta); 3), focal, but only mild FDG uptake or strong diffuse FDG uptake along the graft; 4), focal and intense FDG uptake ( $\pm$  diffuse FDG uptake along the graft); 5), focal and intense FDG uptake plus fluid collections/abscess formation

between infection and inflammation in reference to vascular prosthesis is very challenging, but absolutely crucial for the proper treatment. There are many various diagnostic schemes which include clinical, biochemical, microbiological and imaging procedures [12]. As in the MAGIC recommendation, the clinical criteria of PVGI were the start point of diagnosis [8]. There were major criteria like fistula development and infected pseudoaneurysm as well as minor criteria like erythema, warmth, swelling purulent discharge and pain. They occurred in all patients in various degrees. The serum levels of CRP and WBC belonging to the minor criteria in laboratory categories in MAGIC were increased in the studied patients. The golden standard in the diagnosis of PVGI is confirmation of bacterial colonization of prosthesis. In MAGIC criteria organisms recovered from explanted graft or recovered from intra-operative or radiologically guided aspiration of peri-graft belong to the major criteria of infections. Positive blood culture with no apparent source of infection except of AGI, are the minor criteria of infections [8]. *Staphylococcus* species are the most common causative organisms, *Staphylococcus aureus* are more likely in early infection and *Staphylococcus epidermidis* in late infections [13]. However, many suspected PVGI are treated without knowing the causative organisms, because as described by FitzGerald et al. suitable specimens could not be obtained or antibiotic treatment was applied before collection of samples [13]. Some authors stress that even if the specimens are taken from blood or from the suspicious location, there could be negative bacterial culture in active vascular prosthesis infections [14]. On the other hand, same pathogens isolated from superficial specimens may be misleading, but influence the choice of antimicrobial agents [13]. For this reason, antimicrobial treatment is empirical and based on clinical manifestations and findings, as well as on radiological/nuclear medical imaging.

Contrast-enhanced computed tomography has close to 100% sensitivity and specificity in diagnosis of acute PVGI, whereas in chronic PVGI up to 55% [15]. Presentation of periprosthetic air bubbles, abscesses or infiltration suggests vascular graft infections in CT. Nevertheless, it should be kept in mind that one week after vascular prosthesis implantation, air bubbles are present around the vascular prosthesis in 65% of patients [16]. Moreover, in 100% of patients periprosthetic hematoma is present in CT one week after surgery and in 10% of patients at 100 days post-surgery [17]. However, in all patients presenting air bubbles, periprosthetic infiltration or fluid collections 3 months post-surgery, the possibility of a vascular graft infection should be taken into account [13].

In nuclear medicine procedures there are two main techniques, SPECT and PET, and several radiopharmaceuticals like Gallium 67-citrate, radiolabeled white blood cells, antigranulocyte antibody. In the PET technique there is the main radiotracer 18F-FDG. According to the EANM/SNMMI guidelines [18], the advantage of use of 18F-FDG PET/CT over radiolabeled WBC scintigraphy in detection of infection in vascular prosthesis is unclear. However, the usage of 18F-FDG PET/CT is less time-consuming and much easier to perform compared to radiolabeled WBC scintigraphy. The reported sensitivity, specificity and accuracy of scintigraphy with radiolabeled WBC in PVGI is 100%, 92%, 97% respectively [19], whereas the latest study of 18F-FDG PET/CT presents sensitivity, specificity, positive and negative predictive value 88%, 79%, 67%, and 93% respectively [9].

18F-FDG PET/CT provides information regarding not only of the *anatomy* but also the *metabolism* of lesions. Three cases (12.5%) in the studied population presented increased 18F-FDG uptake in the infected grafts without morphological abnormalities on CT scans. In some patients 18F-FDG PET/CT also revealed extra-prosthetic infection in the lymph nodes. Therefore, an additional value of PET/CT over CT alone was documented in this study. Recently the combination of PET/CT with contrast enhanced CT is postulated in diagnosing PVGI as it was proved to be more accurate than stand-alone imaging and may be supportive in future management of difficult cases [20].

In the studied patients there were two types of vascular graft prosthesis: stent-grafts (EVAR procedure) and classic prostheses. All prostheses were made of either polyester or [7], which are both use in endovascular and open surgery. Synthetic vascular grafts provoke a chronic low-grade inflammation, therefore could be a cause of a false positive diagnosis [21]. Our material revealed higher metabolic activity in stent-grafts than classical prosthesis, but further studies are needed because of potentially higher artifacts from metallic elements contained in the stent-grafts. On the other hand, the number of patients in both groups was not very high.

Testing a short time after implantation could be a source of a false positive finding [22]. The mean time between the surgery and 18F-FDG PET/CT in the studied group of patients was 51 months, but in one patient imaging was performed 1 month after Bentall de Bono procedure, because of rapid progress of infection symptoms. This patient died over the course of the infection. However, generally in cases of very early assessment of vascular prosthesis, the diagnosis should be made very carefully. In the early period after implantation there are post-surgical inflammatory changes in the area of implantation, with physiological activation of leukocytes. Peri-graft fluid and peri-graft gas observed in CT integrated with PET meet the major criteria of aortic graft infection enclosed in MAGIC criteria [8]. They depend on the time after surgery, so persistent peri-graft fluid after more than 3 months and peri-graft gas after more than 7 weeks after insertion, suggest PVGI. In our analysis, except one patient, the time criteria have been met. In this study peri-graft fluid was observed in 16 and peri-graft gas in 15 patients. Presence of pseudoaneurysm and fistula are the minor criteria of MAGIC and in our study were observed in 15 and in 13 patients respectively.

Pattern of 18F-FDG uptake in patients with suspicion of vascular graft infection is very important. Focal or heterogeneous accumulation is highly suggestive of infection whereas moderate, homogeneous, linear uptake in the graft and/or surrounding tissue is often recognized as non-infectious [22, 23]. However, some authors underline that patterns of FDG uptake for uninfected grafts largely overlap with those of infected vascular graft [24]. In these cases it is very important to recognize all the additional signs of potential infection. Concerning the 18F-FDG uptake and distribution patterns, reported sensitivity, specificity, positive predictive value and negative predictive value in PVGI are 93%, 91%, 88%, 96% respectively [25]. In this study of analysis of 18F-FDG uptake in prosthesis and in the surrounding tissues two visual scales were applied [9, 10]. Both of them presented very similar results, FDG uptake was focal (mild to intense) in all patients. 18F-FDG PET/CT as hybrid study additionally revealed in our patients signs of infections in CT, like: gas bubbles, peri-graft fluid retention, thickening of

the graft wall, adjacent blurred fat, soft tissue swelling, fistula and pseudoaneurysm. All the patients in the study were positive in reference to infection. Moreover, in MAGIC criteria increased peri-graft 18F-FDG activity fulfills the minor criteria of aortic graft infection [8].

On the other hand, based only on assessment of 18F-FDG uptake it is very difficult to differentiate a quite rare condition like retroperitoneal fibrosis (RPF), which could be also secondary to vascular graft implantation from a simple inflammatory reaction to a foreign body or the early phase of an infection. In all these conditions there is increased 18F-FDG uptake and serum level of inflammatory markers, as well as clinical symptoms like fever and pain. In RPF treatment is based on glucocorticosteroids application, in inflammation as foreign body reaction – watchful waiting is much advisable, whereas in the last case redo surgery is usually performed. Therefore, it should be kept in mind, that diagnosis of PVGI should be based on multidisciplinary consensus [26].

## Conclusions

18F-FDG PET/CT is a very useful, non-invasive tool for assessment of vascular graft infections. It should be interpreted with caution in multidisciplinary team. CT findings like gas bubbles, peri-graft fluid retention, thickening of the graft wall and adjacent blurred fat soft tissue swelling are associated with significantly higher glucose metabolism: however, in some cases without anatomic alterations, increased metabolic activity is the only sign of infection. A useful marker of infected graft is focal not homogeneous pattern of 18F-FDG uptake found in all examined cases.

## Conflict of interest

The authors declare that they do not have any conflict of interest.

## References

- Legout L, D'Elia PV, Sarraz-Bournet B, et al. Vascular graft infections. *Curr Opin Infect Dis*. 2012; 25(2): 154–158, doi: [10.1097/QCO.0b013e3283501853](https://doi.org/10.1097/QCO.0b013e3283501853), indexed in Pubmed: [22248976](https://pubmed.ncbi.nlm.nih.gov/22248976/).
- Setacci C, Müller-Hülsbeck S, Jamar FX. Common diagnostic flowcharts in vascular and endovascular surgery. *Q J Nucl Med Mol Imaging*. 2014; 58(1): 46–54, indexed in Pubmed: [24231796](https://pubmed.ncbi.nlm.nih.gov/24231796/).
- Baddour LM, Bettmann MA, Bolger AF, et al. AHA. Nonvalvular cardiovascular device-related infections. *Circulation*. 2003; 108(16): 2015–2031, doi: [10.1161/01.CIR.0000093201.57771.47](https://doi.org/10.1161/01.CIR.0000093201.57771.47), indexed in Pubmed: [14568887](https://pubmed.ncbi.nlm.nih.gov/14568887/).
- Keidar Z, Nitecki S. FDG-PET in prosthetic graft infections. *Semin Nucl Med*. 2013; 43(5): 396–402, doi: [10.1053/j.semnuclmed.2013.04.004](https://doi.org/10.1053/j.semnuclmed.2013.04.004), indexed in Pubmed: [23905620](https://pubmed.ncbi.nlm.nih.gov/23905620/).
- Antonios VS, Noel AA, Steckelberg JM, et al. Prosthetic vascular graft infection: a risk factor analysis using a case-control study. *J Infect*. 2006; 53(1): 49–55, doi: [10.1016/j.jinf.2005.10.004](https://doi.org/10.1016/j.jinf.2005.10.004), indexed in Pubmed: [16310254](https://pubmed.ncbi.nlm.nih.gov/16310254/).
- Hasse B, Husmann L, Zinkernagel A, et al. Vascular graft infections. *Swiss Med Wkly*. 2013; 143: w13754, doi: [10.4414/smw.2013.13754](https://doi.org/10.4414/smw.2013.13754), indexed in Pubmed: [23348860](https://pubmed.ncbi.nlm.nih.gov/23348860/).
- Swain TW, Calligaro KD, Dougherty MD. Management of infected aortic prosthetic grafts. *Vasc Endovascular Surg*. 2004; 38(1): 75–82, doi: [10.1177/153857440403800110](https://doi.org/10.1177/153857440403800110), indexed in Pubmed: [14760481](https://pubmed.ncbi.nlm.nih.gov/14760481/).
- Lyons OTA, Baguneid M, Barwick TD, et al. Diagnosis of Aortic Graft Infection: A Case Definition by the Management of Aortic Graft Infection Collaboration (MAGIC). *Eur J Vasc Endovasc Surg*. 2016; 52(6): 758–763, doi: [10.1016/j.ejvs.2016.09.007](https://doi.org/10.1016/j.ejvs.2016.09.007), indexed in Pubmed: [27771318](https://pubmed.ncbi.nlm.nih.gov/27771318/).
- Bowles H, Ambrosioni J, Mestres G, et al. Diagnostic yield of 18F-FDG PET/CT in suspected diagnosis of vascular graft infection: A prospective cohort study. *J Nucl Cardiol*. 2018; 27(1): 294–302, doi: [10.1007/s12350-018-1337-1](https://doi.org/10.1007/s12350-018-1337-1).
- Sah BR, Husmann L, Mayer D, et al. VASGRA Cohort. Diagnostic performance of 18F-FDG-PET/CT in vascular graft infections. *Eur J Vasc Endovasc Surg*. 2015; 49(4): 455–464, doi: [10.1016/j.ejvs.2014.12.024](https://doi.org/10.1016/j.ejvs.2014.12.024), indexed in Pubmed: [25648371](https://pubmed.ncbi.nlm.nih.gov/25648371/).
- Lyons OTA, Patel AS, Saha P, et al. A 14-year experience with aortic endograft infection: management and results. *Eur J Vasc Endovasc Surg*. 2013; 46(3): 306–313, doi: [10.1016/j.ejvs.2013.04.021](https://doi.org/10.1016/j.ejvs.2013.04.021), indexed in Pubmed: [23702108](https://pubmed.ncbi.nlm.nih.gov/23702108/).
- Li HL, Chan YC, Cheng SW. Current Evidence on Management of Aortic Stent-graft Infection: A Systematic Review and Meta-Analysis. *Ann Vasc Surg*. 2018; 51: 306–313, doi: [10.1016/j.avsg.2018.02.038](https://doi.org/10.1016/j.avsg.2018.02.038), indexed in Pubmed: [29772328](https://pubmed.ncbi.nlm.nih.gov/29772328/).
- FitzGerald SF, Kelly C, Humphreys H. Diagnosis and treatment of prosthetic aortic graft infections: confusion and inconsistency in the absence of evidence or consensus. *J Antimicrob Chemother*. 2005; 56(6): 996–999, doi: [10.1093/jac/dki382](https://doi.org/10.1093/jac/dki382), indexed in Pubmed: [16269550](https://pubmed.ncbi.nlm.nih.gov/16269550/).
- McWilliams ET, Yavari A, Raman V. Aortic root abscess: multimodality imaging with computed tomography and gallium-67 citrate single-photon emission computed tomography/computed tomography hybrid imaging. *J Cardiovasc Comput Tomogr*. 2011; 5(2): 122–124, doi: [10.1016/j.jcct.2010.10.004](https://doi.org/10.1016/j.jcct.2010.10.004), indexed in Pubmed: [21130063](https://pubmed.ncbi.nlm.nih.gov/21130063/).
- Legout L, D'Elia PV, Sarraz-Bournet B, et al. Diagnosis and management of prosthetic vascular graft infections. *Med Mal Infect*. 2012; 42(3): 102–109, doi: [10.1016/j.medmal.2012.01.003](https://doi.org/10.1016/j.medmal.2012.01.003), indexed in Pubmed: [22341664](https://pubmed.ncbi.nlm.nih.gov/22341664/).
- O'Hara PJ, Borkowski GP, Hertzner NR, et al. Natural history of periprosthetic air on computerized axial tomographic examination of the abdomen following abdominal aortic aneurysm repair. *J Vasc Surg*. 1984; 1(3): 429–433, doi: [10.1067/mva.1984.av0010429](https://doi.org/10.1067/mva.1984.av0010429), indexed in Pubmed: [6481893](https://pubmed.ncbi.nlm.nih.gov/6481893/).
- Qvarfordt PG, Reilly LM, Mark AS, et al. Computerized tomographic assessment of graft incorporation after aortic reconstruction. *Am J Surg*. 1985; 150(2): 227–231, doi: [10.1016/0002-9610\(85\)90125-4](https://doi.org/10.1016/0002-9610(85)90125-4), indexed in Pubmed: [3161350](https://pubmed.ncbi.nlm.nih.gov/3161350/).
- Jamar F, Buscombe J, Chiti A, et al. EANM/SNMMI guideline for 18F-FDG use in inflammation and infection. *J Nucl Med*. 2013; 54(4): 647–658, doi: [10.2967/jnumed.112.112524](https://doi.org/10.2967/jnumed.112.112524), indexed in Pubmed: [23359660](https://pubmed.ncbi.nlm.nih.gov/23359660/).
- Liberatore M, Iurilli AP, Ponzo F, et al. Clinical usefulness of technetium-99m-HMPAO-labeled leukocyte scan in prosthetic vascular graft infection. *J Nucl Med*. 1998; 39(5): 875–879, indexed in Pubmed: [9591592](https://pubmed.ncbi.nlm.nih.gov/9591592/).
- Husmann L, Huellner MW, Ledergerber B, et al. and the Vasgra Cohort. Comparing diagnostic accuracy of F-FDG-PET/CT, contrast enhanced CT and combined imaging in patients with suspected vascular graft infections. *Eur J Nucl Med Mol Imaging*. 2019; 46(6): 1359–1368, doi: [10.1007/s00259-018-4205-y](https://doi.org/10.1007/s00259-018-4205-y), indexed in Pubmed: [30426151](https://pubmed.ncbi.nlm.nih.gov/30426151/).
- Wassélius J, Malmstedt J, Kalin Bo, et al. High 18F-FDG Uptake in synthetic aortic vascular grafts on PET/CT in symptomatic and asymptomatic patients. *J Nucl Med*. 2008; 49(10): 1601–1605, doi: [10.2967/jnumed.108.053462](https://doi.org/10.2967/jnumed.108.053462), indexed in Pubmed: [18794261](https://pubmed.ncbi.nlm.nih.gov/18794261/).
- Kara PÖ, Gedik GK, Kara T, et al. FDG Uptake Pattern on PET/CT Imaging in Non-Infectious Graft of a Patient with Operated Abdominal Aortic Aneurysm. *Mol Imaging Radionucl Ther*. 2012; 21(3): 110–113, doi: [10.4274/Mirt.98](https://doi.org/10.4274/Mirt.98), indexed in Pubmed: [23486376](https://pubmed.ncbi.nlm.nih.gov/23486376/).
- Granados U, Fuster D, Pericas JM, et al. Hospital Clinic Endocarditis Study Group. Diagnostic Accuracy of 18F-FDG PET/CT in Infective Endocarditis and Implantable Cardiac Electronic Device Infection: A Cross-Sectional Study. *J Nucl Med*. 2016; 57(11): 1726–1732, doi: [10.2967/jnumed.116.173690](https://doi.org/10.2967/jnumed.116.173690), indexed in Pubmed: [27261514](https://pubmed.ncbi.nlm.nih.gov/27261514/).
- Berger P, Vaartjes I, Scholtens A, et al. Differential FDG-PET Uptake Patterns in Uninfected and Infected Central Prosthetic Vascular Grafts. *Eur J Vasc*

- Endovasc Surg. 2015; 50(3): 376–383, doi: [10.1016/j.ejvs.2015.06.007](https://doi.org/10.1016/j.ejvs.2015.06.007), indexed in Pubmed: [26164091](https://pubmed.ncbi.nlm.nih.gov/26164091/).
25. Keidar Z, Engel A, Hoffman A, et al. Prosthetic vascular graft infection: the role of 18F-FDG PET/CT. J Nucl Med. 2007; 48(8): 1230–1236, doi: [10.2967/jnumed.107.040253](https://doi.org/10.2967/jnumed.107.040253), indexed in Pubmed: [17631553](https://pubmed.ncbi.nlm.nih.gov/17631553/).
26. Kim SJ, Lee SW, Jeong S, et al. A systematic review and meta-analysis of 18F-fluorodeoxyglucose positron emission tomography or positron emission tomography/computed tomography for detection of infected prosthetic vascular grafts. J Vasc Surg Venous Lymphat Disord. 2019; 70(1): 307–313, doi: [10.1016/j.jvs.2019.01.051](https://doi.org/10.1016/j.jvs.2019.01.051).

# The diagnostic value of dual-phase SPECT/CT scintigraphy based on transport kinetics of <sup>99m</sup>Tc-sestamibi confirmed with histopathological findings in patients with secondary hyperparathyroidism — practical consideration

Maria H. Listewnik<sup>1</sup> , Hanna Piwowarska-Bilska<sup>1</sup> , Krzysztof Safranow<sup>2</sup> , Marek Ostrowski<sup>3</sup> ,  
 Jacek Iwanowski<sup>1</sup> , Maria Chosia<sup>4</sup> , Bożena Birkenfeld<sup>1</sup> 

<sup>1</sup>Department of Nuclear Medicine, Pomeranian Medical University in Szczecin, Poland

<sup>2</sup>Department of Biochemistry and Medical Chemistry, Pomeranian Medical University in Szczecin, Poland

<sup>3</sup>Department of General Surgery and Transplantology, Pomeranian Medical University in Szczecin, Poland

<sup>4</sup>Department of Pathology, Pomeranian Medical University in Szczecin, Poland

[Received 27 III 2020; Accepted 18 VI 2020]

## Abstract

**BACKGROUND:** Dual phase <sup>99m</sup>Tc-sestamibi SPECT/CT preoperative parathyroid scintigraphy (PPS) is seldom discussed in terms of the transport kinetics of the tracer.

**Objectives:** To assess the relationship between the characteristic type of tracer transport in particular PPS and histopathological findings in patients with secondary hyperparathyroidism (sHPT).

**MATERIAL AND METHODS:** The study comprised 27 patients (13 females and 14 males) with sHPT. Based on tracer accumulation in early phase (EP) and delayed phase (DP), the following types of accumulation for PPS(+) lesions were identified: EP(-)/DP(+) (type I), EP(+)/DP(+) (type II), EP(+)/DP(-) (type III). EP(-)/DP(-) (type IV) lesions constituted PPS(-) group invisible in SPECT/CT. Overall, 69 lesions 59 PPS(+) and 10 PPS(-) were evaluated histopathologically.

**RESULTS:** Among SPECT/CT PPS(+), types I, II and III occurred in 9 (15%), 49 (83%), and 1 (2%) lesions, respectively. The frequency of histopathological diagnosis of normal and abnormal (APG — adenoma or hyperplasia) parathyroid gland, as well as non-parathyroid (thyroid, lymph nodes, or fat) lesions differed significantly between type I, II, and III lesions ( $p = 0.036$ ). APG histopathological diagnosis was significantly more frequent in lesions with type II uptake than in lesions with type I uptake (76% vs. 33%,  $p = 0.0197$ ). Type II lesions had significantly higher odds for histopathological diagnosis of APG or NPG than type IV, PPS(-) lesions [odds ratio = 13.1 (95% CI: 2.75 to 63.27)].

**CONCLUSIONS:** For SHP patients evaluated with SPECT/CT PPS accumulation type I is a weak premise for surgeon to find parathyroid pathology. Only persistent <sup>99m</sup>Tc-sestamibi accumulation in both phases - equivocal with accumulation type II — effectively differentiates parathyroid and non-parathyroid lesions as well as indicates with high probability the presence of adenoma or hyperplasia. Type III consistent with washout pattern is rare in sHPT.

**KEY words:** secondary hyperparathyroidism; single photon emission computed tomography; technetium-99m sestamibi; parathyroid hormone; parathyroid adenoma; hyperplasia

Nucl Med Rev 2020; 23, 2: 71–77

Correspondence to: Maria H. Listewnik  
 Department of Nuclear Medicine, Pomeranian Medical University in  
 Szczecin, Unii Lubelskiej 1, 71–252 Szczecin, Poland  
 e-mail: marlist@fiber.net.pl

## Introduction

Secondary hyperparathyroidism (sHPT) is usually caused by chronic kidney disease in response to hypocalcaemia, which leads to diffused or nodular hyperplasia of the parathyroid glands. Even after successful renal replacement therapy, this condition can be difficult to control using conservative treatments, and hence require parathyroid surgery [1–3]. If surgical intervention is not performed in the optimal time, some patients can develop autonomic adenoma with a constant elevation of PTH [4, 5]. Among various preoperative imaging techniques, single-photon emission computed tomography (SPECT) is an accurate method used for the localization of abnormal parathyroid gland method. Recently, new hybrid imaging using SPECT in combination with computed tomography (CT) has improved precision in the morphological and metabolic assessment of focal lesions [6].

<sup>99m</sup>Tc-methoxyisobutylisonitrile (<sup>99m</sup>Tc-sestamibi) SPECT/CT preoperative parathyroid scintigraphy (PPS) can be performed as dual-phase single-tracer scintigraphy (washout method). There are two patterns of washout from the parathyroid glands: delayed (parathyroid gland retention of radiopharmaceutical on delayed images, usually accompanied by normal washout from the thyroid) and early (minimal or no retention of the radiotracer in the parathyroid gland on delayed-phase images). It was shown that the metabolic activity of the thyroid tissue diminishes with time while in the parathyroid tissue is more protracted; hence, early phase (EP) in SPECT/CT refers to the thyroid washout and the delayed phase (DP) to the parathyroid washout [7, 8]. Accumulation of <sup>99m</sup>Tc-sestamibi may be visible either in one phase only or both phases, thus leading to three different types of trace patterns [9].

The purpose of this study was to evaluate the relationship between the transport kinetics of <sup>99m</sup>Tc-sestamibi in SPECT/CT PPS and histopathological findings in patients with sHPT who underwent parathyroid surgery.

## Material and methods

We included 78 patients with sHPT (30 females, 48 males; mean age of 49.9 years, range: 22–86 years). Patients were examined with planar and SPECT/CT PPS (GE INFINIA Hawkeye 4 with a low-energy high-resolution collimator and 2.0 zoom) following intravenous administration of <sup>99m</sup>Tc-sestamibi  $762 \pm 60.7$  MBq (range: 600–850) with washout technique (dual-phase, single-tracer), in accordance with EANM guidelines [8]. The SPECT/CT study in EP was started following thorax planar acquisition (but not later than 20 min after administration of the tracer), and DP was performed  $127 \pm 28$  min after tracer administration.

Pathological lesions on SPECT/CT were observed in 73 patients, and negative results in 5 patients. Among them, 27 patients (14 males and 13 females; mean age 46.3 years, range: 22–77 years) with abnormal lesions seen in the SPECT/CT study and inadequately controlled sHPT despite standard medical therapy were qualified for parathyroid surgery. PTH plasma concentration exceeding 600 pg/ml was an eligibility criterion for surgery. Among 26 patients with renal sHPT, 25 received kidney replacement therapy. Coeliac disease was diagnosed in one patient with sHPT. Two patients required second parathyroid surgery 4 and 19 months after the first operation.

Sonography of the neck was performed parallel to the scintigraphy at the same department in all cases, but results of the study had only a supportive function in terms of the results of the study [10]. Measurements to estimate accurately their volume were performed in 18.8% of all histopathologically assessed lesions.

We defined a positive result in early and delayed SPECT/CT as the presence of identifiable focus of increased <sup>99m</sup>Tc-sestamibi accumulation in the vicinity of the thyroid gland, or localized outside of the thyroid gland in the neck or mediastinum.

The SPECT/CT method of PPS allowed positioning the anatomic localization of metabolically active lesions in three-dimensional projections. Separate sets of fusion images were delivered to the surgeon to facilitate surgical treatment planning. Removed tissue specimen were secured and, after recording their location, transferred to the pathology lab for histopathological examination.

The specific histopathological diagnoses were correlated with the type of <sup>99m</sup>Tc-sestamibi uptake in the lesions, serum PTH, phosphate, total, and ionized calcium.

In surgical centres, PTH measurements were performed post-operatively. Direct, postoperative PTH assays were performed in 22 patients.

SPECT/CT results were considered true positive (TP) if a lesion was SPECT/CT PPS(+) and diagnosed as an abnormal parathyroid gland (APG — parathyroid adenoma and parathyroid hyperplasia) or normal parathyroid gland (NPG) on histopathological diagnosis; false positive (FP) if a lesion was SPECT/CT PPS(+) but not parathyroid lesions (lymph nodes, fat, thyroid tissue) (Non-PL) on histopathological diagnosis, true negative (TN) was characterized as SPECT/CT PPS(-) and confirmed as not of parathyroid origin on histopathological diagnosis and false negative (FN) as SPECT/CT PPS(-) and diagnosed as APG or NPG histopathologically.

The study was approved by the Pomeranian Medical University Ethics Committee and all patients gave their written consent.

## Statistical analysis

Normality of distribution for serum PTH concentration was examined by the Kolmogorov-Smirnov test. Since the PTH distribution was significantly different from normal, the Kruskal-Wallis test was used to compare PTH between independent groups. Fisher's exact test was used for assessing the significance of the association between types of accumulation and histopathological diagnosis. Statistical analysis was performed with IBM SPSS 23. The threshold for statistical significance was  $p < 0.05$ .

## Results

In 27 patients 65 lesions SPECT/CT PPS(+) on SPECT/CT were detected, but 6 of them were not found during surgery. During operations on 7 patients from this group, the surgeon additionally removed 10 lesions not indicated on SPECT/CT, and then we called it SPECT/CT PPS(-). As a result, 69 lesions were validated on the histopathological diagnosis. In total, 5 patients had a single lesion, 9 patients had 2 lesions, 7 patients had 3 lesions, 5 patients had 4 lesions, and 1 patient had 5 lesions.

The group of 59 lesions SPECT/CT PPS(+) with an additional 10 lesions SPECT/CT PPS(-) had the following histopathological diagnoses: 28 + 0 (40.6%) — parathyroid adenoma, 12 + 2 (20.3%) — parathyroid hyperplasia, 10 + 2 (17.4%) — NPG, 3 + 1

**Table 1.** Baseline biochemical analyses before surgery

Serum concentration (reference range)	Mean ( $\pm$ SD)	Median (Q25–Q75)
Ionized calcium (1.05–1.35 mmol/L)	1.49 $\pm$ 0.47	1.35 (1.15–1.9)
Total calcium (2.1–2.6 mmol/L)	2.29 $\pm$ 0.23	2.32 (2.08–2.51)
Phosphorus (0.87–1.45 mmol/L)	1.90 $\pm$ 0.63	1.76 (1.33–2.54)
PTH (16–65 pg/mL)	1701.92 $\pm$ 763.40	1600.00 (1272–2500)
Creatinine (0.7–1.5 mg/dL)	5.71 $\pm$ 2.18	5.92 (4.90–6.93)
Urea (15–40 mg/dL)	74.18 $\pm$ 37.69	71 (51–91.15)

Q25–Q75 — interquartile range; SD — standard deviation

(5.8%) — lymph node and 6 + 4 (14.5%) — normal thyroid gland tissue, 0 + 1 (1.4%) — fatty tissue.

Biochemistry data obtained before surgery are presented in Table 1.

To analyze the association between PTH and the histopathological diagnosis we compared PTH concentrations between three groups of patients: 1) 16 patients with parathyroid adenoma

in histopathological diagnosis for at least one location, 2) 7 patients with parathyroid hyperplasia in histopathological diagnosis for at least one location, and 3) 4 patients with NPG or other histopathological diagnosis but without parathyroid adenoma or parathyroid hyperplasia at any location. There was no single patient with both parathyroid adenoma and parathyroid hyperplasia in different locations. There was no significant difference between those groups as regards PTH concentration ( $p = 0.18$ , Kruskal-Wallis test).

In a positive SPECT/CT PPS (PPS+), we identified three types of the uptake accumulation: Type I with the absence of accumulation in the early phase and retention in the delayed phase (EP-/DP+), Type 2 with accumulation in both phases (EP+/DP+), Type III with the uptake observed only in the EP(EP+/DP-).

Additionally, we identified Type IV, in which the lesions were not detected by SPECT/CT but were found and removed during surgery (Type IV EP-/DP-). The parathyroid lesion was defined if it was localized dorsally to the thyroid lobe and the uptake in SPECT/CT was classified either as type I or type II [11]. In the type III uptake, the localization criterion was decisive. None of the patients had ectopic localization of lesions.

In the lesion-based analysis, there were 9 (15.3%), 49 (83%) and 1 (1.7%) lesions SPECT/CT PPS(+) characterized as types I, II and III, respectively (Fig 1).

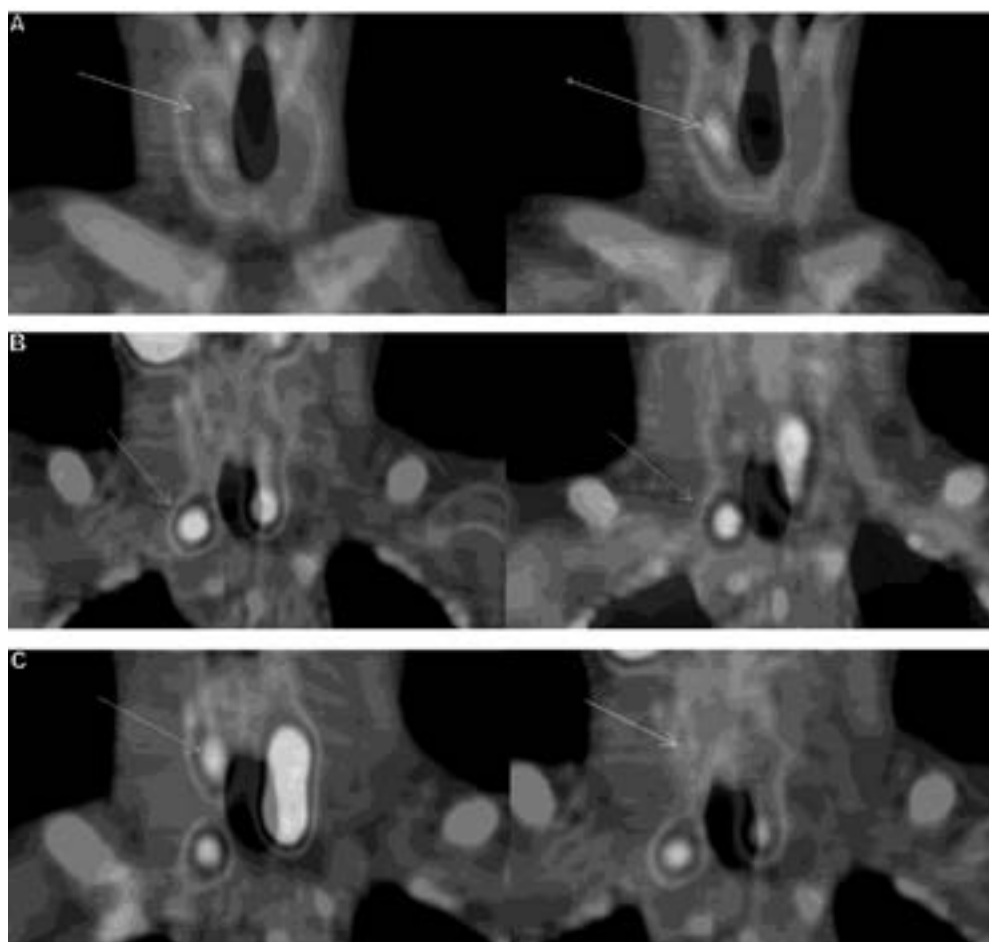


**Figure 1.** Three types of  $^{99m}\text{Tc}$ -sestamibi SPECT/CT uptake in fusion coronal cross-sections; **A.** Type I — the tracer is visible in the delayed phase for right upper parathyroid gland. HP proved as adenoma (patient ZG, 56 y.o.); **B.** Type II — tracer is visible in both phases for right lower parathyroid gland. HP proved as adenoma (patient LM, 57 y.o.); **C.** Type III — the tracer is visible in the early phase for right upper parathyroid gland HP proved as NPT (patient LM, 57 y.o.). White arrows show lesions with or without uptake in corresponding phases of SPECT/CT PPS

**Table 2.** Association of SPECT/CT <sup>99m</sup>Tc-sestamibi results and type of uptake with parathyroid or non-parathyroid lesions in histopathological evaluation

Type of uptake	Parathyroid lesions (n)	Non-parathyroid lesions (n)	P value
TYPE I (EP-/DP+) <sup>a</sup>	5	4	} 0.036*
TYPE II (EP+/DP+) <sup>a</sup>	44	5	
TYPE III (EP+/DP-) <sup>a</sup>	1	0	
TYPE IV (EP-/DP-) <sup>b</sup>	4	6	N/A
Total	54	15	69

\*Fisher exact test for types I-III; EP — early phase; DP — delayed phase; N/A — not applicable; <sup>a</sup>SPECT/CT PPS(+) for types I-III lesions visible in SPECT/CT preoperative parathyroid scintigraphy; <sup>b</sup>SPECT/CT PPS(-) for type IV lesions not visible in SPECT/CT preoperative parathyroid scintigraphy.

Among 69 removed lesions 50 were acknowledged as TP, 9 lesions as FP, 4 lesions as FN, 6 lesions as TN. In type I the rate of TP achieved 5(55%) lesions, in type II — 44 (90%), in type III — 1(100%) lesion, whereas in type IV SPECT/CT PPS(-) achieved 4 (40%) lesions (Tab. 2).

In 13 (18.8%) lesions removed by the surgeon in 3 hyperplasia and 7 adenomas the average volume was 0.38 mL and 0.41 mL, respectively. All those lesions presented as type II on PPS SPECT/CT study.

The statistical analysis for the whole PPS(+) group showed significant differences between accumulation types I, II or III and results of histopathological examination ( $p = 0.036$ ). A comparison between types I and II of <sup>99m</sup>Tc-sestamibi accumulation showed significant ( $p = 0.025$ ) differences in histopathological diagnosis (Tab. 2).

The association of detailed histopathological diagnosis with SPECT/CT uptake type is shown in Table 3.

There were no significant differences between lesions with type I and type II uptake as regards proportions of parathyroid adenomas (33% vs. 51%,  $p = 0.473$ ) and parathyroid hyperplasia (0% vs. 24%,  $p = 0.181$ ) in relation to histopathological diagnosis. However, when parathyroid adenomas and parathyroid hyperplasia were combined as APG, this diagnosis was significantly more frequent in lesions with type II uptake than in lesions with type I uptake (76% vs. 33%,  $p = 0.0197$ ). The frequency of APG was significantly different between types II and IV (76% vs. 20%, respectively,  $p = 0.0016$ ), but not between types I and IV (33% vs. 20%,  $p = 0.628$ ).

Combined lesions with positive uptake (types I, II and III) had significantly higher odds for combined histopathological diagnosis of APG and NPG than lesions with negative uptake (type IV) [OR = 8.33 (95% CI: 1.95–35.54),  $p = 0.004$ ]. Type II lesions had the highest odds ratio for APG or NPG when compared to type IV lesions [OR = 13.1 (95% CI: 2.75 to 63.27),  $p = 0.001$ ], while type I lesions did not have significantly higher odds for APG or NPG than type IV lesions [OR = 1.88 (95% CI: 0.30 to 11.63),  $p = 0.499$ ].

The SPECT/CT <sup>99m</sup>Tc-sestamibi PPS quality parameters for detecting APG or NPG on the basis of positive (type I-III) uptake were sensitivity 92.6%, specificity 40.0%, accuracy 81.2%, positive predictive value 84.7% and negative predictive value 60.0% was achieved.

## Discussion

Even if some articles are focused on parathyroid scanning with <sup>99m</sup>Tc-sestamibi in sHPT, there is limited data about its correlation with histopathology [12, 13]. SPECT/CT PPS has lately been regarded as the method of choice [6, 14, 15]. The main purpose of the study was to find pathological lesions, and the next one was to apply the best procedure to find them effectively. The method of washout analysis was rarely correlated with particular types of uptake and the final results of the study [16]. However, Carpertier, in one of the first articles about the utility of <sup>99m</sup>Tc-sestamibi in preoperative diagnosis of hyperparathyroidism, wrote about the EP and DP phases of the study [17]. Yang compared EP and DP results and pointed out the importance of dual-phase analysis methodology on final results [9].

In our study special attention was paid to the presence or absence of tracer accumulation in particular phases of the study. In this context, our approach is quite innovative. In the current paper, lesions were assessed according to their visibility in both phases of PPS and compared with histopathology.

To our knowledge, this is the first comparison performed between the transport kinetics of <sup>99m</sup>Tc-sestamibi and histopathological results in particular lesions for sHPT patients.

In our material type, I turned out not to be diagnostic for discrimination of whether the lesion is or is not of parathyroid origin. This is depicted by significantly lower odds for histopathological diagnosis of APG or NPG for type I in comparison to type II.

**Table 3.** Association of SPECT/CT <sup>99m</sup>Tc-sestamibi results and uptake types with histopathological diagnosis in sHPT

Histopathological findings			SPECT/CT PPS(+)		SPECT/CT PPS(-)		Total
			Type I EP-/DP+	Type II EP+/DP+	Type III EP+/DP-	Type IV EP-/DP-	
Positive	APG	Parathyroid adenoma	3 <sup>a</sup>	25 <sup>a</sup>	–	–	28
		Parathyroid hyperplasia	–	12 <sup>a</sup>	–	2 <sup>c</sup>	14
	NPG	Normal parathyroid gland	2 <sup>a</sup>	7 <sup>a</sup>	1 <sup>a</sup>	2 <sup>c</sup>	12
Negative	Non-PL	Thyroid tissue	2 <sup>b</sup>	4 <sup>b</sup>	–	4 <sup>d</sup>	10
		Lymph node	2 <sup>b</sup>	1 <sup>b</sup>	–	1 <sup>d</sup>	4
		Fatty tissue	–	–	–	1 <sup>d</sup>	1
Total			9	49	1	10	69

<sup>a</sup>TP — true positive; <sup>b</sup>FP — false positive; <sup>c</sup>FN — false negative; <sup>d</sup>TN — true negative; APG — abnormal parathyroid gland; NPG — normal parathyroid gland; SPECT/CT PPS(+) — lesions visible in SPECT/CT preoperative parathyroid scintigraphy; SPECT/CT PPS(-) — lesions not visible in SPECT/CT preoperative parathyroid scintigraphy; EP — early phase; DP — delayed phase

Type II uptake was predominant in the examined group. As a practical remark, it might be valuable to point out in the report of the PPS study the type  $^{99m}\text{Tc}$ -sestamibi uptake. Such lesions would have higher odds of being APG or NPG. The explanation might be the greater number of mitochondrias, and the ability of parathyroid cells to persistently capture  $^{99m}\text{Tc}$ -sestamibi in comparison with Non-PL.

For parathyroid adenomas and parathyroid hyperplasias, type II accumulation was observed in 90% and 86%, respectively, while type I accumulation was noted in 10% of adenoma lesions. The examined group consisted of patients with relatively high ratios of parathyroid adenoma to hyperplasia (ratio 2:1) and was different compared with data obtained by Yuan [6]. The explanation for this fact might be the relatively long waiting time for kidney transplantation in our country [18]. This fact in patients with sHPT refractory to medical treatment promoted the evolution of parathyroid gland hyperplasia into adenoma [2, 19, 20]. This happens because of alternation in parathyroid tissue growth pattern from polyclonal to monoclonal or multiclonal proliferation [21].

The presence of increased uptake of  $^{99m}\text{Tc}$ -sestamibi only in DP or increased activity of a tracer in both phases (EP and DP) are the main principles of the washout protocol [22, 23]. The  $^{99m}\text{Tc}$ -sestamibi clearance from the lesion is a well-known phenomenon in the case of pHPT patients, and it is assessed as from 17% to 40% of all cases of parathyroid scintigraphy [24–27]. In our material type III uptake was presented only in one case, perhaps because there is a different aetiology of primary hyperparathyroidism (pHPT) and sHP [6, 28]. The lesion with this kind of uptake misleads nuclear medicine practitioners suggesting the thyroid origin of the lesion. Quick clearance typical of thyroid tissue is a cause of false-negative findings, and researchers overcome it by performing thyroid scans with  $^{123}\text{I}$  after the  $^{99m}\text{Tc}$ -sestamibi scan [14]. On the other hand, it leads to a disadvantage in image interpretation because of the “shine through” phenomenon [29]. In our opinion, it is not necessary when the SPECT-CT technique is applied. Localization of the lesion behind the thyroid gland indicates its parathyroid rather than thyroid origin regardless of the type of transport kinetics type [14, 30]. Furthermore, the better technical possibilities related to the use of hybrid techniques and structural imaging have resulted in better sensitivity compared to previous planar or SPECT modality, even if in sHPT lesions are multiple and smaller [6, 14, 31, 32].

Surgeons removed 12 (17.4%) lesions of NPT because they were visible in parathyroid scintigraphy. These findings are similar to the 15.8% noted in the publication by Yuan [6]. High PTH plasma concentration (greater than in pHPT) might influence and stimulate to some extent NPG [7, 33]. However, Bolasco found one case of sHPT treated with cinacalcet where despite the lowering PTH plasma level  $^{99m}\text{Tc}$ -sestamibi uptake in APG was unchanged [34].

SPECT/CT PPS helped in choosing lesions to be removed. Nowadays, it is believed that if four glands exploration parathyroid surgery is necessary, surgeons should remove three glands and a half of the fourth with the most normal appearance, leaving the remaining half in situ [6]. For the 27 patients, the estimated number of removed parathyroid glands should have been minimum 81 glands, but 69 glands were removed. So, SPECT/CT PPS results helped to limit the number of resected glands, shortened the duration time of the surgery, and diminished the failure rate. However, it is possible

that in the operating theatre lesions suspected of pathology by the surgeon would be removed during the exploration, even if there is no indication in preoperative diagnosis. It is important to admit this in terms of the limitation of our study. The study was conducted in just one university centre. The surgeons' skills, preoperative assessment, and the experience of nuclear medicine specialists will affect the outcome of the study.

A sensitivity of 92.6% and accuracy of 81.2% is comparable with the literature data [2, 30]. A specificity of 40% is much lower than that achieved by other authors [2, 6, 9, 30, 35]. This could have been affected by including Type IV lesions in the calculation. Type IV consisted of lesions removed by the surgeon despite the lack of accumulation of the tracer in scintigraphy. It is worth mentioning in this context that our study provides additional quality parameters not available in other papers as the odds ratio for successful surgery in particular transport kinetics types in patients with sHPT.

In the current study as well as in the literature there was no statistical relation between histopathological diagnosis and PTH level. The explanation may be that pharmacological treatment in sHPT patients influences their PTH level [36]. In our study, the recommendation for surgery was PTH level of more than 600 pg/mL. The same criteria were applied by Souberbielle and Rosato [33, 37].

Separation into three groups of tracer uptake was used in previous studies with  $^{99m}\text{Tc}$ -sestamibi performed for different indications. For example, the kinetics of the tracer was used as a predictor of tumour response to chemotherapy treatment. It combined imaging findings with prognostic value in patients with breast cancer, lymphoma, and small and non-small cell lung cancer [38]. Different kinetics of  $^{99m}\text{Tc}$ -sestamibi depicted a multidrug resistance phenotype prior to preoperative diagnosis or any treatment. The above idea inspired us to perform the comparison between  $^{99m}\text{Tc}$ -sestamibi uptake in SPECT/CT PPS and different histopathological diagnosis in sHPT.

The genetic factors influencing parathyroid uptake in patients with hyperparathyroidism were postulated in some publications [39–41]. But there is still a limited number of genetics studies investigating the background of the transport kinetics of  $^{99m}\text{Tc}$ -sestamibi in patients with sHPT. Also, different mathematical models of transport kinetics have been created but there is a lack of clinical studies [42]. The authors of the presented study performed genetic studies in patients with hyperparathyroidism and proved the significant negative correlation of mRNA expression for the *ABCC1* gene with maximal  $^{99m}\text{Tc}$ -sestamibi uptake values in patients with hyperparathyroidism [43, 44]. There is a need for further investigation in this field.

## Conclusions

For sHPT patients evaluated with SPECT/CT PPS accumulation type, I is a weak premise for a surgeon to find parathyroid pathology. Only persistent  $^{99m}\text{Tc}$ -sestamibi accumulation in both phases — equivocal with accumulation type II — effectively differentiates parathyroid and non-parathyroid lesions as well as indicates with high probability the presence of adenoma or hyperplasia. Type III, consistent with washout pattern, is rare in sHPT.

## Conflict of interest

The authors declare no conflicts of interest.

## Acknowledgments

The authors are deeply indebted to Ms. Krystyna Jasiakiewicz, MSc for her great commitment and excellent work.

## Funding

This study was supported by a grant from budget resources for science in the years 2010–2015 as research project No. N N402 463339.

## References

- Chen JB, Chou FF, Yang CH, et al. Association between clinical variables and mortality after parathyroidectomy in maintenance hemodialysis patients. *Am J Surg*. 2017; 213(1): 140–145, doi: [10.1016/j.amjsurg.2016.03.012](https://doi.org/10.1016/j.amjsurg.2016.03.012), indexed in Pubmed: [27469221](https://pubmed.ncbi.nlm.nih.gov/27469221/).
- Zeng M, Liu W, Zha X, et al. MIBI SPECT/CT imaging had high sensitivity in accurate localization of parathyroids before parathyroidectomy for patients with secondary hyperparathyroidism. *Ren Fail*. 2019; 41(1): 885–892, doi: [10.1080/0886022x.2019.1662804](https://doi.org/10.1080/0886022x.2019.1662804).
- Ballinger AE, Palmer SC, Nistor I, et al. Calcimimetics for secondary hyperparathyroidism in chronic kidney disease patients. *Cochrane Database Syst Rev*. 2014(12): CD006254, doi: [10.1002/14651858.CD006254.pub2](https://doi.org/10.1002/14651858.CD006254.pub2), indexed in Pubmed: [25490118](https://pubmed.ncbi.nlm.nih.gov/25490118/).
- Tominaga Y, Johansson H, Johansson H, et al. Secondary hyperparathyroidism: pathophysiology, histopathology, and medical and surgical management. *Surg Today*. 1997; 27(9): 787–792, doi: [10.1007/BF02385267](https://doi.org/10.1007/BF02385267), indexed in Pubmed: [9306599](https://pubmed.ncbi.nlm.nih.gov/9306599/).
- Konturek A, Barczyński M, Stopa M, et al. Subtotal parathyroidectomy for secondary renal hyperparathyroidism: a 20-year surgical outcome study. *Langenbecks Arch Surg*. 2016; 401(7): 965–974, doi: [10.1007/s00423-016-1447-7](https://doi.org/10.1007/s00423-016-1447-7), indexed in Pubmed: [27233241](https://pubmed.ncbi.nlm.nih.gov/27233241/).
- Yuan LL, Kan Y, Ma DQ, et al. Combined application of ultrasound and SPECT/CT has incremental value in detecting parathyroid tissue in SHPT patients. *Diagn Interv Imaging*. 2016; 97(2): 219–225, doi: [10.1016/j.diii.2015.08.007](https://doi.org/10.1016/j.diii.2015.08.007), indexed in Pubmed: [26432401](https://pubmed.ncbi.nlm.nih.gov/26432401/).
- Olaizola I, Zingraff J, Heuguerot C, et al. [(99m)Tc]-sestamibi parathyroid scintigraphy in chronic haemodialysis patients: static and dynamic explorations. *Nephrol Dial Transplant*. 2000; 15(8): 1201–1206, doi: [10.1093/ndt/15.8.1201](https://doi.org/10.1093/ndt/15.8.1201), indexed in Pubmed: [10910445](https://pubmed.ncbi.nlm.nih.gov/10910445/).
- Hindié E, Ugur O, Fuster D, et al. Parathyroid Task Group of the EANM. 2009 EANM parathyroid guidelines. *Eur J Nucl Med Mol Imaging*. 2009; 36(7): 1201–1216, doi: [10.1007/s00259-009-1131-z](https://doi.org/10.1007/s00259-009-1131-z), indexed in Pubmed: [19471928](https://pubmed.ncbi.nlm.nih.gov/19471928/).
- Yang J, Hao R, Yuan L, et al. Value of dual-phase (99m)Tc-sestamibi scintigraphy with neck and thoracic SPECT/CT in secondary hyperparathyroidism. *AJR Am J Roentgenol*. 2014; 202(1): 180–184, doi: [10.2214/AJR.13.11053](https://doi.org/10.2214/AJR.13.11053), indexed in Pubmed: [24370142](https://pubmed.ncbi.nlm.nih.gov/24370142/).
- Assante R, Zampella E, Nicolai E, et al. Incremental Value of Sestamibi SPECT/CT Over Dual-Phase Planar Scintigraphy in Patients With Primary Hyperparathyroidism and Inconclusive Ultrasound. *Front Med (Lausanne)*. 2019; 6: 164, doi: [10.3389/fmed.2019.00164](https://doi.org/10.3389/fmed.2019.00164), indexed in Pubmed: [31380379](https://pubmed.ncbi.nlm.nih.gov/31380379/).
- Yip L, Pryma DA, Yim JH, et al. Can a lightbulb sestamibi SPECT accurately predict single-gland disease in sporadic primary hyperparathyroidism? *World J Surg*. 2008; 32(5): 784–92; discussion 793, doi: [10.1007/s00268-008-9532-x](https://doi.org/10.1007/s00268-008-9532-x), indexed in Pubmed: [18324345](https://pubmed.ncbi.nlm.nih.gov/18324345/).
- Sheu-Grabellus SY, Schmid KW. [Pathology of parathyroid glands: Practical aspects for routine pathological investigations]. *Pathologe*. 2015; 36(3): 229–236, doi: [10.1007/s00292-015-0016-0](https://doi.org/10.1007/s00292-015-0016-0), indexed in Pubmed: [25898935](https://pubmed.ncbi.nlm.nih.gov/25898935/).
- Uchida K, Tominaga Y, Tanaka Y, et al. Renal transplantation and secondary hyperparathyroidism. *Semin Surg Oncol*. 1997; 13(2): 97–103, doi: [10.1002/\(sici\)1098-2388\(199703/04\)13:2<97::aid-ssu5>3.0.co;2-x](https://doi.org/10.1002/(sici)1098-2388(199703/04)13:2<97::aid-ssu5>3.0.co;2-x).
- Caldarella C, Treglia G, Pontecorvi A, et al. Diagnostic performance of planar scintigraphy using mTc-MIBI in patients with secondary hyperparathyroidism: a meta-analysis. *Ann Nucl Med*. 2012; 26(10): 794–803, doi: [10.1007/s12149-012-0643-y](https://doi.org/10.1007/s12149-012-0643-y), indexed in Pubmed: [22875577](https://pubmed.ncbi.nlm.nih.gov/22875577/).
- Hindié E, Zanotti-Fregonara P, Just PA, et al. Parathyroid scintigraphy findings in chronic kidney disease patients with recurrent hyperparathyroidism. *Eur J Nucl Med Mol Imaging*. 2010; 37(3): 623–634, doi: [10.1007/s00259-009-1313-8](https://doi.org/10.1007/s00259-009-1313-8), indexed in Pubmed: [19946686](https://pubmed.ncbi.nlm.nih.gov/19946686/).
- Spanu A, Schillaci O, Piras B, et al. SPECT/CT in hyperparathyroidism. *Clin Transl Imaging*. 2014; 2(6): 537–555, doi: [10.1007/s40336-014-0089-4](https://doi.org/10.1007/s40336-014-0089-4).
- Carpentier A, Jeannotte S, Verreault J, et al. Preoperative localization of parathyroid lesions in hyperparathyroidism: relationship between technetium-99m-MIBI uptake and oxyphil cell content. *J Nucl Med*. 1998; 39(8): 1441–1444, indexed in Pubmed: [9708524](https://pubmed.ncbi.nlm.nih.gov/9708524/).
- Rutkowski B, Ciechanowski K, Durlik M, et al. Availability of different therapeutic option in patients with secondary hyperthyroidism in Poland. *Forum Nefrol*. 2012; 5(4): 333–338.
- Tominaga Y, Tanaka Y, Sato K, et al. Histopathology, pathophysiology, and indications for surgical treatment of renal hyperparathyroidism. *Seminars in Surgical Oncology*. 1997; 13(2): 78–86, doi: [10.1002/\(sici\)1098-2388\(199703/04\)13:2<78::aid-ssu3>3.0.co;2-z](https://doi.org/10.1002/(sici)1098-2388(199703/04)13:2<78::aid-ssu3>3.0.co;2-z).
- DeLellis RA. Parathyroid tumors and related disorders. *Mod Pathol*. 2011; 24 Suppl 2: S78–S93, doi: [10.1038/modpathol.2010.132](https://doi.org/10.1038/modpathol.2010.132), indexed in Pubmed: [21455204](https://pubmed.ncbi.nlm.nih.gov/21455204/).
- Zitt E, Lhotta K. [Management of secondary hyperparathyroidism-current impact of parathyroidectomy]. *Wien Med Wochenschr*. 2016; 166(7-8): 254–258, doi: [10.1007/s10354-016-0444-3](https://doi.org/10.1007/s10354-016-0444-3), indexed in Pubmed: [26913524](https://pubmed.ncbi.nlm.nih.gov/26913524/).
- Coakley AJ, Kettle AG, Wells CP, et al. 99Tcm sestamibi—a new agent for parathyroid imaging. *Nucl Med Commun*. 1989; 10(11): 791–794, doi: [10.1097/00006231-198911000-00003](https://doi.org/10.1097/00006231-198911000-00003), indexed in Pubmed: [2532313](https://pubmed.ncbi.nlm.nih.gov/2532313/).
- Taillefer R, Boucher Y, Potvin C, et al. Detection and localization of parathyroid adenomas in patients with hyperparathyroidism using a single radionuclide imaging procedure with technetium-99m-sestamibi (double-phase study). *J Nucl Med*. 1992; 33(10): 1801–1807, indexed in Pubmed: [1328564](https://pubmed.ncbi.nlm.nih.gov/1328564/).
- Bénard F, Lefebvre B, Beuvon F, et al. Rapid washout of technetium-99m-MIBI from a large parathyroid adenoma. *J Nucl Med*. 1995; 36(2): 241–243, indexed in Pubmed: [7830122](https://pubmed.ncbi.nlm.nih.gov/7830122/).
- Perez-Monte JE, Brown ML, Shah AN, et al. Parathyroid adenomas: accurate detection and localization with Tc-99m sestamibi SPECT. *Radiology*. 1996; 201(1): 85–91, doi: [10.1148/radiology.201.1.8816526](https://doi.org/10.1148/radiology.201.1.8816526), indexed in Pubmed: [8816526](https://pubmed.ncbi.nlm.nih.gov/8816526/).
- Lorberboym M, Minski I, Macadziob S, et al. Incremental diagnostic value of preoperative 99mTc-MIBI SPECT in patients with a parathyroid adenoma. *J Nucl Med*. 2003; 44(6): 904–908, indexed in Pubmed: [12791817](https://pubmed.ncbi.nlm.nih.gov/12791817/).
- Fröberg AC, Valkema R, Bonjer HJ, et al. 99mTc-tetrofosmin or 99mTc-sestamibi for double-phase parathyroid scintigraphy? *Eur J Nucl Med Mol Imaging*. 2003; 30(2): 193–196, doi: [10.1007/s00259-002-1030-z](https://doi.org/10.1007/s00259-002-1030-z), indexed in Pubmed: [12552335](https://pubmed.ncbi.nlm.nih.gov/12552335/).
- Vulpio C, Bossola M, De Gaetano A, et al. Usefulness of the combination of ultrasonography and 99mTc-sestamibi scintigraphy in the preoperative evaluation of uremic secondary hyperparathyroidism. *Head Neck*. 2010; 32(9): 1226–1235, doi: [10.1002/hed.21320](https://doi.org/10.1002/hed.21320), indexed in Pubmed: [20091692](https://pubmed.ncbi.nlm.nih.gov/20091692/).
- Liu Y, Chun KJ, Freeman LM. ‘Shine through’ on dual tracer parathyroid scintigraphy: a potential pitfall in interpretation. *Clin Nucl Med*. 2005; 30(3): 145–149, doi: [10.1097/00003072-200503000-00001](https://doi.org/10.1097/00003072-200503000-00001), indexed in Pubmed: [15722816](https://pubmed.ncbi.nlm.nih.gov/15722816/).
- Zhen L, Li H, Liu X, et al. The application of SPECT/CT for preoperative planning in patients with secondary hyperparathyroidism. *Nucl Med Commun*. 2013; 34(5): 439–444, doi: [10.1097/MNM.0b013e32835f9447](https://doi.org/10.1097/MNM.0b013e32835f9447), indexed in Pubmed: [23458854](https://pubmed.ncbi.nlm.nih.gov/23458854/).
- Taieb D, Ureña-Torres P, Zanotti-Fregonara P, et al. Parathyroid scintigraphy in renal hyperparathyroidism: the added diagnostic value of SPECT and SPECT/CT. *Clin Nucl Med*. 2013; 38(8): 630–635, doi: [10.1097/RLU.0b013e32829af5bf](https://doi.org/10.1097/RLU.0b013e32829af5bf), indexed in Pubmed: [23751837](https://pubmed.ncbi.nlm.nih.gov/23751837/).

32. Monzen Y, Tamura A, Okazaki H, et al. SPECT/CT Fusion in the Diagnosis of Hyperparathyroidism. *Asia Oceania J Nucl Med Biol.* 2015; 3(1): 61–65, indexed in Pubmed: [27408883](#).
33. Souberbielle JC. Measurement of Parathormone in Chronic Kidney Disease: An Easy Task? In: Delanaye P. ed. *Nephrology and Clinical Chemistry: The Essential Link.* Bentham Books, Belgium 2012: 91–105.
34. Bolasco P, Serra A, Loi M, et al. Failed Switching off in the MIBI-Parathyroid Scintigraphy in a Dialyzed Patient with Secondary Hyperparathyroidism Responsive to Cinacalcet Therapy. *Int J Endocrinol.* 2010; 2010: 206801, doi: [10.1155/2010/206801](#), indexed in Pubmed: [20652073](#).
35. Raruenrom Y, Theerakulpisut D, Wongsurawat N, et al. Diagnostic accuracy of planar, SPECT, and SPECT/CT parathyroid scintigraphy protocols in patients with hyperparathyroidism. *Nucl Med Rev Cent East Eur.* 2018; 21(1): 20–25, doi: [10.5603/NMR.a2018.0003](#), indexed in Pubmed: [29319134](#).
36. Fang Li, Tang B, Hou D, et al. Relationship between parathyroid mass and parathyroid hormone level in hemodialysis patients with secondary hyperparathyroidism. *BMC Nephrol.* 2015; 16: 82, doi: [10.1186/s12882-015-0077-6](#), indexed in Pubmed: [26058796](#).
37. Rosato L, Raffaelli M, Bellantone R, et al. Diagnostic, therapeutic and healthcare management protocols in parathyroid surgery: II Consensus Conference of the Italian Association of Endocrine Surgery Units (U.E.C. CLUB). *J Endocrinol Invest.* 2014; 37(2): 149–165, doi: [10.1007/s40618-013-0022-0](#), indexed in Pubmed: [24497214](#).
38. Del Vecchio S, Zannetti A, Aloj L, et al. MIBI as prognostic factor in breast cancer. *Q J Nucl Med Mol Imaging.* 2003; 47(1): 46–50, indexed in Pubmed: [12714954](#).
39. Kasai ETP, da Silva JWE, Mandarim de Lacerda CA, et al. Parathyroid glands: combination of sestamibi-(99m)Tc scintigraphy and ultrasonography for demonstration of hyperplastic parathyroid glands. *Rev Esp Med Nucl.* 2008; 27(1): 8–12, doi: [10.1157/13114364](#), indexed in Pubmed: [18208776](#).
40. Kao A, Shiao YC, Tsai SC, et al. Technetium-99m methoxyisobutylisonitrile imaging for parathyroid adenoma: relationship to P-glycoprotein or multidrug resistance-related protein expression. *Eur J Nucl Med Mol Imaging.* 2002; 29(8): 1012–1015, doi: [10.1007/s00259-002-0817-2](#), indexed in Pubmed: [12173014](#).
41. Yamaguchi S, Kobayashi Y, Tsujikawa K, et al. [Usefulness of 99mTc-methoxy-isobutyl-isonitrile scintigraphy for preoperative localization of adenoma in primary hyperparathyroidism]. *Hinyokika Kyo.* 2001; 47(9): 619–623, indexed in Pubmed: [11692597](#).
42. Shevtsova ON, Shevtsova VK. Mathematical Simulation of Transport Kinetics of Tumor-Imaging Radiopharmaceutical Tc-MIBI. *Comput Math Methods Med.* 2017; 2017: 2414878, doi: [10.1155/2017/2414878](#), indexed in Pubmed: [28702073](#).
43. Listewnik M, Piowarska-Bilska H, Kurzawski M, et al. The relationship of mRNA ABCC1 expression and uptake of MIBI-Tc99m in patients with hyperparathyroidism. (Meeting Abstract). *Eur J Nucl Med Mol Imaging.* 2016; 43(S70): WOS:000391801600160.
44. Xue J, Liu Y, Yang D, et al. Dual-phase 99mTc-MIBI imaging and the expressions of P-gp, GST- $\alpha$ , and MRP1 in hyperparathyroidism. *Nucl Med Commun.* 2017; 38(10): 868–874, doi: [10.1097/MNM.0000000000000721](#), indexed in Pubmed: [28806349](#).

# Kidney Efficiency Index — quantitative parameter of a dynamic renal scintigraphy. I. Theory and preliminary verification

Krzysztof Grzegorz Filipczak<sup>1</sup> , Paweł Cichoński<sup>2</sup> , Jacek Kusmirek<sup>2</sup> , Anna Plachcińska<sup>1</sup> 

<sup>1</sup>Department of Quality Control and Radiation Protection, Medical University of Lodz, Poland

<sup>2</sup>Department of Nuclear Medicine, Medical University of Lodz, Poland

[Received 6 V 2020; Accepted 28 VIII 2020]

## Abstract

**BACKGROUND:** One of the basic clinical indications for dynamic renal scintigraphy (DRS) is a diagnosis of obstructive uropathy and/or nephropathy. Currently, a basic quantitative criterion for diagnosing nephropathy is the percentage of individual kidney's contribution in the global uptake of a radiopharmaceutical from the blood (so-called Split Function - SF). From a clinical point of view, a parameter evaluating a radiopharmaceutical uptake and reflecting the efficiency of a specific kidney, determined independently of the total uptake of both kidneys, would be much more useful. Based on a Rutland theory, a kidney uptake constant  $K$  proportional to a radiotracer uptake by individual kidney was introduced and applied to DRS with <sup>99m</sup>Tc-ethylene-1-dicysteine (<sup>99m</sup>Tc-EC). In addition, a kidney efficiency index (KEi) was also worked out as a new parameter obtained by dividing the uptake constant  $K$  by the surface of the ROI of a given kidney, which can be interpreted as the average "efficiency" of clearance of a kidney.

**MATERIAL AND METHODS:**  $K$  and KEi values were verified in 72 studies selected retrospectively from patients referred routinely for DRS, with available current level of blood creatinine, used for calculation of estimated GFR (eGFR) according to a CKD-EPI formula. After splitting of eGFR values into individual kidneys according to SF, single kidney eGFR values (SKeGFR) were obtained and then used as a verification method for SF,  $K$  and KEi values.

**RESULTS:** Correlation between SF and SKeGFR values,  $r_{sp} = 0.64$ , was significantly weaker ( $p < 0.0022$ ) than the correlation of SKeGFR values with  $K$  uptake constants and KEi indices: 0.90 and 0.84, respectively.

**CONCLUSIONS:** Uptake constant  $K$  and KEi, as quantitative parameters, give the opportunity to analyze a function of each kidney separately and in an absolute way. KEi also allows for a reliable assessment of kidneys of atypical sizes (larger or smaller than average). It also gives the opportunity to create normative values for this parameter and may be useful in a number of clinical situations where the diagnostic effectiveness of such a relative parameter as SF, is severely limited, e.g. in assessing a large kidney with hydronephrosis or while differing a cirrhotic from hypoplastic (i.e. a small but properly functioning) kidney.

**KEY words:** dynamic renal scintigraphy; renal clearance; split function; uropathy; nephropathy; kidney efficiency index; uptake constant

Nucl Med Rev 2020; 23, 2: 78–83

## Introduction

In dynamic renal scintigraphy (DRS), imaging of a radiopharmaceutical passage through a patient's kidneys allows the assessment of uptake, transport, and excretion of radiopharmaceutical by these

organs. One of the basic clinical indications for DRS is diagnosis of obstructive uropathy and/or nephropathy. Persistent obstructive uropathy (obstruction of the urinary outflow from the calico-pelvic system), manifesting in DRS as a radiopharmaceutical excretion impairment, can lead to damage to the renal parenchyma - obstructive nephropathy, characterized by impairment of radiopharmaceutical uptake and transport function. Currently, a basic quantitative criterion for diagnosing nephropathy is the percentage of individual kidney's contribution in the global uptake of a radiopharmaceutical from the blood [so-called Split Function (SF)]. In a healthy patient, the share of both kidneys in total radiopharmaceutical uptake

Correspondence to: Krzysztof Grzegorz Filipczak  
Department of Quality Control and Radiation Protection, Medical University of Lodz, Czechoslowacka 8/10, 92–216 Lodz, Poland  
e-mail: krzysztof.filipczak.fiz+NMR@gmail.com

is similar - normal SF values are in the range between 42% and 58% [1, 2].

Although the SF parameter is the basic, routinely used criterion for the diagnosis of nephropathy, it has its significant limitations due to its relative nature. The problem is manifested i.a. in cases of absence or only a trace function of one of kidneys (when the SF of the other kidney will always be close to or equal to 100%, even despite its damage), nephropathy of similar severity affecting both kidneys (both SF values remain in the normal range despite the disease process ongoing in both kidneys) and in case of large differences in the size of kidneys, e.g. hypoplasia of one of them (the share of SF of the smaller kidney will be significantly reduced, despite a normal function of nephrons). From a clinical point of view, a parameter evaluating a radiopharmaceutical uptake and reflecting the efficiency of a given kidney, determined independently of the total uptake of both kidneys, would be much more useful.

In 1984, Rutland [3], taking into account the method of graphic analysis of Patlak [4], presented a comprehensive theory applied to DRS images analysis. In his mathematical model, there was an uptake constant  $K$ , which he describes as "a fraction of the blood activity taken up per second". This value was successfully applied to calculate a glomerular filtration rate (GFR) for a single kidney using  $^{99m}\text{Tc}$ -DTPA [5], and in studies using  $^{99m}\text{Tc}$ -MAG3 to determine tubular extraction rate (TER) [6,7]. Despite its potential usefulness, the Rutland method has not gained much popularity and has not yet been applied to a newer radiopharmaceutical —  $^{99m}\text{Tc}$ -ethylene-1-dicysteine ( $^{99m}\text{Tc}$ -EC) [8].

The aim of this study was therefore to present a relatively simple method for generating parameters proportional to the uptake function of a single kidney, independent of the total uptake function of both kidneys. An additional goal was to obtain a parameter independent of kidney size. The parameter should be useful not only in the situations described earlier in which SF is of limited value, but also, for example, in the differentiation between the cirrhotic and hypoplastic kidney (with normal nephron function).

## Material and Methods

### Material

72 patients (47 women, 25 men) aged 17-81 (average 52) years were qualified for the study. They were selected retrospectively from patients routinely referred for DRS, and the entry criterion - qualifying for the study group - was the available current serum creatinine level results in archived medical documentation, which enabled the determination of the approximate glomerular filtration rate eGFR. A total of 138 kidneys were assessed (some patients had only one kidney).

### Study Acquisition

DRS was performed according to a standard procedure. A patient was placed in the supine position with a gamma camera detector (GE Infinia Hawkeye 4) in the posterior projection. Image acquisition was started at the time of intravenous injection of 111 MBq of  $^{99m}\text{Tc}$ -EC. A sequence of 60 images was acquired of 20 seconds each. Counts were stored in a  $128 \times 128$  matrix. The camera detector, equipped with a LEHR collimator, was positioned so that its field of view covered — in addition to kidneys — also a heart.

### Preprocessing

Before processing, images were smoothed twice with a typical filter that replaces each pixel with the average of its  $3 \times 3$  neighbourhood. An additional image was also created showing the summed counts from the 2 and 3 minutes of the study (parenchymal phase). The images prepared in this way were further processed using the standard and alternative — in house modified method for data processing.

### Regions of interest (ROIs)

To determine areas of kidneys, the image presenting smoothed counts from the 2 and 3 minutes of the study was used. In this image, an isocontour was drawn automatically extracting pixels with values equal to or higher than 30% of the maximum in the image — the ROI generated in this way, if necessary, could be corrected by the operator. ROI areas were also stored for use at a later processing stage. Extra-renal background areas were determined automatically around the lower kidney poles.

Determining a heart ROI — whose size and correct location significantly affect the repeatability of final results — has been automated. An operator used an image showing the first 20 seconds of the study, in which he outlined (with a large margin) the heart area. Twenty pixels with maximum values were automatically searched in the outlined area — and a curve from these pixels (sum of values) was considered a heart curve. Examples of ROIs placement are shown in Figure 1.

### Split Function (SF)

Software available on the Xeleris Functional Imaging Workstation 4.0 (GE Healthcare) dedicated to dynamic renal studies was used for routine study processing. Split Function (SF) was determined from renographic curves after background subtraction, normalized to the areas of respective ROIs. Counts collected during radiotracer

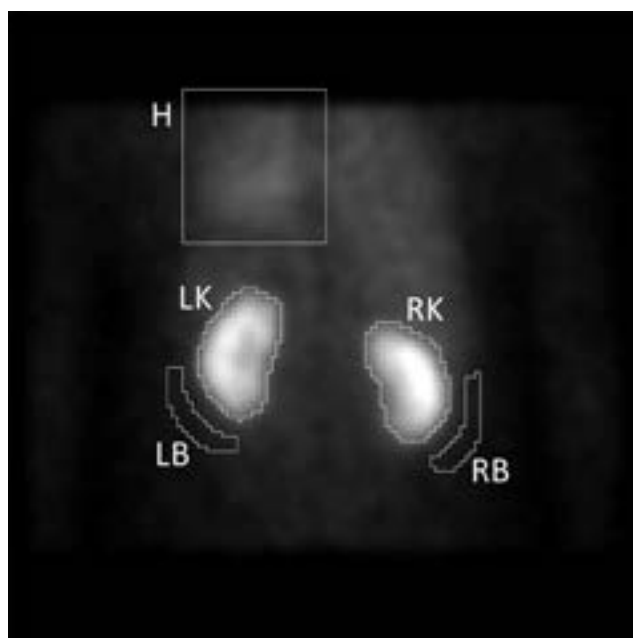


**Figure 1.** Example of heart (H), kidneys (LK, RK), and extrarenal background (LB, RB) ROIs

uptake phase (from 2 to 3 min) were added (integrated) for each curve and then divided by the sum of counts from both kidneys. The result, presented in percent, was the SF value for a given kidney.

### Uptake Constant $K$

$K$  uptake constants were calculated on the basis of the Rutland method, in which background-corrected kidney and cardiac curves were transformed into so-called Rutland space (Appendix). After transforming the curves, an uptake constant  $K$  was determined for each kidney. This value was calculated as an angular coefficient (slope) of line, formed over a time interval between 2 and 3 minutes of the study (from 60 to 160s). According to the theory, the uptake constant value is proportional to clearance function of the individual kidney but has no specific unit. In this paper, phrase "uptake index" was used for description of the graph's axis.

### Kidney Efficiency index

A kidney efficiency index (KEi) is a new parameter obtained by dividing the uptake constant  $K$  by the surface of the ROI of a given kidney. This parameter can be interpreted as the average

"efficiency" of clearance of a kidney, and it has a unit marked as "uptake index/pixel". Such independence of clearance from a kidney size (in this case from its surface) opens the field for comparing KEi parameters between different kidneys, as well as determining a range of normal values, which should help determine the degree of impairment of kidney function.

### Single Kidney Estimated GFR (SKeGFR)

The reliability of KEi, as an absolute index of renal function, was assessed by comparing its values with the estimated glomerular filtration rate (eGFR) values, which was calculated according to the CKD-EPI formula [9]. This formula takes into account serum creatinine level as well as age, sex, and race of a patient. Serum creatinine levels were obtained from patients' documentation. Testing for serum creatinine level was performed in different labs, but with the same, enzymatic, method. After multiplying eGFR values by the SF percentage values, calculated earlier for each kidney, a parameter determining estimated eGFR value for individual kidneys (Single Kidney estimated GFR — SKeGFR) was obtained. Unit for the SKeGFR was the same as eGFR unit,

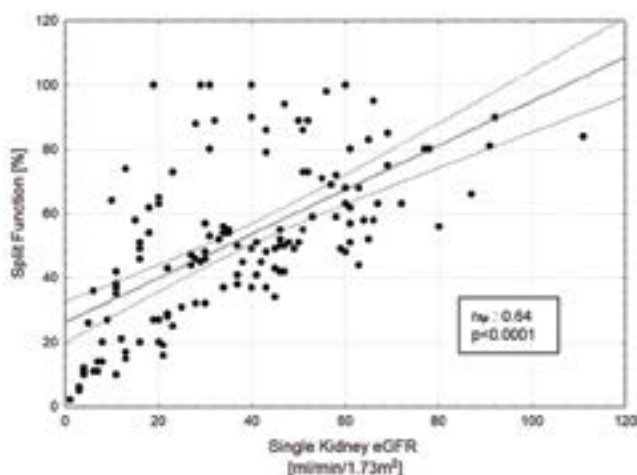


**Figure 2.** Scatter plot of Split Function (SF) and SKeGFR ( $r_{sp} = 0.64$ ) with regression line and its 95% confidence interval

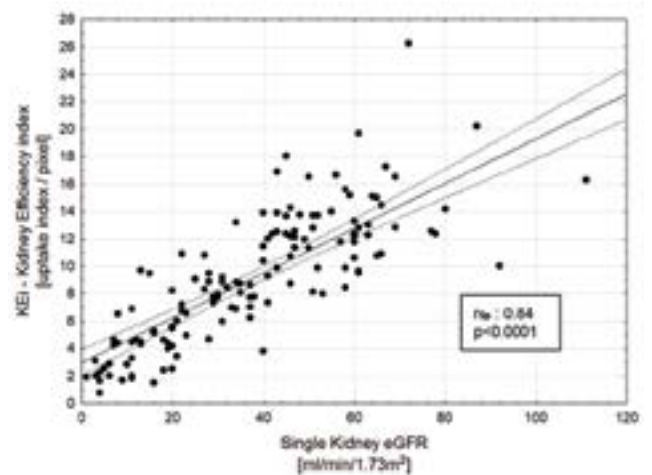


**Figure 4.** Scatter plot of KEi and SKeGFR ( $r_{sp} = 0.84$ ) with regression line and its 95% confidence interval

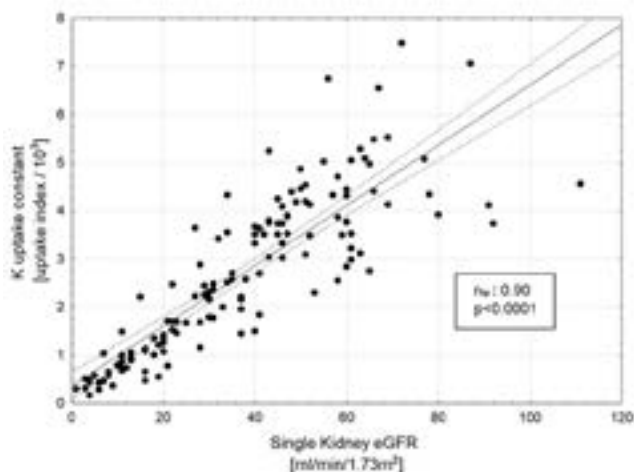


**Figure 3.** Scatter plot of uptake constant  $K$  and SKeGFR ( $r_{sp} = 0.90$ ) with regression line and its 95% confidence interval

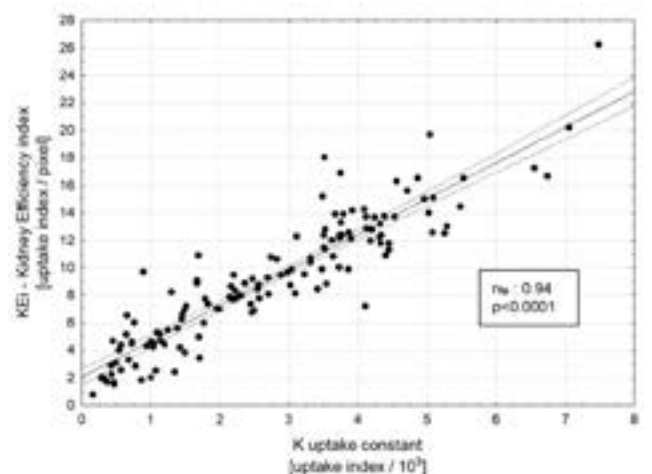


**Figure 5.** Scatter plot of KEi and  $K$  uptake constant ( $r_{sp} = 0.94$ ) with regression line and its 95% confidence interval

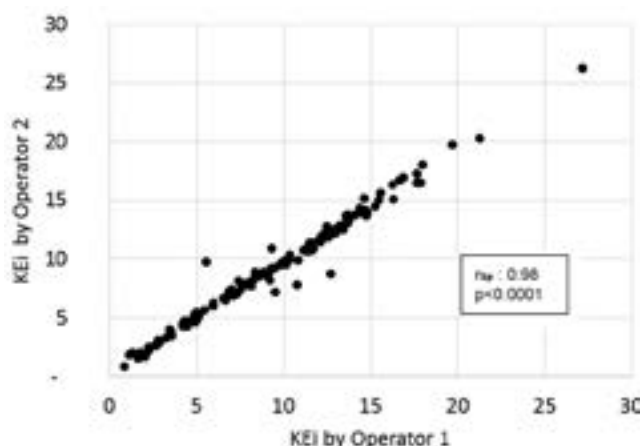


**Figure 6.** KEI values: Operator 1 and Operator 2

which is [mL/min/1.73 m<sup>2</sup>]. SKeGFR values were compared with previously obtained SF parameters and K uptake constants.

### Inter-observer variability

All activities related to the study results were carried out twice, by different operators. Before processing, both operators underwent training unifying their proceedings, in particular how to determine ROIs. Values obtained by both operators were compared in order to assess the repeatability of study results.

### Statistical analysis

The least squares method was used to approximate straight lines. Spearman's coefficients ( $r_{sp}$ ) examined correlations between the SF and SKeGFR parameters, between the uptake constant K and SKeGFR, and between KEI parameters calculated by both operators.

### Results

The correlation between SF and SKeGFR values turned out to be statistically significant  $r_{sp} = 0.64$  ( $p < 0.0001$ , Fig. 2), but this relationship was significantly weaker ( $p < 0.0022$ ) than the correlation of SKeGFR values with K uptake constants and KEI indices: 0.90 and 0.84, respectively ( $p < 0.0001$ ). Figures 3 and 4 present scatter plots of these values. Correlation between K uptake constants and KEI values (Fig. 5) was very high and statistically significant  $r_{sp} = 0.94$  ( $p < 0.0001$ ). The repeatability of the KEI parameter determination by various operators turned out to be very high  $r_{sp} = 0.986$  (Fig. 6).

### Discussion

Gamma camera methods determining clearance function separately for each kidney were introduced in the seventies of the twentieth century [10, 11], and in the eighties and nineties, a methodology of these studies was improved [5, 12, 13]. The method for clearance calculation was based on a relationship between a radiotracer uptake by a kidney (in per cent) and its concentration in blood plasma. Based on proportionality coefficients between

these values, the clearance functions of both kidneys were estimated separately. Initially, this method was used to determine only a glomerular filtration rate — GFR [10, 11], because <sup>99m</sup>Tc-DTPA was the only radiopharmaceutical labelled with radiotechnetium available at that time. At the beginning of the nineties, a similar methodology was used to estimate clearance of a newly introduced radiopharmaceutical — <sup>99m</sup>Tc-MAG3, secreted in renal tubules [7, 13]. For normalization purposes, however, these methods required measurement of a patient's blood sample as well as consideration of a camera sensitivity while converting counts into activity. This was done by measuring by gamma camera a syringe with a radiopharmaceutical prepared for administration and a residual of activity in the syringe after injection. In addition, the need to apply corrections for extra-renal background, radiation absorption dependent on the kidney depth, radiation absorption by a couch and normalization of clearance values to patient body surface were emphasized. In subsequent versions of the methodology, the blood sample was no longer necessary. Clearance, expressed as a percentage of uptake of administered activity by kidneys, was then converted to clearance-specific units by using appropriate nomograms [14]. However, none of these methods has been used so far for the radiopharmaceutical <sup>99m</sup>Tc-ethylenedicycysteine (<sup>99m</sup>Tc-EC) [8].

The Rutland method used in this work [3] is based on the determination of a regression line between two quantities that change during the first 3 minutes after administration of a radiotracer, that is, before it begins to leave a kidney.

This applies, on one side of the equation, to the ratio of radiopharmaceutical uptake in a kidney, normalized to its level in the blood (approximated by a curve from the heart as a large reservoir of blood) and on the other side of the equation, to the total (integrated) flow of the radiopharmaceutical through the heart, also related to its level in blood (Appendix). In the classic Rutland method, a slope of a straight line of regression referred to as the "uptake index" [5], is proportional to the radiotracer clearance of a given kidney. It is assumed in this method, that the intravascular part of the extra-renal background changes proportionally to the curve determined from above the heart as the largest blood reservoir.

Peters [15] believes that this method has the smallest statistical error among other gamma camera methods used for clearance calculation. However, despite the fact that the possibility of using this method to determine the clearance of <sup>99m</sup>Tc-DTPA of each kidney was presented as early as in 1985, it did not find application, with a few exceptions [7, 16], in later works — probably due to its relatively high mathematical complexity [17]. However, it has been mentioned in the literature, mainly in the context of calculating split function [1, 18], although it was not adopted in this application either [19]. Instead, it was successfully used to generate parametric images of the kidneys [20–22].

Advantages of this method used to separately assess the function of each kidney, are significant. It is a simplified version of a gamma camera clearance measurement based only on the automated determination of areas of kidneys, heart, and the extra-vascular background. The fact that this method does not require normalization of calculated values to administered activity facilitates its application. Disregarding administered activity causes that parameters determining the efficiency of each kidney (K uptake constant and KEI index) are unnamed quantities proportional to their clearance function [5].

In case of the KEi parameter, dividing K uptake value by the surface of the kidney (its ROI) made the value independent of kidney size. Such a quantitative parameter not only gives the opportunity to analyze a function of each kidney separately and in an absolute way, but also allows for reliable assessment of kidneys of atypical sizes (larger or smaller than average). It also gives the opportunity to create normative values for this parameter. KEi may be useful in a number of clinical situations where the diagnostic effectiveness of basic parameters of dynamic renal scintigraphy, such as SF, is severely limited. Its absolute nature allows reliable differential diagnosis of uropathy and obstructive nephropathy in case of a single kidney or bilateral renal impairment. Its independence from kidney size will be important, e.g. in assessing a large kidney with hydronephrosis. Due to the greater initial amount of parenchyma of such a kidney, SF can remain within the normal range despite damage to some of its nephrons, while KEi will decrease already in the initial phase of obstructive nephropathy. A similar problem is met while differing a cirrhotic from hypoplastic (i.e. a small but properly functioning) kidney, where SF will be below the normal limit in both cases, while KEi will be lowered only in the kidney damaged.

The comparison of the K uptake constant (reflecting the clearance of individual kidney) and the KEi index with estimated GFR values (calculated on the basis of creatinine level, each time converted to individual kidney in accordance with its relative contribution to radiopharmaceutical uptake) was used in this paper as a verification of these parameters' usefulness in the assessment of renal function.

The two presented parameters, K uptake constant and KEi index (Fig. 5), correlate highly with each other (0.94) but their meanings are slightly different. According to Rutland theory, K uptake constant corresponds strictly to kidney clearance, which is dependent on kidney size, and this is why the correlation coefficient between K and SKeGFR has the highest value (0.90). KEi parameter, because of its average nature, corresponds more to kidney efficiency and is independent of kidney size. For this reason, correlation coefficient between KEi and SKeGFR is lower (0.84), but KEi still correlates strongly with kidney clearance.

A greater spread of the K uptake constant around a regression line in patients with higher eGFR levels (Fig. 3) is caused by errors of eGFR values at such levels [9], i.e. due to the imperfections of the verification method. Another source of the scatter on the graphs (Fig. 3, 4) might be the fact that testing for serum creatinine level was performed in different labs, using tests from different producers. However, higher correlation coefficients between the K and SKeGFR uptake constant and KEi and SKeGFR than between SF and SKeGFR (0.90 and 0.84 vs 0.64) indicate higher usefulness of those parameters in assessment of uptake function of individual kidneys by these values than SF.

Due to the retrospective character of this preliminary analysis, it was impossible to use more accurate, measured GFR (e.g. using  $^{99m}\text{Tc}$ -DTPA clearance) as a reference method. This will be the subject of a future prospective study.

The presented method ensures high repeatability mainly due to the high automation of data processing. The most important was a reproducibility of a method generating a heart curve. Using an average value of the highest 20 pixels within heart ROI means that shape and area under a cardiac curve remained the same regardless of an operator processing the study. In case of

renal curves, an isocontour method (30% of the maximum value in the kidney) applied to summed images of second and third minutes of the study was of great importance. However, in cases when fragments of renal parenchyma were omitted by isocontour or when kidney shape was atypical — it was necessary to manually draw a fragment or the entire kidney ROI.

The method also avoids errors introduced by the need to measure the administered activity. Thanks to this, even a paravenous injection should not affect negatively the quantitative parameters of kidney function.

Our method also assumes, as demonstrated by Rehling et al. [5], that the absorption of radiation emitted by kidneys is similar to the absorption of radiation coming from the heart (these effects cancel each other out), hence it is not necessary to apply corrections accounting for the absorption of radiation. As Rehling et al. showed, these corrections can be omitted, especially in the light of the fact that differences in the depth of the kidneys in patient in the lying position, exceeding 1 cm, are relatively rare [23].

## Conclusions

A method of calculating the uptake constant K (value proportional to kidney clearance) presented here in application to  $^{99m}\text{Tc}$ -EC, due to its high degree of automation, is characterized by high repeatability. In clinical situations where the classic parameters of dynamic renal scintigraphy are unreliable, the use of the KEi parameter (average clearance per pixel) should improve the diagnostic effectiveness of this study, including differential diagnosis of uropathy and obstructive nephropathy or cirrhotic and hypoplastic kidney.

## Appendix

Rutland space — a space described by variables created on renographic and cardiac curves. At the initial stage of the renoscintigraphic examination (2–3 minutes of the study), the distribution of points in this space is approximated by a straight line described by the equation:

$$\frac{R(t)}{H(t)} = K \cdot \frac{\int_0^t H(t)dt}{H(t)} + F \quad (\text{E1})$$

where:

R(t) — kidney (renographic) curve after background subtraction

H(t) — cardiac curve. The author's modification of the method

uses of a sum of 20 pixels with maximum values within the heart ROI,

F — blood background subtraction factor,

K — uptake constant, fraction of blood activity taken up per time unit — can be calculated as a slope of the straight line described by equation E1. This value reflects the clearance of individual kidneys and is dependent on kidney size. After dividing this value by kidney ROI area, the KEi parameter was obtained, reflecting the average efficiency of the kidney in filtering blood.

## References

1. Taylor AT, Brandon DC, de Palma D, et al. SNMMI Procedure Standard/EANM Practice Guideline for Diuretic Renal Scintigraphy in Adults With Suspected Upper Urinary Tract Obstruction 1.0. *Semin Nucl Med.*

- 2018; 48(4): 377–390, doi: [10.1053/j.semnuclmed.2018.02.010](https://doi.org/10.1053/j.semnuclmed.2018.02.010), indexed in Pubmed: [29852947](https://pubmed.ncbi.nlm.nih.gov/29852947/).
2. Esteves FP, Taylor A, Manatunga A, et al. 99mTc-MAG3 renography: normal values for MAG3 clearance and curve parameters, excretory parameters, and residual urine volume. *AJR Am J Roentgenol.* 2006; 187(6): W610–W617, doi: [10.2214/AJR.05.1550](https://doi.org/10.2214/AJR.05.1550), indexed in Pubmed: [17114514](https://pubmed.ncbi.nlm.nih.gov/17114514/).
  3. Rutland MD. A comprehensive analysis of renal DTPA studies. I. Theory and normal values. *Nucl Med Commun.* 1985; 6(1): 11–20, doi: [10.1097/00006231-198501000-00003](https://doi.org/10.1097/00006231-198501000-00003), indexed in Pubmed: [3916534](https://pubmed.ncbi.nlm.nih.gov/3916534/).
  4. Patlak CS, Goldstein DA, Hoffman JF. The flow of solute and solvent across a two-membrane system. *J Theor Biol.* 1963; 5(3): 426–442, doi: [10.1016/0022-5193\(63\)90088-2](https://doi.org/10.1016/0022-5193(63)90088-2), indexed in Pubmed: [5875168](https://pubmed.ncbi.nlm.nih.gov/5875168/).
  5. Rehling M, Möller ML, Lund JO, et al. 99mTc-DTPA gamma-camera renography: normal values and rapid determination of single-kidney glomerular filtration rate. *Eur J Nucl Med.* 1985; 11(1): 1–6, doi: [10.1007/BF00440952](https://doi.org/10.1007/BF00440952), indexed in Pubmed: [3899656](https://pubmed.ncbi.nlm.nih.gov/3899656/).
  6. Bubeck B, Brandau W, Eisenhut M, et al. The tubular extraction rate (TER) of 99mTc-MAG3: a new quantitative parameter of renal function. *Nuc Compact.* 1987; 18(5).
  7. Tondeur M, Piepsz A, Dobbeleir A, et al. Technetium 99m mercaptoacetyltriglycine gamma camera clearance calculations: methodological problems. *Eur J Nucl Med.* 1991; 18(2): 83–86, doi: [10.1007/BF00950751](https://doi.org/10.1007/BF00950751), indexed in Pubmed: [1828421](https://pubmed.ncbi.nlm.nih.gov/1828421/).
  8. Kabasakal L. Technetium-99m ethylene dicysteine: a new renal tubular function agent. *Eur J Nucl Med.* 2000; 27(3): 351–357, doi: [10.1007/s002590050045](https://doi.org/10.1007/s002590050045), indexed in Pubmed: [10774890](https://pubmed.ncbi.nlm.nih.gov/10774890/).
  9. Levey AS, Stevens LA, Schmid CH, et al. CKD-EPI (Chronic Kidney Disease Epidemiology Collaboration). A new equation to estimate glomerular filtration rate. *Ann Intern Med.* 2009; 150(9): 604–612, doi: [10.7326/0003-4819-150-9-200905050-00006](https://doi.org/10.7326/0003-4819-150-9-200905050-00006), indexed in Pubmed: [19414839](https://pubmed.ncbi.nlm.nih.gov/19414839/).
  10. Piepsz A, Dobbeleir A, Erbsmann F. Measurement of separate kidney clearance by means of 99mTc-DTPA complex and a scintillation camera. *Eur J Nucl Med.* 1977; 2(3): 173–177, doi: [10.1007/BF00257276](https://doi.org/10.1007/BF00257276), indexed in Pubmed: [913431](https://pubmed.ncbi.nlm.nih.gov/913431/).
  11. Schlegel JU, Halikiopoulos HL, Prima R. Determination of filtration fraction using the gamma scintillation camera. *J Urol.* 1979; 122(4): 447–450, doi: [10.1016/s0022-5347\(17\)56457-5](https://doi.org/10.1016/s0022-5347(17)56457-5), indexed in Pubmed: [480482](https://pubmed.ncbi.nlm.nih.gov/480482/).
  12. Galli G, Rufini V, Vellante C, et al. Estimation of glomerular filtration rate with 99Tc(m)-DTPA: a comparative assessment of simplified methods. *Nucl Med Commun.* 1997; 18(7): 634–641, doi: [10.1097/00006231-199707000-00007](https://doi.org/10.1097/00006231-199707000-00007), indexed in Pubmed: [9342101](https://pubmed.ncbi.nlm.nih.gov/9342101/).
  13. Taylor AJr, Corrigan PL, Galt J, et al. Measuring technetium-99m-MAG3 clearance with an improved camera-based method. *J Nucl Med.* 1995; 36(9): 1689–1695.
  14. Taylor AT, Taylor AT. Radionuclides in nephrourology, part 1: Radiopharmaceuticals, quality control, and quantitative indices. *J Nucl Med.* 2014; 55(4): 608–615, doi: [10.2967/jnumed.113.133447](https://doi.org/10.2967/jnumed.113.133447), indexed in Pubmed: [24549283](https://pubmed.ncbi.nlm.nih.gov/24549283/).
  15. Peters AM. Quantification of renal haemodynamics with radionuclides. *Eur J Nucl Med.* 1991; 18(4): 274–286, doi: [10.1007/BF00186653](https://doi.org/10.1007/BF00186653), indexed in Pubmed: [2070806](https://pubmed.ncbi.nlm.nih.gov/2070806/).
  16. Bocher M, Shrem Y, Tappiser A, et al. Tc-99m mercaptoacetyltriglycine clearance: comparison of camera-assisted methods. *Clin Nucl Med.* 2001; 26(9): 745–750, doi: [10.1097/00003072-200109000-00001](https://doi.org/10.1097/00003072-200109000-00001), indexed in Pubmed: [11507290](https://pubmed.ncbi.nlm.nih.gov/11507290/).
  17. Wesolowski MJ, Conrad GR, Šámal M, et al. A simple method for determining split renal function from dynamic (99m)Tc-MAG3 scintigraphic data. *Eur J Nucl Med Mol Imaging.* 2016; 43(3): 550–558, doi: [10.1007/s00259-015-3216-1](https://doi.org/10.1007/s00259-015-3216-1), indexed in Pubmed: [26537286](https://pubmed.ncbi.nlm.nih.gov/26537286/).
  18. Prigent A, Cosgriff P, Gates G, et al. Consensus report on quality control of quantitative measurements of renal function obtained from the renogram: International consensus committee from the scientific committee of radionuclides in nephrourology. *Seminars in Nuclear Medicine.* 1999; 29(2): 146–159, doi: [10.1016/s0001-2998\(99\)80005-1](https://doi.org/10.1016/s0001-2998(99)80005-1).
  19. Blaufox MD. Renal background correction and measurement of split renal function: The challenge : Editorial Comment: *EJNM-D-15-00322*, M Donald Blaufox, MD, PhD. *Eur J Nucl Med Mol Imaging.* 2016; 43(3): 548–549, doi: [10.1007/s00259-015-3253-9](https://doi.org/10.1007/s00259-015-3253-9), indexed in Pubmed: [26572761](https://pubmed.ncbi.nlm.nih.gov/26572761/).
  20. Surma MJ, Anderson P. The functional imaging of kidney clearance. Pt. 1. Methodology. *Problemy Medycyny Nuklearnej.* 1993; 7(14): 185–198.
  21. Kuśmierek J, Pietrzak-Stelmasiak E, Bieńkiewicz M, et al. Diagnostic efficacy of parametric clearance images in detection of renal scars in children with recurrent urinary tract infections. *Ann Nucl Med.* 2015; 29(3): 313–318, doi: [10.1007/s12149-014-0944-4](https://doi.org/10.1007/s12149-014-0944-4), indexed in Pubmed: [25563578](https://pubmed.ncbi.nlm.nih.gov/25563578/).
  22. Gordon I, Anderson PJ, Lythgoe MF, et al. Technetium-99m-mercaptoacetyltriglycine replace technetium-99m-dimercaptosuccinic acid in the exclusion of a focal renal defect? *J Nucl Med.* 1992; 33(12): 2090–2093.
  23. Tonnesen KH. Influence on the radiorenogram of variation in skin to kidney distance and the clinical importance hereof. *Radionuclide in Nephrology.* 1975: 79–86.

# Kidney efficiency index quantitative parameter of a dynamic renal scintigraphy. II. usefulness in the diagnosis of obstructive nephropathy

Paweł Cichoński<sup>1</sup>, Krzysztof Filipczak<sup>2</sup>, Anna Plachcińska<sup>2</sup>, Jacek Kusmierk<sup>1</sup>

<sup>1</sup>Medical University of Łódź, Department of Nuclear Medicine, Poland

<sup>2</sup>Medical University of Łódź, Department of Quality Control and Radiological Protection, Poland

[Received 8 V 2020; Accepted 24 VII 2020]

## Abstract

**BACKGROUND:** One of the main indications for DRS is a diagnosis of obstructive uro-/nephropathy. In standard practice, this study includes the assessment of sequential scintigraphic images, renographic curves and such quantitative parameters as  $T_{MAX}$ ,  $T_{1/2}$  and split function of each kidney (SF). Due to the relative nature of SF and limitations of diagnostic capabilities of  $T_{MAX}$  and  $T_{1/2}$ , DRS was expanded to include new quantitative parameters describing kidney function in absolute values. This study aims to evaluate the usefulness of kidney efficiency index (KEi) — new, in-house developed parameter proportional to the average clearance function of the kidney.

**MATERIAL AND METHODS:** The study included 156 people aged 18–84 (average 51) years. The first group, from which normative values of new parameters were determined, consisted of 20 healthy volunteers. The second group consisted of 136 patients selected retrospectively, based on archived scintigraphic data. “Normalcy rate” (percentage of normal results among selected 62 patients with a low likelihood of obstructive uro-/nephropathy) was used to evaluate the reliability of KEi. A comparative differential analysis of obstructive uro-/nephropathy, based on standard and new DRS parameters, was performed on selected 74 patients (92 kidneys) with single functioning kidney or bilateral obstructive uropathy, where SF is unreliable.

**RESULTS:** Normative values:  $KEi \geq 8$ ; Normalcy rate for KEi: 95%. In comparison with standard DRS evaluation, application of KEi changed the diagnosis in 1/3 of assessed kidneys (from uropathy to nephropathy in 27/92 kidneys and vice versa in 4 kidneys).

**CONCLUSIONS:** KEi enables reproducible, quantitative assessment of absolute kidney function without any modifications of the standard DRS protocol. Its values can be compared between independent studies (e.g. follow-up examinations). KEi corrected the diagnosis of obstructive uro-/nephropathy in cases of single functioning kidney or bilateral obstructive uropathy.

**KEY words:** humans; kidney; radioisotope renography; radiopharmaceuticals; technetium Tc 99m-ethylenedicysteine

Nucl Med Rev 2020; 23, 2: 84–88

## Introduction

Dynamic renal scintigraphy (DRS) allows the evaluation of two functions of the kidney — uptake function and transport function. Interpretation of this study consists of visual assessment of sequential scintigraphic images, renographic curves and

analysis of quantitative parameters, such as an individual contribution of each kidney to their total function (SF — split function) as well as times  $T_{MAX}$  and  $T_{1/2}$  [1–3].

SF is the most important quantitative parameter in the standard DRS study and is often critical when making crucial clinical decisions (e.g. qualification of patients for nephrectomy). However, it has a significant limitation. Due to the fact that it shows the function of one kidney relative to the other, there are situations in which its value loses credibility, e.g. when assessing the function of a single kidney, or in case of disorders affecting both kidneys. Due to significant, often fundamental importance of DRS in making decisions about further management of patients, there are attempts to expand this study with additional parameters allowing

Correspondence to: Paweł Cichoński  
8/10 Czechosłowska St, 92–216 Łódź  
phone: 42 675–72–90; fax: 42 675–72–85  
e-mail: pawelcichoński.zmn@gmail.com

**Table 1.** Demographic data of all examined groups

	Number of people (number of kidneys in parentheses) and their sex					Age
	Total	Women	Men	Min.	Max.	Avg. ± SD
Group I	20 (40)	15	5	26	66	50 ± 11
Group II	136 (216)	94	42	18	84	52 ± 18
Subgroup IIA	62 (124)	48	14	18	79	48 ± 17
Subgroup IIB	74 (92)	46	28	18	84	57 ± 19

the assessment and monitoring of absolute renal function also in the above-mentioned situations.

One such option is to determine the value of glomerular filtration rate (GFR) and compare it with SF to calculate single-kidney GFR (SKGFR) [4]. However, this requires additional radioisotope studies of blood samples taken from the patient after intravenous administration of the radiopharmaceutical ( $^{99m}\text{Tc}$ -DTPA), which are not widely available. Assessment of renal function in absolute values within the DRS itself, without the need for additional tests, is made possible by calculating clearance of radiopharmaceuticals using gamma-cameras (camera-based clearance), but its determination requires extending the DRS protocol by accurate measurement of injected activity and the depth of kidneys [5, 6].

This study evaluates the diagnostic potential of a new, original parameter — Kidney Efficiency index (KEi), generated using software developed in our Department [7, 8], that allows the assessment of renal function in absolute values, but without the need for additional tests or modification of the standard DRS protocol. A model clinical problem for analyzing the usefulness of the above-mentioned parameters is the differential diagnosis of obstructive uro- and nephropathy, which is the most common indication for DRS.

## Material and methods

The study covered 156 people aged 18–84 (average 51) years.

The subjects were separated into two groups. Group I — control, consisting of 20 healthy, adult volunteers (40 kidneys), which was used to determine normative values of evaluated parameters. Inclusion criteria for this group were as follows:

- no history of past or ongoing urinary tract diseases or other conditions that may lead to impaired renal function (such as systemic lupus, diabetes or uncontrolled hypertension)
- no features of urolithiasis, hydronephrosis, scarring or other focal lesions (e.g. cysts) in the kidneys in ultrasound, performed on the same day as DRS
- serum urea and creatinine levels within normal limits in tests performed on the same day as DRS

Group II included 136 adult patients, retrospectively selected from among those who underwent DRS in our Department in the years 2016–2019, based on archived medical documentation, including full data from the DRS study. In total, 216 kidneys were assessed (some patients from group IIB had only one functioning kidney). This group consisted of:

Subgroup IIA — 62 patients without scintigraphic features of obstructive uropathy or nephropathy (124 kidneys)

Subgroup IIB — 74 patients with no or trace function of one kidney (defined as SF < 10%); or with features of obstructive uropathy of both kidneys in standard study (92 kidneys in total)

Demographic data of all examined groups is summarized in Table 1.

All subjects underwent DRS performed according to the standard protocol used in our Department. All subjects drank 0.5 l of water about 30 minutes before the study and urinated just before commencing image acquisition. DRS was performed in the supine position using one of the GE scintillation cameras: Infinia Hawkeye 1, Infinia Hawkeye 4 or Optima NM/CT 640, equipped with low-energy general-purpose collimators (LEGP), after administration of standard activity of 111 MBq  $^{99m}\text{Tc}$ -EC [9, 10]. Field of view of the detectors covered both the kidneys and the heart of the subject and the images were recorded in a 128 x 128 pixel matrix. In case of a significantly slowed down urine outflow, i.e. renographic curve remaining above 30% of the peak level for the entirety of the base study (20 min.), DRS was extended by a diuretic test, carried out in accordance with the "F+20" protocol for additional 10 minutes [11].

Routine visual assessment of 2-minute sequential scintigraphic images and renographic curves were performed in all subjects, as well as the assessment of basic quantitative parameters obtained after conventional scintigraphic data processing. In group II, kidneys with features of obstructive uropathy or nephropathy were distinguished on this basis. Kidneys meeting at least 2 of the following 3 criteria were considered nephropathic: SF < 42%,  $T_{\text{MAX}} > 7$  min. or presence of uptake defect(s) in the peripheral part of the kidney cortex determined as a consensus by two specialists based on visual assessment of sequential images obtained in the uptake phase. On the other hand, absence of renographic curve decrease, or its decrease by less than 50% from the end of the case study after the diuretic test, were considered as features of obstructive uropathy (total or incomplete obstructive uropathy, respectively).

Afterwards, additional post-processing of scintigraphic data was performed, using the ImageJ program with the original plugin developed in our Department. The method of determining ROIs of heart, kidneys and extrarenal background was shown in the work by Filipczak et al. [7, 8]. ROIs plotted in this way were then used to generate time-activity curves showing changes of the radiopharmaceutical concentration in the heart and kidneys (the latter being corrected by subtracting non-renal background activity). These curves served as the basis for the calculation of all assessed parameters.

Based on Rutland's theory [12], uptake constant K was determined for each kidney [7, 8]. Its value is proportional to the

clearance function of a kidney. Then the average value of this parameter per pixel of whole kidney ROI was calculated, to make it independent from the size of the organ, which leads to obtaining KEi.

Reliability of assessed parameters was evaluated in multiple ways. KEi values, as shown in work by Filipczak et al. [7, 8], were strongly correlated with single-kidney eGFR (SKeGFR), where eGFR was calculated using the CKD-EPI formula [13–15] and multiplying it by SF value of each kidney.

“Normalcy rate” — the percentage of results within the normal range (according to normative values determined in the group of healthy volunteers) in group IIA, that is, in patients with no scintigraphic features of uropathy or obstructive nephropathy in standard DRS, was also used as a verification of the reliability of the method.

Next, a comparative analysis of the differentiation of obstructive uro-/nephropathy was performed based on standard and new DRS parameters in IIB subgroup, i.e. in situations where SF is unreliable.

Statistica version 13.1 was used for statistical analysis. Normality of data distributions was tested using Shapiro-Wilk’s test. In group I, the distribution of KEi values was normal, while values of  $T_{MAX}$  deviated from normal distribution. In group II and each of its subgroups, values of both parameters deviated from normal distribution. The statistical significance level (p) used in the study was 0.05.

## Results

Due to normal distribution of KEi values in the control group (I), its normative value was assumed as mean — 2 standard deviations, while for  $T_{MAX}$ , mean + 3 standard deviations were taken as normal limit. The results are summarized in Table 2.

KEi was within normal range in 118/124 kidneys from subgroup IIA (with very low probability of obstructive uro-/nephropathy) — “normalcy rate” 95%. The distribution of KEi values in group I and subgroup IIA was very similar (Fig. 1A and 1B, respectively).

In subgroup IIB (patients with bilateral uropathy or single active kidney), according to the standard DRS criteria assumed in this study, obstructive uropathy was found in 18/92 kidneys, and obstructive nephropathy was diagnosed in 25/92 kidneys. Distribution of KEi values in this subgroup was significantly different than in groups of healthy kidneys (Fig. 1C). Use of KEi changed the qualification in 31/92 kidneys (1/3) — in 4 cases (4%) corrected the qualification from nephropathy to uropathy, while in 27 cases (29%) KEi was below normal limit despite of lack of features of nephropathy in the evaluation of standard scintigraphic parameters (Fig. 2).

**Table 2.** Values of assessed parameters in examined groups with assumed normative limits

	TMAX [min]	KEi
Group I	3,6 ± 1,1	12,78 ± 2,46
Normal limits	< 7	≥ 8
Group II		
Subgroup IIA	4,4 ± 2,2	12,20 ± 2,87
Subgroup IIB	13,8 ± 11,3	9,32 ± 5,45

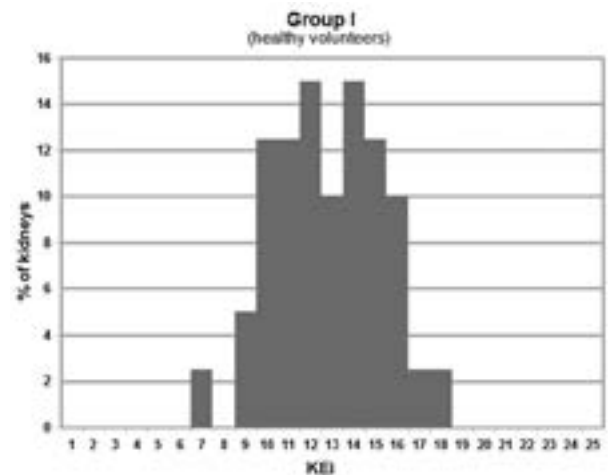


**Figure 1A.** Distribution of KEi values in kidneys from group I

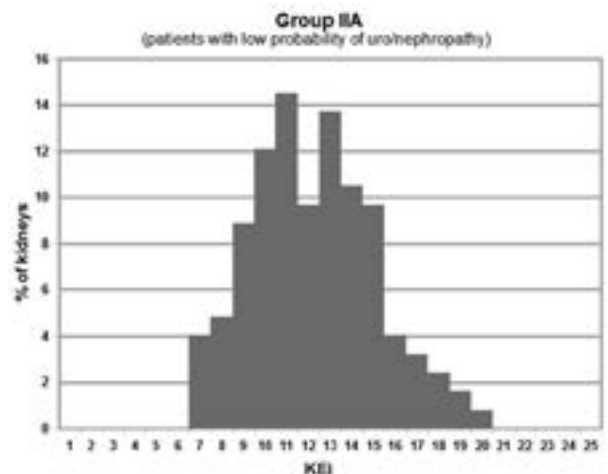


**Figure 1B.** Distribution of KEi values in kidneys from subgroup IIA

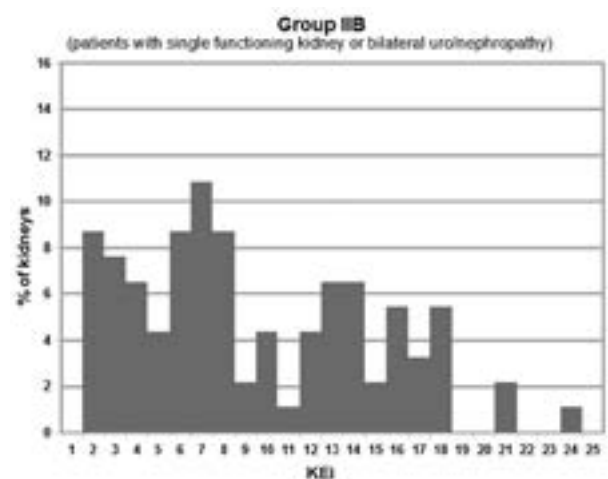


**Figure 1C.** Distribution of KEi values in kidneys from subgroup IIB

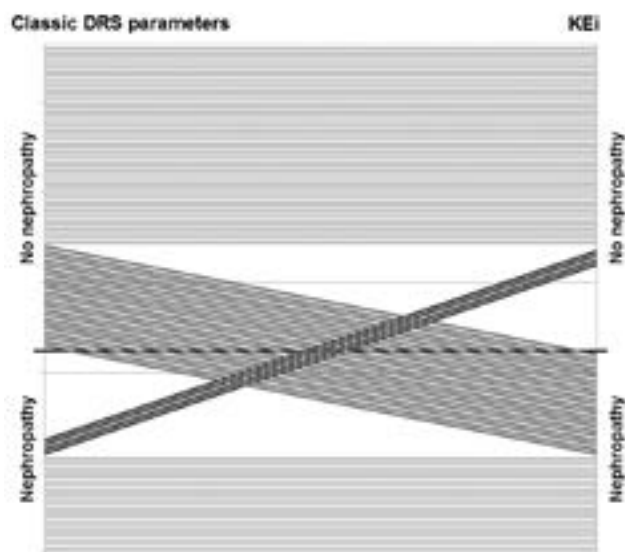


**Figure 2.** Change of kidney qualification in group IIB based on the values of KEi

There were 3 patients qualified as bilateral uropathy, whose kidneys had SF well within normal ranges and displayed no significant uptake defects, while KEi showed features of bilateral nephropathy. In the group of patients with single functioning kidney, in 7 cases KEi changed the classification to nephropathy while all 3 standard criteria suggested normal function of the kidney, that is SF was between 90 and 100%,  $T_{MAX}$  between 3 and 6 min. and visual assessment revealed no uptake defects at all.

## Discussion

SF, which is the main quantitative parameter of DRS, due to its relative nature has significant limitations reducing its usefulness in certain clinical situations. In case of bilateral renal dysfunction or only a single functioning kidney, reliable assessment of renal function is only possible by supplementing SF with the value of GFR of a given patient. However, this requires performing additional studies, e.g. using accurate, but time-consuming and labor-intensive methods for determining glomerular filtration with radioisotopes ( $^{99m}\text{Tc}$ -DTPA clearance) or as a simpler, but less accurate method for calculating estimated GFR using biochemical studies (e.g. serum creatinine level).

Therefore, methods that allow an assessment of renal cortex function in absolute values are being developed, based only on scintigraphic data obtained with gamma-cameras in DRS, without the need for taking blood samples or urine collection. Several such protocols have been created and camera-based clearance methods are even an integral part of modern scintillation camera software. However, for these techniques acquisition of additional - non-standard data is necessary, as described in the work by Filipczak et al. [7, 8], which in turn requires modification and expansion of the standard DRS protocol.

Original parameter KEi does not have these disadvantages. It is relatively easy to determine and relies only on post-processing

of standard scintigraphic data. Hence it can be used both routinely, or only in cases in which assessment of classic DRS parameters does not provide a conclusive diagnosis. It can also be applied retrospectively with ease, for example for scientific purposes.

One of the important arguments supporting the usefulness of this parameter, apart from its strong correlation with SKeGFR shown in work by Filipczak et al. [7, 8], is its high normalcy rate. In a group of patients with a very low probability of uropathy or nephropathy according to the standard DRS evaluation — subgroup IIA, KEi also showed values within the normal range in 95% of cases and the distribution of its values was very similar to group I. This confirms the accuracy of the normative limit established on a selected group of healthy volunteers. Distribution of KEi values in subgroup IIB, which consisted of both normally functioning and nephropathic kidneys, was significantly different.

Value of KEi, that represents the average clearance function of a kidney, is completely independent of its size. This allows determination of normative values, based on a group of healthy volunteers with no impairments of kidney function, that can later be used for evaluation of other kidneys, regardless of their size. This parameter can be useful not only in the diagnosis of obstructive nephropathy, but also for the differentiation of a small, but normally functioning (hypoplastic) kidney from an insufficient one (e.g. cirrhotic), and in assessing a small kidney in the diagnosis of renovascular hypertension. This will be the subject of our further research.

In summary, it should be noted that KEi extends the capabilities of DRS with a repeatable, quantitative assessment of absolute, individual kidney function. This parameter does not require any modifications of a routine protocol of the study (and thus can be determined in post-processing, e.g. only if the standard DRS result is ambiguous). It was shown that use of this parameter improves the diagnostic effectiveness of DRS in the differential diagnosis of obstructive uropathy and nephropathy.

## References

1. Taylor AT, Brandon DC, de Palma D, et al. SNMMI Procedure Standard/EANM Practice Guideline for Diuretic Renal Scintigraphy in Adults With Suspected Upper Urinary Tract Obstruction 1.0. *Semin Nucl Med.* 2018; 48(4): 377–390, doi: [10.1053/j.semnuclmed.2018.02.010](https://doi.org/10.1053/j.semnuclmed.2018.02.010), indexed in Pubmed: [29852947](https://pubmed.ncbi.nlm.nih.gov/29852947/).
2. Durand E, Blaufox MD, Britton KE, et al. International Scientific Committee of Radionuclides in Nephrourology (ISCORN). International Scientific Committee of Radionuclides in Nephrourology (ISCORN) consensus on renal transit time measurements. *Semin Nucl Med.* 2008; 38(1): 82–102, doi: [10.1053/j.semnuclmed.2007.09.009](https://doi.org/10.1053/j.semnuclmed.2007.09.009), indexed in Pubmed: [18096466](https://pubmed.ncbi.nlm.nih.gov/18096466/).
3. Taylor A, Nally JV. Clinical applications of renal scintigraphy. *AJR Am J Roentgenol.* 1995; 164(1): 31–41, doi: [10.2214/ajr.164.1.7998566](https://doi.org/10.2214/ajr.164.1.7998566), indexed in Pubmed: [7998566](https://pubmed.ncbi.nlm.nih.gov/7998566/).
4. Piepsz A, Dobbeleir A, Erbsmann F. Measurement of separate kidney clearance by means of  $^{99m}\text{Tc}$ -DTPA complex and a scintillation camera. *European Journal of Nuclear Medicine.* 1977; 2(3), doi: [10.1007/bf00257276](https://doi.org/10.1007/bf00257276).
5. Schlegel JU, Halikiopoulos HL, Prima R. Determination of filtration fraction using the gamma scintillation camera. *J Urol.* 1979; 122(4): 447–450, doi: [10.1016/s0022-5347\(17\)56457-5](https://doi.org/10.1016/s0022-5347(17)56457-5), indexed in Pubmed: [480482](https://pubmed.ncbi.nlm.nih.gov/480482/).
6. Gates GF. Glomerular filtration rate: estimation from fractional renal accumulation of  $^{99m}\text{Tc}$ -DTPA (stannous). *AJR Am J Roentgenol.* 1982; 138(3): 565–570, doi: [10.2214/ajr.138.3.565](https://doi.org/10.2214/ajr.138.3.565), indexed in Pubmed: [7039273](https://pubmed.ncbi.nlm.nih.gov/7039273/).

7. Filipczak K, Cichocki P, Surma M, et al. Renal Clearance Function Index—a New Quantitative Parameter of a Dynamic Renal Scintigraphy. *Eur J Nucl Med Mol Imaging*. 2019; 46: 243–4.
8. Filipczak K, Cichocki P, Kuśmierk J, et al.. Kidney Efficiency Index — quantitative parameter of a dynamic renal scintigraphy. I. Theory and preliminary verification. *Nucl Med Rev* 2020; 23, 2:53-58
9. Surma MJ, Wiewiórka J, Szadkowska A, et al. Pharmacokinetic characteristics of <sup>99m</sup>Tc-Ethylene-l-dicysteine (<sup>99m</sup>Tc-EC). *Nucl Med Rev Cent East Eur*. 1999; 2(1): 20–27, indexed in Pubmed: [14600996](#).
10. Surma MJ, Wiewióra J, Liniecki J. Usefulness of <sup>99m</sup>Tc-N,N'-ethylene-1-dicysteine complex for dynamic kidney investigations. *Nucl Med Commun*. 1994; 15(8): 628–635, doi: [10.1097/00006231-199408000-00007](#), indexed in Pubmed: [7970444](#).
11. O'Reilly P, Aurell M, Britton K, et al. Consensus on diuresis renography for investigating the dilated upper urinary tract. *Radionuclides in Nephrourology Group. Consensus Committee on Diuresis Renography. J Nucl Med*. 1996; 37(11): 1872–1876, indexed in Pubmed: [8917195](#).
12. Rutland MD. A comprehensive analysis of renal DTPA studies. I. Theory and normal values. *Nucl Med Commun*. 1985; 6(1): 11–20, doi: [10.1097/00006231-198501000-00003](#), indexed in Pubmed: [3916534](#).
13. Kidney Disease: Improving Global Outcomes (KDIGO) CKD Work Group. Clinical practice guideline for the evaluation and management of chronic kidney disease. *Kidney Int.* ; 3(1): 1–150.
14. Levey A. A More Accurate Method To Estimate Glomerular Filtration Rate from Serum Creatinine: A New Prediction Equation. *Annals of Internal Medicine*. 1999; 130(6): 461, doi: [10.7326/0003-4819-130-6-199903160-00002](#).
15. Dias AH, Pintão S, Almeida P et al. Comparison of GFR calculation methods: MDRD and CKD-EPI vs. (<sup>99m</sup>Tc-DTPA tracer clearance rates. *Scand J Clin Lab Invest*. 2013; 73(4): 334–338, doi: [10.3109/00365513.2013.780663](#), indexed in Pubmed: [23586782](#).

# The levels of oxidative and nitrosative stress in patients who had <sup>99m</sup>Tc-MIBI myocardial perfusion scintigraphy and <sup>99m</sup>Tc-DMSA, <sup>99m</sup>Tc-MAG-3 renal scintigraphy

Ebru Salmanoglu<sup>1</sup> , Ergul Belge Kurutas<sup>2</sup> 

<sup>1</sup>Department of Nuclear Medicine, Kahramanmaraş Sutcu Imam University, Faculty of Medicine, Kahramanmaraş, Turkey

<sup>2</sup>Department of Medical Biochemistry, Kahramanmaraş Sutcu Imam University, Faculty of Medicine, Kahramanmaraş, Turkey

[Received 4 V 2020; Accepted 18 VI 2020]

## Abstract

**BACKGROUND:** Ionizing radiation is a strong stimulator of reactive oxygen species (ROS) and reactive nitrogen species (RNS). These reactive species may cause oxidative and nitrosative stress. In this study, we aimed to evaluate possible effects of <sup>99m</sup>Technetium (<sup>99m</sup>Tc)-methoxyisobutylisonitrite (MIBI), <sup>99m</sup>Tc-dimercaptosuccinic acid (DMSA), <sup>99m</sup>Tc-mercaptoacetyltriglycine (MAG-3) on oxidative and nitrosative stress biomarkers in patients who were performed myocardial perfusion scintigraphy (MPS) and renal scintigraphy.

**MATERIAL AND METHODS:** Patients (n = 29) who were referred to nuclear medicine department were chosen as the patient group. They were divided into three subgroups according to the type of disease and <sup>99m</sup>Tc labelled agent. The first patient group had MPS (n = 9). The second patient group had <sup>99m</sup>Tc-DMSA renal scintigraphy (n = 12). The third patient group had <sup>99m</sup>Tc-MAG-3 renal scintigraphy (n = 8). The blood samples were taken from first, second and third patient groups 1 h, 3 h, 45 min after injection of the agent, respectively. The samples were taken from healthy volunteers (n = 25) as a control group. Alterations in catalase (CAT), superoxide dismutase (SOD), malondialdehyde (MDA) levels as oxidative stress biomarkers and nitric oxide (NO) and 3-Nitrotyrosine (3-NTx) levels as nitrosative stress biomarkers in all blood samples were evaluated.

**RESULTS:** Results of MPS and renal scintigraphy performed patients were compared with control group separately. CAT, SOD, MDA and 3-NTx levels were higher in the first group than the control group (p < 0.05). Although NO levels were higher in the first group than the control group, it was not statistically significant (p > 0.05). CAT and SOD levels were lower in second and third groups than the control group (p < 0.05). However, MDA, NO, 3-NTx levels were higher in second and third groups than the control group (p < 0.05).

**CONCLUSIONS:** These results show that oxidative and nitrosative balance is impaired due to ionization radiation. These reactive species might stimulate an adaptive and protective cellular defense mechanism in irradiated cells soon after exposure to radiation. Thereby, this mechanism protect organism from the effects of low dose ionizing radiation.

**KEY words:** ionizing radiation; oxidative stress; nitrosative stress

Nucl Med Rev 2020; 23, 2: 89–96

Correspondence to: Ebru Salmanoglu  
 Department of Nuclear Medicine, Kahramanmaraş Sutcu Imam University,  
 Faculty of Medicine, Avsar Kampus, 46040, Kahramanmaraş, Turkey  
 Phone: +903443003747, Fax: +903443003409  
 e-mail: ebrusalmanoglu@yahoo.co

## Introduction

<sup>99m</sup>Technetium (<sup>99m</sup>Tc) and <sup>99m</sup>Tc-labeled radiopharmaceuticals widely are used more than 50 years in clinical nuclear medicine applications. <sup>99m</sup>Tc has both 140 keV gamma emission

and approximately 5 low energy Auger and internal conversion electrons per decay.  $^{99m}\text{Tc}$ 's half-life ( $t_{1/2}$ ) is six hours.  $^{99m}\text{Tc}$ -methoxyisobutylisonitrite (MIBI) is used for myocardial perfusion scintigraphy (MPS) [1, 2].  $^{99m}\text{Tc}$ -dimercaptosuccinic acid (DMSA) is used for renal cortical scintigraphy and  $^{99m}\text{Tc}$ -mercaptoacetyltriglycine (MAG-3) is used for dynamic renal scintigraphy [3]. Although the importance of  $^{99m}\text{Tc}$  has been accepted in the worldwide, it results high ionization radiation intensity near the radionuclide's decay position due to emitted beams [2]. After intravenous (i.v.) injection of the radiopharmaceutical, it distributes into living cells and ionizing radiation is absorbed by these living cells. Cellular exposure to ionizing radiation initiates oxidizing process. This process damages cells and their structures at the atomic level via direct interactions with macromolecules such as DNA, RNA, proteins and lipids or radiolysis of water. Furthermore, this damage might spread to neighbour cells via bystander effect and persist in the progeny for many generations [4–7].

During the radiolysis of water-reactive oxygen species (ROS) including superoxide anion, hydrated electron, hydroxyl radical, hydrogen peroxide, organic hydroperoxides, alkoxy and peroxy radicals, hypochlorite, peroxyxynitrite are produced. Ionizing radiation also causes the production of reactive nitrogen species (RNS). As a result of that, large amounts of nitric oxide and peroxyxynitrite anion are produced [7, 8].

ROS/RNS initiate harmful process in cells. Different signalling cascades adaptive responses including DNA repair, antioxidant reactions and different signalling cascades are stimulated to overcome these harmful process. Ionizing radiation regulates antioxidant enzyme activity depending on dose and linear energy transfer. While a low dose of LET radiation (gamma rays) at low dose-rate stimulates antioxidant defense system, high LET radiation spreads oxidative stress both in the irradiated cells and nearby cells by means of bystander effect [7]. Antioxidants defense systems play a crucial role for preventing damage caused by ROS/RNS and eliminating ROS/RNS. The imbalance in the production and the elimination of ROS/RNS and various reducing or antioxidant systems of the body causes oxidative/nitrosative stress [7, 9, 10].

To our knowledge, this is the first study in the current literature that investigates the effects of  $^{99m}\text{Tc}$ -MIBI,  $^{99m}\text{Tc}$ -DMSA and  $^{99m}\text{Tc}$ -MAG-3 oxidative/nitrosative damage in human. The present study was aimed to evaluate levels of both oxidative stress biomarkers including catalase (CAT), superoxide dismutase (SOD), malondialdehyde (MDA) and nitrosative stress biomarkers including nitric oxide (NO) and 3-Nitrotyrosine (3-NTx) in patients who were clinically indicated and underwent  $^{99m}\text{Tc}$ -MIBI MPS,  $^{99m}\text{Tc}$ -DMSA renal cortical scintigraphy and  $^{99m}\text{Tc}$ -MAG-3 dynamic renal scintigraphy.

## Material and methods

### Ethics

This study was conducted after obtaining approval from the local ethical committee of Sutcu Imam University, Medical Faculty, Kahramanmaraş, Turkey. Also, the study was conducted in accordance with the Declaration of Helsinki on medical protocols and ethics. As we used routinely generated data with no identifying information, the study carries no harm whatsoever to patients. Data were

used only for scientific purposes. All participants were informed extensively about this study and signed an informed-consent form before they were enrolled in this study.

### Study population

A total of 29 patients who were referred to the nuclear medicine department and who were routine scintigraphic imaging methods were indicated were chosen as the patient group. The patients were divided into three subgroups based on the type of disease and  $^{99m}\text{Tc}$  labelled agent. The  $^{99m}\text{Tc}$  labelled imaging agents were administered at clinical doses.

In 9 patients (2 female, 7 male) with a mean age of  $52 \pm 9.7$  years (range 38–67 years), MPS with  $^{99m}\text{Tc}$ -MIBI was obtained (group 1).

In 12 patients (8 female, 4 male) with a mean age of  $20 \pm 21.6$  years (range 1–66 years), renal cortical scintigraphy with  $^{99m}\text{Tc}$ -DMSA was carried out (group 2).

In 8 patients (6 female, 2 male) with a mean age of  $28 \pm 21.4$  years (range 6 and 66 years) dynamic renal scintigraphy with  $^{99m}\text{Tc}$ -MAG-3 was performed (group 3).

The blood samples were taken from first group 1h after intravenous (i.v.) injection of  $^{99m}\text{Tc}$ -MIBI, from second group 3h after i.v. injection of  $^{99m}\text{Tc}$ -DMSA, from third group 45min, after i.v. injection of  $^{99m}\text{Tc}$ -MAG-3. The samples were also taken from a total of 25 healthy volunteers with a mean age of  $39 \pm 13.1$  years (range 18–63 years) as a control group.

Alterations in both CAT, SOD, MDA levels as oxidative stress biomarkers and NO and 3-NTx levels as nitrosative stress biomarkers in all blood samples were evaluated.

### Biochemical analysis in erythrocytes

The blood samples were centrifuged at 3000 g for 10 minutes at 4°C. Plasma was separated and the buffy coat was discarded by aspiration. Erythrocytes were washed 4 times with cold physiological saline and stored at  $-70^\circ\text{C}$  until analysis. The CAT activity in erythrocyte was measured in samples by the method applied by Beutler [11]. The decomposition of the substrate  $\text{H}_2\text{O}_2$  was monitored spectrophotometrically at 240 nm. The activity of CAT was expressed as U/g Hb. The SOD activities in erythrocyte were estimated by the use of the method described by Fridovich [12]. SOD activity was expressed as U/g Hb. Lipid peroxidation level in the plasma samples was expressed in MDA. Measurement was based on the method of Ohkawa [13]. MDA levels were expressed as nmol/mL. NO and 3-NTx levels in plasma samples were determined with a "sandwich" enzyme-linked immunosorbent assay kits (mybio-source human elisa kits, USA) according to the manufacturers' protocol. Then, 3-NTx levels were given as nmol/L.

### Statistical analysis

Data were analyzed using the statistical package SPSS for Windows version 20.0 (SPSS Inc., Chicago, IL.). Results were expressed as mean  $\pm$  SD. The conformability of the quantitative data to the normal distribution was examined by the Kolmogorov–Smirnov test. The Mann–Whitney U-test was used to compare mean values for all parameters between patients and control groups. p value  $< 0.05$  was accepted as statistically significant.

## Results

Results of MPS and renal scintigraphy performed patients were compared with control group separately.

Initially, MPS performed patients group were evaluated. The antioxidant enzyme activities of CAT and SOD were statistically significantly higher in the first patient group than the control group ( $p < 0.05$ ) as shown in Figure 1A and 1B. CAT and SOD levels were approximately 1.9 and 1.7 fold higher in the first patient group than healthy subjects, respectively. In addition, MDA levels were also statistically significantly higher in the first patient group than the control group ( $p < 0.05$ ) and its levels were nearly 1.6 fold higher in the first patient group as shown in Figure 1C. 3-NTx levels were statistically significantly nearly 1.8 fold higher in the first patient group than control group ( $p < 0.05$ ) as shown in Figure 2B. NO levels were nearly 1.2 fold higher in the first patient group than control group ( $p > 0.05$ ) as shown in Figure 2A.

Then, renal scintigraphy performed patients group were evaluated. CAT and SOD levels were statistically significantly lower in second, third and total renal scintigraphy performed patient groups than control group ( $p < 0.05$ ). CAT and SOD levels were nearly 2 and 3 fold lower in the second patient group than control group, respectively (Fig. 3A and 3B). CAT and SOD levels were nearly 1.7 and 3 fold lower in the third patient group than control group, respectively (Fig. 5A and 5B). CAT and SOD levels were nearly 2 and 3 fold lower in total renal scintigraphy performed patients group than control group, respectively (Fig. 7A and 7B). MDA levels were statistically significantly higher in second, third and total renal scintigraphy performed patient groups than the control group ( $p < 0.05$ ). MDA levels were nearly 2, 2 and 1.8 fold higher in second, third and total renal scintigraphy performed patient groups than the control group, respectively (Fig. 3C, 5C and 7C). NO levels were nearly 1.5, 2 and 1.6 fold higher in second, third and total renal scintigraphy performed patient groups than the control group, respectively ( $p < 0.05$ ) (Fig. 4A, 6A and 8A). 3-NTx levels were nearly 2.3, 2.85 and 2.6 fold higher in second, third and total renal scintigraphy performed patient groups than the control group, respectively ( $p < 0.05$ ) (Fig. 4B, 6B and 8B).

## Discussion

In this study, we investigated the effect of ionizing radiation on both oxidative and nitrosative stress parameters in patients who were clinically indicated  $^{99m}\text{Tc}$ -MIBI MPS,  $^{99m}\text{Tc}$ -DMSA renal cortical scintigraphy,  $^{99m}\text{Tc}$ -MAG-3 dynamic renal scintigraphy. This is the first study that evaluates levels of nitrosative stress parameters in patients with these scintigraphic imaging agents.

$^{99m}\text{Tc}$ -MIBI is a lipophilic cationic complex, enters cells by passive diffusion. It is localized mostly in the mitochondria of myocytes due to negative mitochondrial membrane potential [1, 2, 15].  $^{99m}\text{Tc}$ -DMSA is a renal cortical agent that primarily bound in the proximal tubule in the renal cortex for a prolonged time after injection.  $^{99m}\text{Tc}$ -MAG-3 is commonly used renal tubular agent in nuclear medicine practice [3]. It is known that the DNA-binding traits of  $^{99m}\text{Tc}$  labelled agents augments radiotoxicity of these agents [1, 2, 14–16].

CAT, SOD, MDA, 3-NTx levels were found statistically significantly higher in MPS performed patients than control group ( $p < 0.05$ )

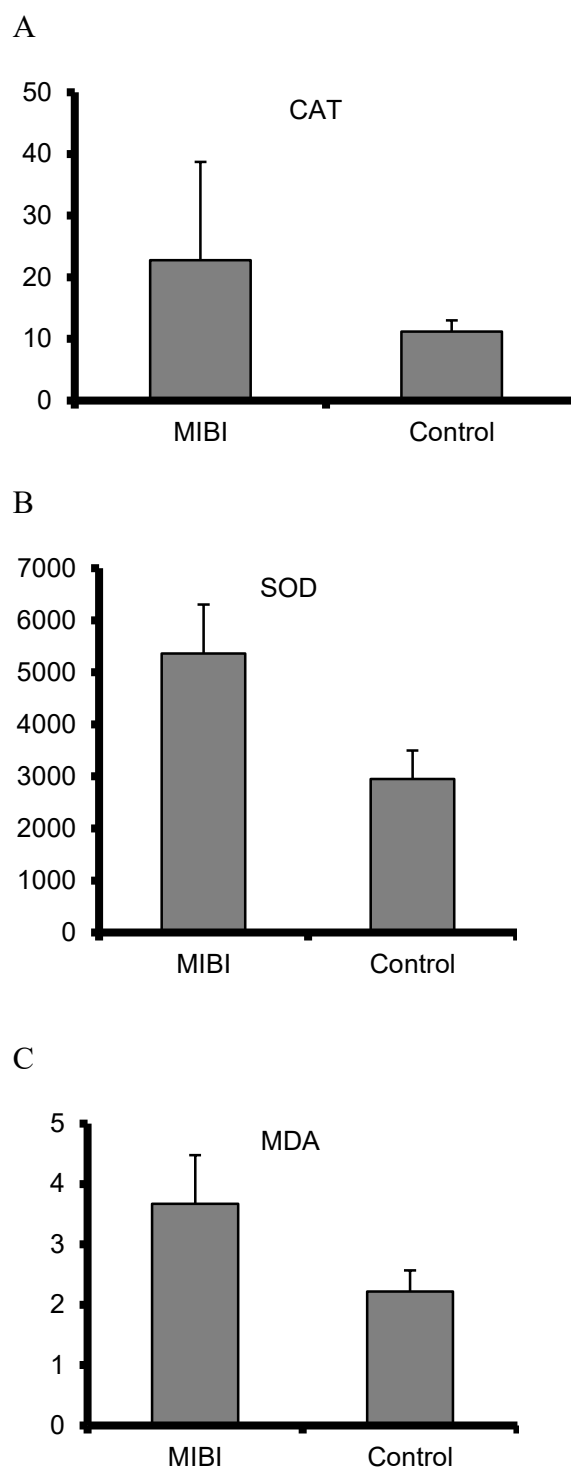


**Figure 1.** The activities of catalase (CAT); A. Superoxide dismutase (SOD); B. and malondialdehyde (MDA); C. Levels as oxidative stress biomarkers in first patient group and control group

and 1.9, 1.7, 1.6, 1.8 fold higher in patients, respectively. NO levels were 1.2 fold higher in patients than control group ( $p > 0.05$ ). The results of this study showed that antioxidant enzyme activities of CAT and SOD levels were significantly higher in  $^{99m}\text{Tc}$ -MIBI administered group than the control group ( $p < 0.05$ ). Because shortly after exposure to  $^{99m}\text{Tc}$ -MIBI, cellular protective pathways are triggered to overcome radiation-induced ROS. In addition, we

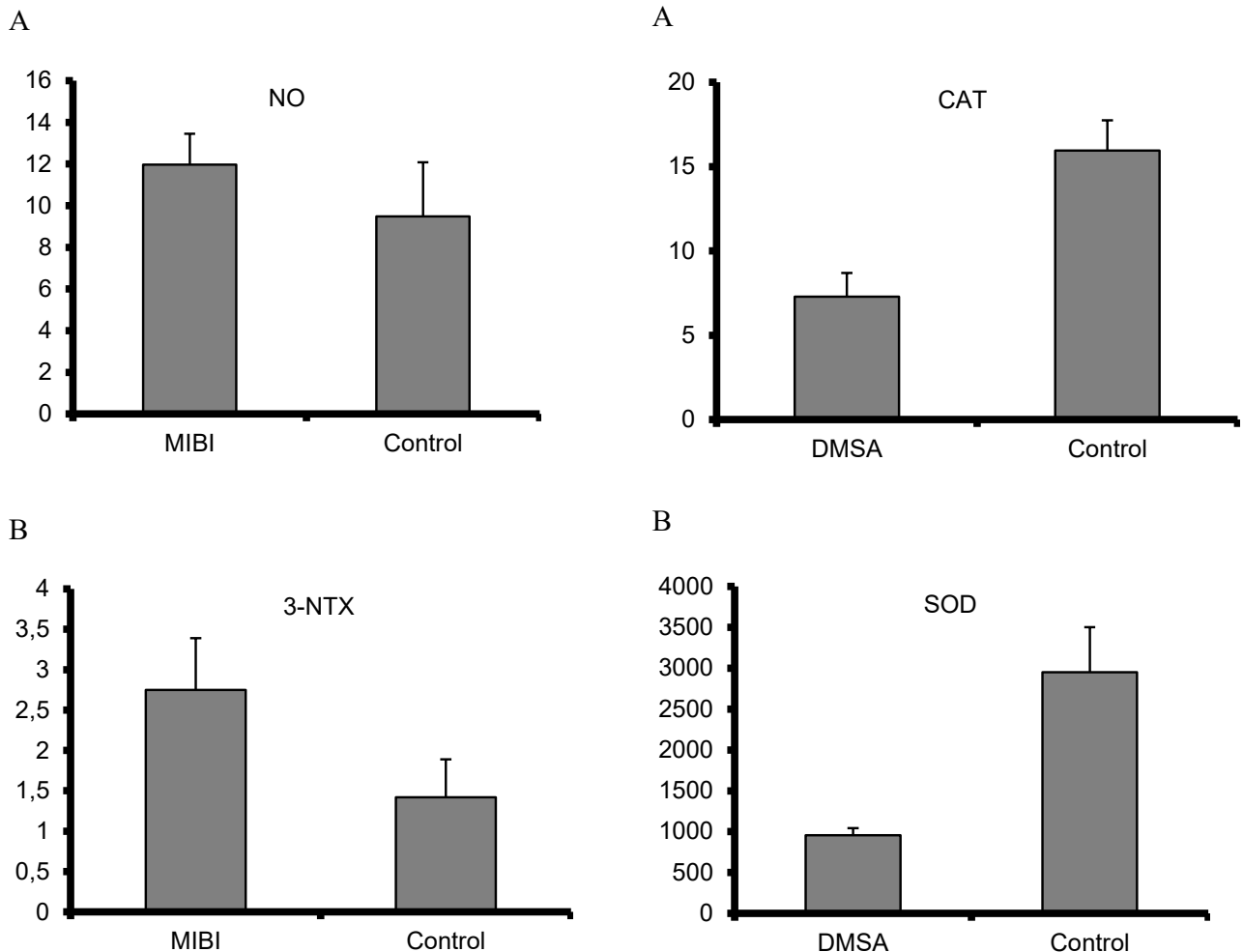


**Figure 2.** The activities of nitric oxide (NO); A. and nitrotyrosine (3-NTx); B. Levels as nitrosative stress biomarkers in first patient group and control group

previously reported same results in patients have thyroid and bone scintigraphy [17, 18]. However,  $^{99m}\text{Tc}$ -MIBI caused decreased SOD levels in mice [19].

In contrast to MIBI administered group, CAT and SOD levels were significantly lower in  $^{99m}\text{Tc}$ -DMSA,  $^{99m}\text{Tc}$ -MAG-3 administered patients and total renal scintigraphy performed patients than control group in this study ( $p < 0.05$ ).  $^{99m}\text{Tc}$ -DMSA stays in the proximal tubule in the renal cortex for a prolonged time after injection.  $^{99m}\text{Tc}$ -MAG-3 is a renal tubular agent. Renal imaging agents might induce free radical production more than MPS imaging agent. In addition, renal diseases cause oxidative stress. Therefore, antioxidant enzyme levels decreased in this group of patients. It has also been reported in the literature that exposure to radiation due to different radiopharmaceuticals including  $^{99m}\text{Tc}$ -diethylene trimine pentaacetic acid (DTPA) [20],  $^{99m}\text{Tc}$ -MIBI,  $^{201}\text{Tl}$ Thallium,  $^{99m}\text{Tc}$ -MIBI,  $^{99m}\text{Tc}$ -methylendiphosphonate (MDP) [19, 21–23] and 2.45 GHz microwave radiation [24] caused same results in animal and human studies.

MDA levels were significantly higher in  $^{99m}\text{Tc}$ -DMSA,  $^{99m}\text{Tc}$ -MAG-3 administered patients and total renal scintigraphy performed patient groups than the control group ( $p < 0.05$ ). In addition,

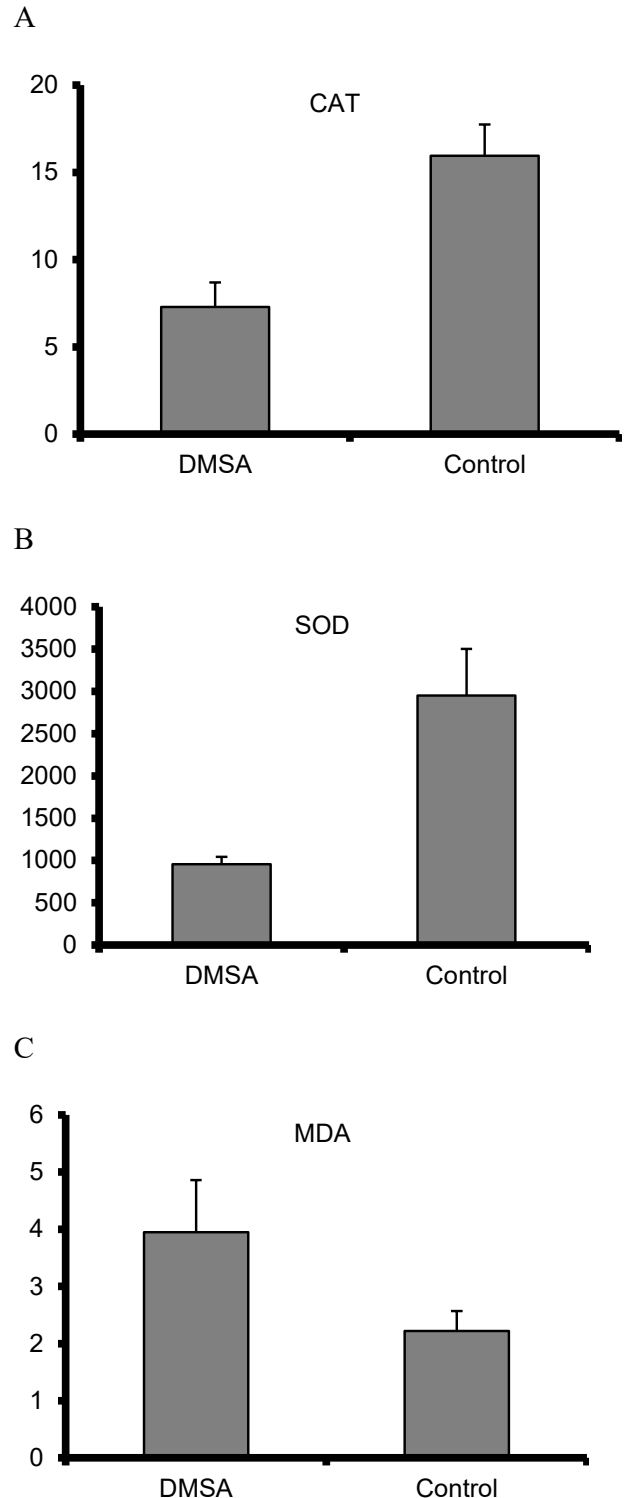


**Figure 3.** The activities of catalase (CAT); A. Superoxide dismutase (SOD); B. and malondialdehyde (MDA); C. Levels as oxidative stress biomarkers in second patient group and control group

researchers stated that gamma radiation at clinically used doses stimulates lipid peroxidation in human red cells [25]. ROS can initiate lipid peroxidation that is a chain reaction. Once lipid peroxidation is initiated, it results in the oxidative deterioration of polyunsaturated fatty acids and caused increased MDA levels [25].

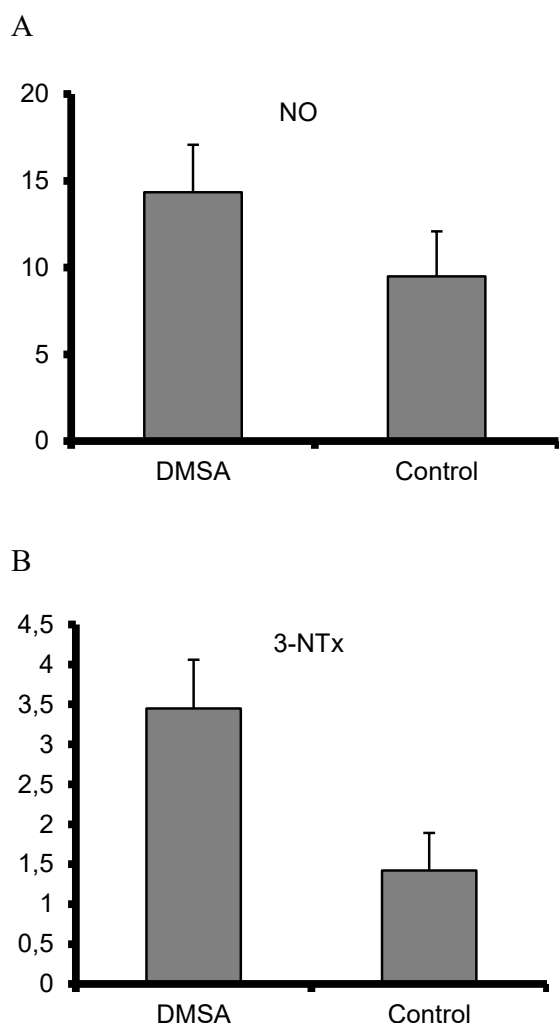


**Figure 4.** The activities of nitric oxide (NO); A. and nitrotyrosine (3-NTx); B. Levels as nitrosative stress biomarkers in second patient group and control group

Furthermore, these results are in agreement with previous animal and human studies that demonstrated <sup>99m</sup>Tc-DTPA [20], <sup>99m</sup>Tc-MIBI [21] and microwave radiation [24] caused increased MDA levels. However, <sup>99m</sup>Tc pertechnetate caused decreased MDA levels in patients [26].

The results acquired in this research study confirms that ionizing radiation causes different changes at antioxidant enzyme levels. However, to the best of our knowledge there is no similar clinical study reports on the effect of ionizing radiation due to <sup>99m</sup>Tc-MIBI and <sup>99m</sup>Tc-MDP on nitrosative stress parameters (NO, 3-NTx) in human. Therefore, we could not compare our results with those of others. We only could compare our findings on nitrosative stress parameters only with our previous reports that were performed in different patients groups and with different radiopharmaceutical agents including <sup>99m</sup>Tc pertechnetate and <sup>99m</sup>Tc-MDP.

NO levels were higher in the first patient group than the control group but it was not statistically significant ( $p > 0.05$ ). 3-NTx levels were statistically significantly higher in the first patient group than the control group ( $p < 0.05$ ).

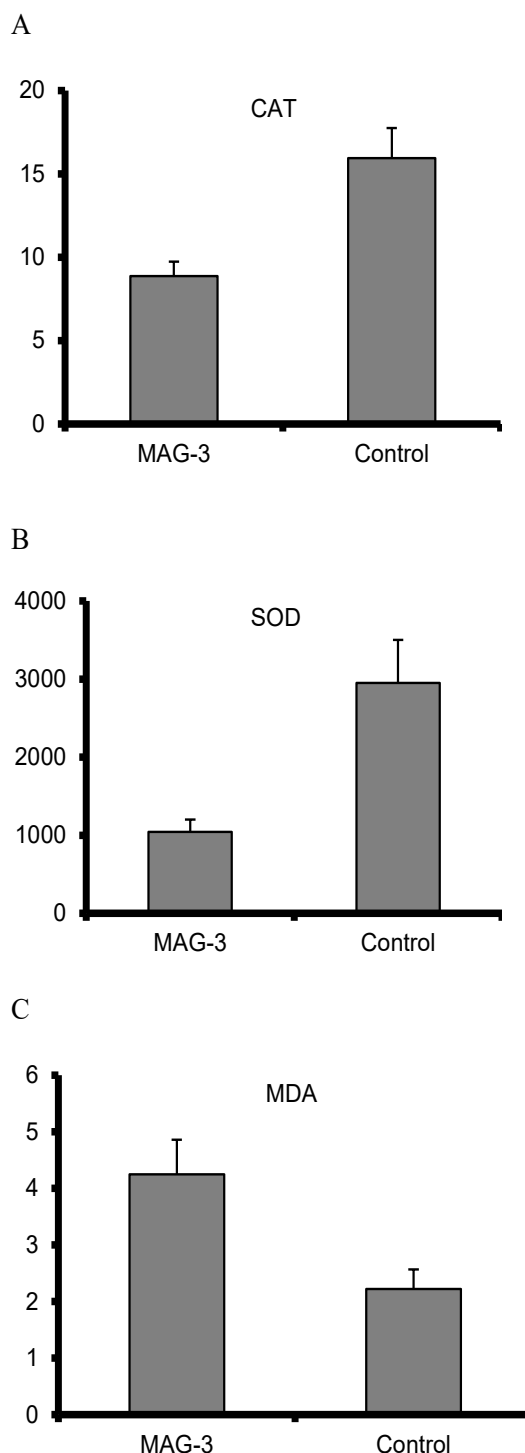


**Figure 5.** The activities of catalase (CAT); A. Superoxide dismutase (SOD); B. and malondialdehyde (MDA); C. Levels as oxidative stress biomarkers in third patient group and control group

NO, 3-NTx levels were higher in <sup>99m</sup>Tc-DMSA, <sup>99m</sup>Tc-MAG-3 administered patients and total renal scintigraphy performed patient groups than the control group ( $p < 0.05$ ).

We reported that NO and 3-NTx levels were increased in patients who have performed thyroid scintigraphy with <sup>99m</sup>Tc pertechnetate and bone scintigraphy with <sup>99m</sup>Tc-MDP [17–18].

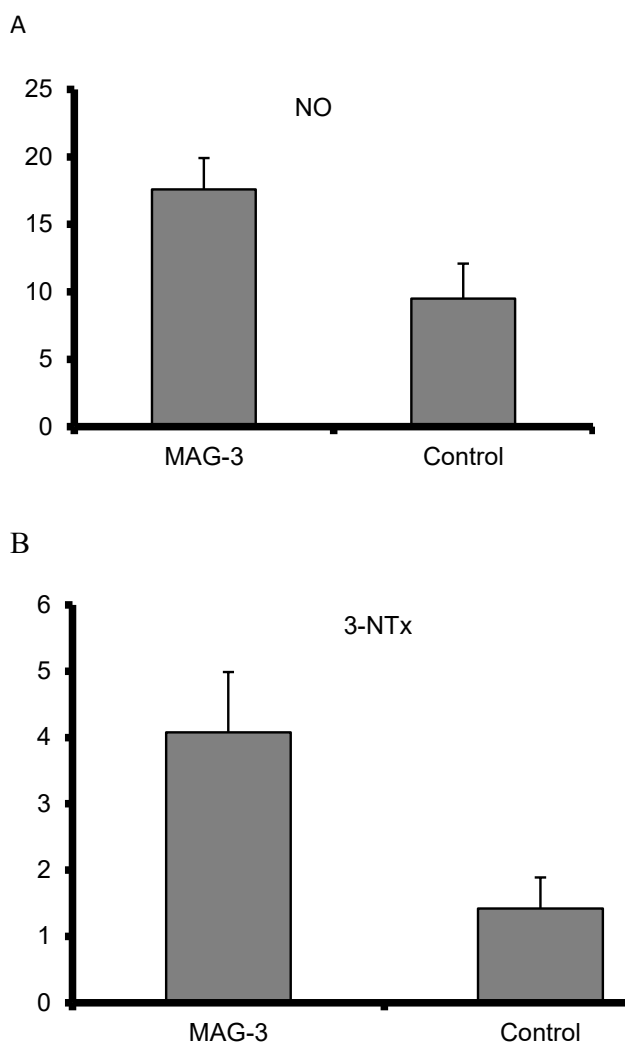


**Figure 6.** The activities of nitric oxide (NO); A. and nitrotyrosine (3-NTx); B. Levels as nitrosative stress biomarkers in third patient group and control group

Nitric oxide (NO) has one unpaired electron, hence it is accepted as a radical. NO is produced in biological systems via specific nitric oxide synthases (NOSs). NO plays an important role in various physiological conditions, such as neurotransmission, blood pressure regulation, defence mechanisms, smooth muscle relaxation and immune regulation. NO chemically reacts with oxygen and water, as a result of that nitrate and nitrite anions are produced. NO also reacts with superoxide anion and peroxynitrite (ONOO<sup>-</sup>) is produced. Reactivity of ONOO<sup>-</sup> is higher than NO. ONOO<sup>-</sup> reacts with proteins, thus nitrotyrosine (3-NTx) is produced. 3-NTx is a characteristic marker of nitrosative stress. It is known that NO and 3-NTx levels are increased in various diseases such as skin cancers, systemic lupus erythematosus, and atopic dermatitis [27].

NO, is produced by endothelial and endocardial tissue, has a significant effect on myocard and its vascular function. Coronary heart disease (CHD) is a chronic inflammatory process that becomes against vascular damage. Endothelial dysfunction causes CHD when endothelial cells cannot perform their functions including NO production. Furthermore, free oxygen

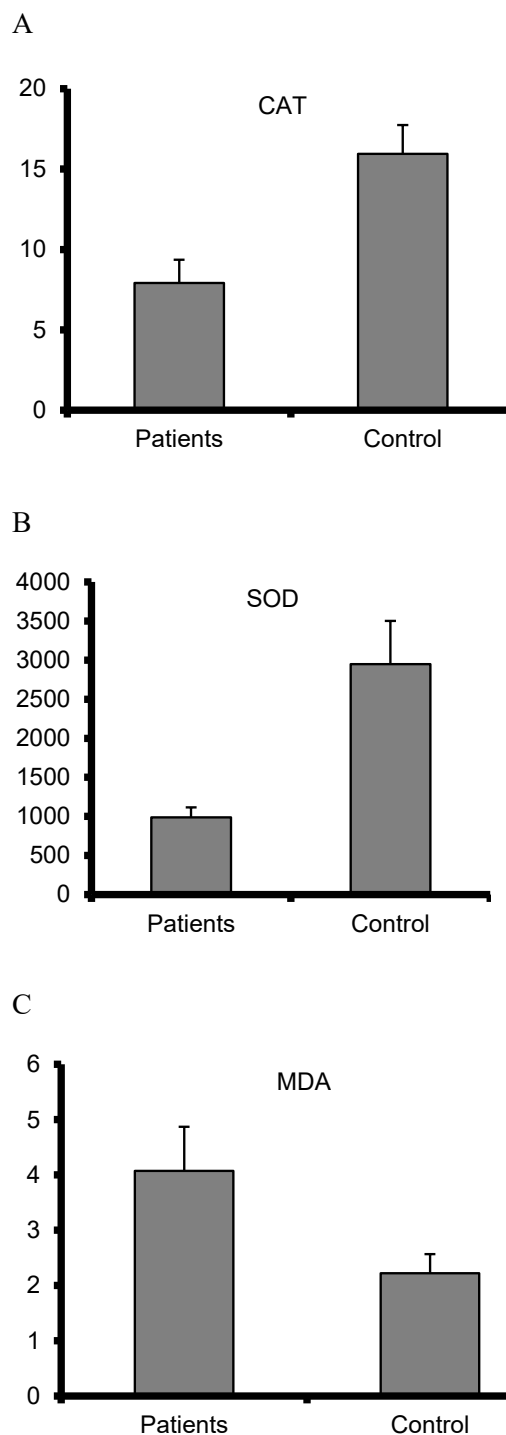


**Figure 7.** The activities of catalase (CAT); A. Superoxide dismutase (SOD); B. and malondialdehyde (MDA); C. Levels as oxidative stress biomarkers in total renal scintigraphy performed patient groups and control group

radicals negatively effect NO production in MPS performed patients. Because of that, NO levels might not statistically increased in <sup>99m</sup>Tc-MIBI administered group in this study [28–30].

This research, however, is subject to some limitations. There were an insufficient number of patients and number of blood samples. The samples were only taken after radiopharmaceutical

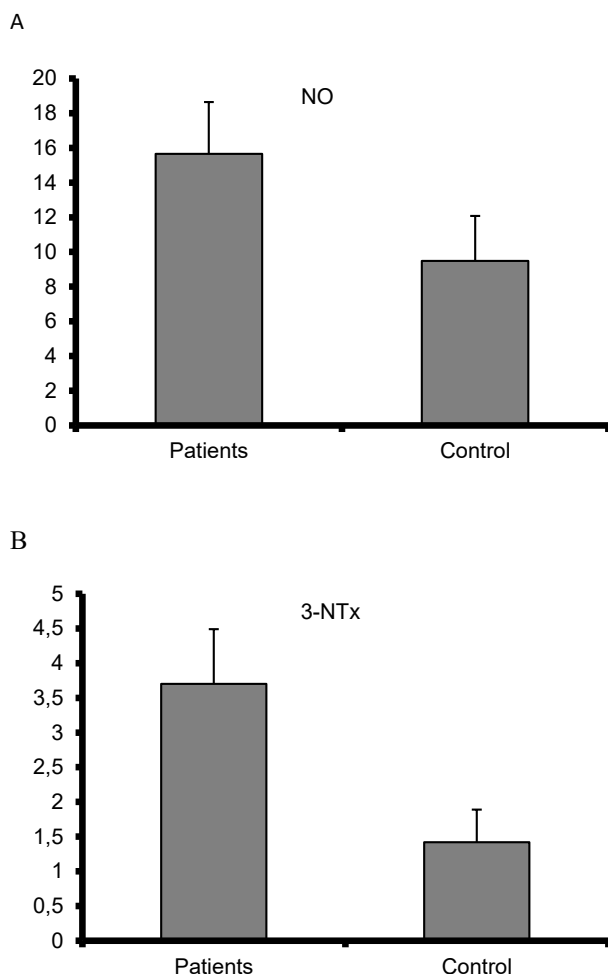


**Figure 8.** The activities of nitric oxide (NO); A. and nitrotyrosine (3-NTx); B. Levels as nitrosative stress biomarkers in total renal scintigraphy performed patient groups and control group

administration. If the samples were taken before agent injection, it would be more clear to understand whether oxidative/nitrosative stress parameters were changed due to ionizing radiation or cardiac and renal disease of patients.

## Conclusion

Taking the results of current study into consideration, we able to show alterations in oxidative/nitrosative stress parameters due to ionizing radiation. Although, the effects of scintigraphic imaging methods on free radicals are yet to be completely elucidated, shortly after ionizing radiation exposure, cellular protective pathways are activated to overcome harmful effects of ROS/RNS production due to ionizing radiation. In the literature there are no studies evaluating nitrosative stress levels in patients who undergone MPS, dynamic renal scintigraphy and renal cortical scintigraphy. This present study demonstrated that ionizing radiation due to MPS, dynamic renal scintigraphy and renal cortical scintigraphy applications have different effects on antioxidant enzyme levels. All of these methods increased MDA levels and nitrosative stress parameters. Our study will contribute current literature understanding radiobiological

effects of scintigraphic imaging agents on especially nitrosative stress parameters. However, further studies in a larger number of the population are needed to fully understand this topic.

## Acknowledgement: not applicable

Support for the work in the form of grants, equipment or drugs: not applicable.

## References

- Papagiannopoulou D. Technetium-99m radiochemistry for pharmaceutical applications. *J Labelled Comp Radiopharm.* 2017; 60(11): 502–520, doi: [10.1002/jlcr.3531](https://doi.org/10.1002/jlcr.3531), indexed in Pubmed: [28618064](https://pubmed.ncbi.nlm.nih.gov/28618064/).
- Maucksch U, Runge R, Wunderlich G, et al. Comparison of the radiotoxicity of the Tc-labeled compounds Tc-pertechnetate, Tc-HMPAO and Tc-MIBI. *Int J Radiat Biol.* 2016; 92(11): 698–706, doi: [10.3109/09553002.2016.1168533](https://doi.org/10.3109/09553002.2016.1168533), indexed in Pubmed: [27117205](https://pubmed.ncbi.nlm.nih.gov/27117205/).
- Blaufoux MD, De Palma D, Taylor A, et al. SNMMI Procedure Standard/EANM Practice Guideline for Diuretic Renal Scintigraphy in Adults With Suspected Upper Urinary Tract Obstruction 1.0. *Semin Nucl Med.* 2018; 48(4): 377–390, doi: [10.1053/j.semnuclmed.2018.02.010](https://doi.org/10.1053/j.semnuclmed.2018.02.010), indexed in Pubmed: [29852947](https://pubmed.ncbi.nlm.nih.gov/29852947/).
- Santos-Cuevas CL, Ferro-Flores G, Rojas-Calderón EL, et al. 99mTc-N2S2-Tat (49-57)-bombesin intern alized in nuclei of prostate and breast cancer cells: kinetics, dosimetry and effect on cellular proliferation. *Nucl Med Commun.* 2011; 32(4): 303–313, doi: [10.1097/MNM.0b013e328341b27f](https://doi.org/10.1097/MNM.0b013e328341b27f), indexed in Pubmed: [21304415](https://pubmed.ncbi.nlm.nih.gov/21304415/).
- Piron B, Paillas S, Boudousq V, et al. DNA damage-centered signaling pathways are effectively activated during low dose-rate Auger radioimmunotherapy. *Nucl Med Biol.* 2014; 41: e75–e83, doi: [10.1016/j.nuclmedbio.2014.01.012](https://doi.org/10.1016/j.nuclmedbio.2014.01.012).
- Spitz DR, Azzam EI, Li JJ, et al. Metabolic oxidation/reduction reactions and cellular responses to ionizing radiation: a unifying concept in stress response biology. *Cancer Metastasis Rev.* 2004; 23(3-4): 311–322, doi: [10.1023/B:CANC.0000031769.14728.bc](https://doi.org/10.1023/B:CANC.0000031769.14728.bc), indexed in Pubmed: [15197331](https://pubmed.ncbi.nlm.nih.gov/15197331/).
- Azzam EI, Jay-Gerin JP, Pain D. Ionizing radiation-induced metabolic oxidative stress and prolonged cell injury. *Cancer Lett.* 2012; 327(1-2): 48–60, doi: [10.1016/j.canlet.2011.12.012](https://doi.org/10.1016/j.canlet.2011.12.012), indexed in Pubmed: [22182453](https://pubmed.ncbi.nlm.nih.gov/22182453/).
- Dröge W. Free radicals in the physiological control of cell function. *Physiol Rev.* 2002; 82(1): 47–95, doi: [10.1152/physrev.00018.2001](https://doi.org/10.1152/physrev.00018.2001), indexed in Pubmed: [11773609](https://pubmed.ncbi.nlm.nih.gov/11773609/).
- Sies H. Oxidative stress: oxidants and antioxidants. *Exp Physiol.* 1997; 82(2): 291–295, doi: [10.1113/expphysiol.1997.sp004024](https://doi.org/10.1113/expphysiol.1997.sp004024), indexed in Pubmed: [9129943](https://pubmed.ncbi.nlm.nih.gov/9129943/).
- Klandorf H, Dyke KV. Oxidative and Nitrosative Stresses: Their Role in Health and Disease in Man and Birds. *Oxidative Stress-Molecular Mechanisms and Biological Effects.* Volodymyr Lushchak (ed.), 2012. InTech. <http://www.intechopen.com/books/oxidative-stress-molecular-mechanisms-and-biological-effects/oxidativeand-nitrosative-stresses-their-role-in-health-and-disease-in-man-and-birds>.
- Beutler E. *Red Cell Metabolism. A Manual of Biochemical Methods.* 2<sup>nd</sup> ed. Grune and Stratton Inc, New York 1984: 68–70.
- Fridovich I. Superoxide dismutase. *Adv Enzymol.* 1974; 41: 35–97.
- Ohkawa H, Ohishi N, Yagi K. Assay for lipid peroxides in animal tissues by thiobarbituric acid reaction. *Anal Biochem.* 1979; 95(2): 351–358, doi: [10.1016/0003-2697\(79\)90738-3](https://doi.org/10.1016/0003-2697(79)90738-3), indexed in Pubmed: [36810](https://pubmed.ncbi.nlm.nih.gov/36810/).
- Backus M, Piwnica-Worms D, Hockett D, et al. Microprobe analysis of Tc-MIBI in heart cells: calculation of mitochondrial membrane potential. *Am J Physiol.* 1993; 265(1 Pt 1): C178–C187, doi: [10.1152/ajpcell.1993.265.1.C178](https://doi.org/10.1152/ajpcell.1993.265.1.C178), indexed in Pubmed: [8338127](https://pubmed.ncbi.nlm.nih.gov/8338127/).
- Arbab AS, Koizumi K, Toyama K, et al. Technetium-99m-tetrofosmin, technetium-99m-MIBI and thallium-201 uptake in rat myocardial cells. *J Nucl Med.* 1998; 39(2): 266–271, indexed in Pubmed: [9476934](https://pubmed.ncbi.nlm.nih.gov/9476934/).

16. Kotzerke J, Punzet R, Runge R, et al. 99mTc-labeled HYNIC-DAPI causes plasmid DNA damage with high efficiency. *PLoS One*. 2014; 9(8): e104653, doi: [10.1371/journal.pone.0104653](https://doi.org/10.1371/journal.pone.0104653), indexed in Pubmed: [25098953](https://pubmed.ncbi.nlm.nih.gov/25098953/).
17. Salmanoglu E, Kurutas EB. Induction of oxidative/nitrosative stress following Tc-99m pertechnetate thyroid scintigraphy in human. *Cumhuriyet Medical Journal*. 2019, doi: [10.7197/cmj.vi.486246](https://doi.org/10.7197/cmj.vi.486246).
18. Salmanoglu E, Kurutas EB. Effects of 99mTc-MDP bone scintigraphy on oxidative/nitrosative stress biomarkers in patients. *Adv Lab Med Int*. 2017; 7: 12–22.
19. El-Gebaly RH, Rageh MM, Maamoun IK. Radio-protective potential of lipoic acid free and nano-capsule against 99mTc-MIBI induced injury in cardio vascular tissue. *J Xray Sci Technol*. 2019; 27(1): 83–96, doi: [10.3233/XST-180438](https://doi.org/10.3233/XST-180438), indexed in Pubmed: [30507603](https://pubmed.ncbi.nlm.nih.gov/30507603/).
20. Cicek E, Yildiz M, Delibas N, et al. Effects of Dynamic Renal Scintigraphy and Bone Scintigraphy Studies on Oxidative Damage in Patients. *Spectroscopy Letters*. 2009; 42(2): 63–66, doi: [10.1080/00387010802428468](https://doi.org/10.1080/00387010802428468).
21. Cesur G, Doguc DK, Yildiz M, et al. Effects of (99m)Tc sestamibi on antioxidant defense system and lipid peroxidation in the heart of Sprague Dawley rats. *Toxicol Ind Health*. 2014; 30(2): 154–159, doi: [10.1177/0748233712452599](https://doi.org/10.1177/0748233712452599), indexed in Pubmed: [22773438](https://pubmed.ncbi.nlm.nih.gov/22773438/).
22. Cicek E, Yildiz M, Delibas N, et al. The effects of 201Tl myocardial perfusion scintigraphy studies on oxidative damage in patients. *West Indian Med J*. 2009; 58(1): 50–53, indexed in Pubmed: [19565998](https://pubmed.ncbi.nlm.nih.gov/19565998/).
23. Gurbuz N, Aydin F, et al. Boz, A, The Effects of 99mTechnetium-methylendiphosphonate and 99mTechnetium-methoxyisobutylisonitrile on Erythrocyte Antioxidant Enzyme Activities. *Türk Biyokimya Dergisi [Turkish Journal of Biochemistry–Turk J Biochem]*. 2010; 35(3): 172–176.
24. Shahin S, Singh SP, Chaturvedi CM. 2.45 GHz microwave radiation induced oxidative and nitrosative stress mediated testicular apoptosis: Involvement of a p53 dependent bax-caspase-3 mediated pathway. *Environ Toxicol*. 2018; 33(9): 931–945, doi: [10.1002/tox.22578](https://doi.org/10.1002/tox.22578), indexed in Pubmed: [29968967](https://pubmed.ncbi.nlm.nih.gov/29968967/).
25. Anand AJ, Dzik WH, Imam A, et al. Radiation-induced red cell damage: role of reactive oxygen species. *Transfusion*. 1997; 37(2): 160–165.
26. Çiçek E, Yildiz M, Delibaş N, et al. The effects of thyroid scintigraphy studies on oxidative damage in patients. *Acta Physiol Hung*. 2006; 93(2-3): 131–136, doi: [10.1556/APhysiol.93.2006.2-3.3](https://doi.org/10.1556/APhysiol.93.2006.2-3.3), indexed in Pubmed: [17063624](https://pubmed.ncbi.nlm.nih.gov/17063624/).
27. Kurutas EB. The importance of antioxidants which play the role in cellular response against oxidative/nitrosative stress: current state. *Nutr J*. 2016; 15(1): 71, doi: [10.1186/s12937-016-0186-5](https://doi.org/10.1186/s12937-016-0186-5), indexed in Pubmed: [27456681](https://pubmed.ncbi.nlm.nih.gov/27456681/).
28. Lahera V, Goicoechea M, de Vinuesa SG, et al. Endothelial dysfunction, oxidative stress and inflammation in atherosclerosis: beneficial effects of statins. *Curr Med Chem*. 2007; 14(2): 243–248, doi: [10.2174/092986707779313381](https://doi.org/10.2174/092986707779313381), indexed in Pubmed: [17266583](https://pubmed.ncbi.nlm.nih.gov/17266583/).
29. Tritto I, Ambrosio G. The multi-faceted behavior of nitric oxide in vascular "inflammation": catchy terminology or true phenomenon? *Cardiovasc Res*. 2004; 63(1): 1–4, doi: [10.1016/j.cardiores.2004.04.028](https://doi.org/10.1016/j.cardiores.2004.04.028), indexed in Pubmed: [15194454](https://pubmed.ncbi.nlm.nih.gov/15194454/).
30. Atzeni F, Sarzi-Puttini P, Sitia S, et al. From endothelial dysfunction to atherosclerosis. *Autoimmun Rev*. 2010; 9(12): 830–834, doi: [10.1016/j.autrev.2010.07.016](https://doi.org/10.1016/j.autrev.2010.07.016), indexed in Pubmed: [20678595](https://pubmed.ncbi.nlm.nih.gov/20678595/).

# PET/CT in thyroid cancer — the importance of BRAF mutations

Vincenzo Cuccurullo<sup>1</sup> , Giuseppe Danilo Di Stasio<sup>1</sup> , Giuseppe Lucio Cascini<sup>2</sup> 

<sup>1</sup>Nuclear Medicine Unit, Department of Precision Medicine, Università della Campania “Luigi Vanvitelli”, Napoli, Italy

<sup>2</sup>Department of Diagnostic Imaging, Nuclear Medicine Unit, Magna Graecia University of Catanzaro, Catanzaro, Italy

[Received 20 XI 2019; Accepted 5 V 2020]

## Abstract

Thyroid cancer (TC) represents less than 1% of all newly diagnosed malignancies. In some selected cases, with a high clinical suspicion for disease but negative I-131 scan, positron emission tomography/computed tomography (PET) with F-18-Fluorodeoxyglucose (FDG) could be helpful in the detection of disease and the definition of its extent. FDG PET/CT, better if performed after TSH stimulation analogously to patient preparation done for radioiodine scintigraphy, could be useful mainly in the detection of metastatic and recurrent disease since the uptake and diagnostic sensitivity of FDG are increased by TSH stimulation. Recently, the role of oncogenic mutations in the tumorigenesis of TCs has become clearer. Among such mutations, BRAF<sup>V600E</sup> represents the most common genetic alteration. Mutated BRAF may define a more aggressive papillary carcinoma with poorer prognosis and therefore its analysis has been extensively studied as a rule-in test for thyroid carcinoma.

In this paper, we try to outline the possible role of FDG PET/CT in the management of patients with TC and positive BRAF mutations and the impact that it could have on their therapeutic algorithm, in terms of thyroidectomy and radioactive iodine (RAI) therapy.

**KEY words:** BRAF mutation; fluorodeoxyglucose F18; positron emission tomography; thyroid neoplasms

Nucl Med Rev 2020; 23, 2: 97–102

## Introduction

Thyroid nodules (TN) are extremely common in general population and also thanks to their subclinical detection via ultrasound imaging (US), the incidence of thyroid cancer is increasing [1]; in Europe for example, it has increased in the last decade by 69% in men and 65% in women. In fact, it has been estimated that one person out of five, despite gender, age and other epidemiological characteristics has a palpable thyroid nodule, which can be detected by US in most of cases [2]. The prevalence of TN is greater in women than in men, with multiple nodules that are more common than solitary ones [3]. In the diagnostic algorithm of TN, the differential diagnosis includes numerous clinical entities, both benign and malignant; therefore, the pathological examination has an important role in their evaluation. Thanks to fine needle aspiration cytology (FNAC) biopsy the identification of high-risk situations has significantly improved so that their management has now become more effective [4]. However, there are still cases in which patients require surgery for further confirmation of the disease, thus relying upon the pathologist to correctly characterize their nodule [4].

Thyroid cancer (TC) instead, despite being the most common endocrine tumor, represents less than 1% of all newly diagnosed malignancies [2]. From a histological point of view, follicular cells within the thyroid gland are responsible for tumorigenesis and generate three main types of differentiated thyroid cancer (DTC): papillary (PTC), follicular (FTC) and mixed cell variants, which account for approximately 95% of all thyroid carcinoma, all of which are commonly well differentiated therefore these tumors are iodine avid and diagnosed/treated with I-123 or I-131, although they also include many subtypes that have different outcomes in terms of response to therapy and prognosis [5]. Undifferentiated and anaplastic tumors are not always iodine avid due to tumor dedifferentiation, which can occur even in case of tumor recurrence [5]. When thyroid neoplastic lesions lose the ability to synthesize hormones from iodine, they show increased glucose metabolism; therefore, patients will have high human thyroglobulin levels and negative I-131 scans. In such selected cases, with a high clinical suspicion for disease but negative I-131 scan, positron emission tomography/computed tomography (PET) with F-18-Fluorodeoxyglucose (FDG) could be helpful in the detection of disease and the definition of its extent [6]. The most recent American Thyroid Association (ATA 2015) guidelines for the management of adult patients with Thyroid Nodules and Differentiated Thyroid Cancer recommend total thyroidectomy for tumors greater than 1 cm and possible lobectomy for tumors ≤ 1 cm. In general, PTC and FTC prognoses are very good, with low risk of recurrence and distant

Correspondence to: Vincenzo Cuccurullo  
 Medicina Nucleare, Università della Campania “Luigi Vanvitelli”.  
 P.zza Miraglia 2, 80138 Napoli, Italy  
 e-mail: vincenzo.cuccurullo@unicampania.it

metastases; however, there are marked differences between the two groups [7]. In fact, PTC patients are usually younger than 50 years old, with smaller tumors and higher incidence of lymph node metastases, whereas FTC patients show more frequently distant metastatic disease and receive radioiodine [8]. In addition to these prognostic factors, more recently, the role of oncogenic mutations in the tumorigenesis of TCs has become clearer [9]. Among such mutations, BRAF<sup>V600E</sup> represents the most common genetic alteration in PTC, with approximately 45% prevalence. In fact, compared to PTC patients without BRAF mutation, positive ones tend to present at higher stage and with more frequent distant metastases [10]. Thus, mutated BRAF may define a more aggressive papillary carcinoma with poorer prognosis and therefore its analysis has been extensively studied as a rule-in test for thyroid carcinoma [11].

In this paper, we try to outline the possible role of FDG PET/CT in the management of patients with DTC and positive BRAF mutations and the impact that it could have on their therapeutic algorithm, in terms of thyroidectomy and radioactive iodine (RAI) therapy.

### Molecular pathophysiology

Thyroid epithelial cells have a transport mechanism, the sodium/iodide symporter (NIS), which enables thyroid concentration of iodide to subsequently undergo organification and incorporation into thyroid hormones [12]. This mechanism is influenced primarily by a pituitary hormone, the thyroid-stimulating hormone (TSH), which increases the transport of iodide [13]. B-type RAF kinase (BRAF) is a serine-threonine kinase that belongs to the rapidly accelerated fibrosarcoma (RAF) family, and represents the most potent mitogen activated protein kinase (MAPK) pathway activator [14]. The MAPK pathway is a signal transduction cascade driven by phosphorylation that leads to intracellular responses such as cell proliferation [15]. Thus, BRAF acts as a protooncogene and has an important function in cell growth, differentiation and apoptosis, with its point mutations that have been noted in various human cancers [16]. In PTC, a common mutation in the BRAF gene comprises a missense mutation that consists of a thymine-to-adenine transversion at nucleotide 1799 (T1799A) within exon 15, which leads to the substitution of a valine residue for a glutamate one at position 600 of the protein (V600E), with consequent gain of function, constitutive activation of MAPK pathway, *i.e.* BRAF<sup>V600E</sup> activating mutation is associated with tumorigenesis [17].

FDG PET/CT is routinely used to evaluate disease burden in a variety of neoplasms, with FDG uptake that is based on enhanced aerobic glycolysis in cancer cells, known as Warburg effect. In TC there is an inverse relationship between FDG avidity and radioiodine uptake mainly in case of metastatic lesions, a phenomenon which was originally described as 'flip-flop' [18–20].

### Thyroid nuclear medicine imaging

Thyroid gland imaging is routinely done with different radiopharmaceuticals that are used in specific clinical contexts. Among them, Tc-99m-pertechnetate is widely used and owes its popularity to easy availability, low absorbed radiation dose compared to I-123 or I-131 and lower costs. The tracer is trapped by the thyroid, but it does not undergo organification, remaining in the gland for a relatively short period which allows imaging for diagnostic

purposes mainly related to thyroid morphology and function, *i.e.* hypo- or hyper-thyroidism [21].

<sup>99m</sup>Tc-MIBI scintigraphy instead is more suitable than <sup>99m</sup>Tc-pertechnetate scintigraphy for TN differentiation between benign and malignant lesions, since nodules with increased uptake and late retention of <sup>99m</sup>Tc-MIBI are more suspicious for malignancy (sensitivity 82%, specificity 63%) [22].

Iodide radioisotopes (I-123, I-131) are trapped and organified inside the thyroid providing higher thyroid-to-background uptake ratios; however, in order to achieve sufficient iodine uptake into tumor cells, high levels of TSH are required (serum TSH levels > 30 mIU/L), thus implying either thyroid hormone withdrawal or intramuscular injection of rh-TSH (Thyrogen®). I-123 and I-131 could be used to interrogate the NIS symporter to assess thyroid nodule functioning in order to distinguish "hot" (autonomous) from "cold" (hypofunctioning) nodules but their main application is the detection of thyroid cancer metastases, which as the primary tumor are usually iodine avid [23].

### FDG PET/CT in the management of patients with DTCs

As stated above, due to either BRAF<sup>V600E</sup> mutation or tumor dedifferentiation, when the ability to synthesize hormones from iodine is lost, tumors show increased glucose metabolism [24]. In such cases, patients will present with elevated human thyroglobulin levels (*i.e.* serum specific marker of TC) and with negative post-therapeutic I-131 whole body scans. Here, FDG PET/CT, better if performed after TSH stimulation analogously to patient preparation done for radioiodine scintigraphy, could be useful mainly in the detection of metastatic and recurrent disease since the uptake and diagnostic sensitivity of FDG are increased by TSH stimulation [25]. In fact, although the current ATA guidelines do not routinely recommend FDG-PET/CT for the diagnostic workup of indeterminate thyroid nodules due to limited clinical validation, several studies and meta-analysis already demonstrated the opposite [7].

More in particular in a recent paper by Piccardo et al., the Authors compared the accuracy of FDG PET/CT with Tc-99m-MIBI scintigraphy and multiparametric neck ultrasonography (US) demonstrating that the former has significantly higher performances in terms of sensitivity and NPV than the latter [26]. They also evaluated the possible role of FDG PET/CT in different diagnostic contexts in terms of impact on clinical management. It emerged that FDG PET/CT could be of use already at a preoperative stage to define the nature of indeterminate TNs thanks to its high sensitivity and NPV, especially in patients with lesions > 15mm with sensitivity ranging from 77 to 100% and NPV from 81 to 100% [26]. More specifically, we know that focal uptake of FDG within the thyroid gland, as incidental finding during evaluation of non-thyroid cancers, may be related to both benign and malignant pathology [27]. In this sense, De Koster et al. suggested that the number of futile hemithyroidectomies for benign nodules could be reduced thanks to the implementation of FDG-PET/CT by 66%, implying the cost-effectiveness of this technique in the pre-operative setting [28]. However, overall reported sensitivity and specificity of FDG-PET/CT in this specific scenario ranged from 77% to 100% and from 33% to 64%, respectively, with small nodule size being the main reason for false-negativity, since FDG-avidity in very small nodules may

be missed due to both low volume of malignant cells and partial volume effect, which underestimate the real FDG-concentration [28]. Moreover, the radiation exposure of FDG-PET/CT that patients should undergo before surgery represents another limitation to this possible application since it is largely accounted for by the FDG dosage (approximately 3 to 4 mSv for a typical activity of 185 MBq administered to an average adult) whereas the CT radiation dose greatly varies, being less than 0.5 mSv for a low-dose CT of the neck region only [29].

Pre-operative FDG PET/CT could also be used in the assessment of biological behavior of DTCs in order to predict the aggressiveness of the tumor pre-surgically [30]. In this sense, BRAF molecular test already represents the most reliable tool to identify the most aggressive subgroup of papillary thyroid carcinomas, but due to the relatively high costs and low availability, its use in clinical practice remains not applicable [31, 32]. Therefore, as some studies report, FDG PET/CT could be used to reduce costs and provide analogous information, with a more intense FDG uptake at pre-operative PET/CT that might be associated with a poorer prognosis and more aggressive histological subtype [33]. In this sense, Trimboli and colleagues used a SUV ratio of 3.0 as a cut-off to distinguish patients with higher rather than lower risk of disease progression. However, after a multivariate analysis, they concluded that only tumor size remained associated with disease persistence/progression; therefore, the evidence of this possible application of FDG PET/CT remains to be further evaluated [34].

Recent 2015 ATA Guidelines recommend neck US as first-line imaging technique to stage DTCs before thyroidectomy, whereas the use of CT or multiparametric magnetic resonance imaging (MRI) is reserved for high risk patients in which the probability to have distant metastases or mediastinal/neck nodal involvement at time of diagnosis is elevated [7]. In this context PET/CT does not have a role yet, even if some studies have been already published in this sense [35]. Specifically, Agate et al. compared the performance of FDG PET/CT, CT alone and US in the diagnosis of cervical lymph node metastasis in patients with PTC and concluded that US had the best diagnostic accuracy among the three (64.9%, 61.9% and 82% respectively) thus confirming ATA guidelines preference of neck US as best methodology for preoperative assessment of nodal status. However, FDG PET/CT might still be useful in aggressive DTC subtypes such as tall-cell, solid/trabecular, insular and diffuse sclerosing or in patients with suspected distant metastases for staging purposes and to predict the preoperatively the risk of recurrence [37]. A Japanese group retrospectively analyzed in a recent paper the benefit of FDG PET/CT at initial diagnosis in 114 patients with DTC for predicting the high-risk for recurrence by assessing seven parameters including among the others SUVmax, SUVmean and MTV (metabolic tumor volume expressed in cm<sup>3</sup>). They identified 88 patients with FDG-avid tumor and 26 patients with FDG-non-avid tumor and demonstrated that the former group resulted to have significantly larger lesions (21 vs 13 mm), more advanced ATA-risk classification, but at the same time, only 10 out of 88 patients were classified as high-risk and the parameters themselves revealed a wide range of sensitivity, specificity and accuracy. So, they divided patients according MTV, if greater than 10.0 cm<sup>3</sup> or not, and introduced a scoring system that takes in consideration each of the seven diagnostic parameters assigning a score of 0 if negative for high-risk or 1 if positive using each threshold

criterion. Summing these scores to differentiate between high-risk and non-high-risk patients they demonstrated that a summed score  $\geq 5$  in 44 patients with an MTV  $> 10.0$  cm<sup>3</sup> was associated with 100% sensitivity, 91.7% specificity and 93.2% accuracy (AUC: 0.98) in predicting the high-risk for recurrence. Therefore, they concluded that FDG-non-avid primary DTCs are less inclined to post-operative recurrence whereas in FDG-avid primary DTCs with MTV  $> 10.0$  cm<sup>3</sup>, the combination of SUV-related, volumetric and texture parameters could significantly increase the ability to identify high-risk patients, thus confirming the prognostic value of FDG PET in advanced thyroid cancer [38].

Apart from the aforementioned scenarios in which FDG PET/CT might have or not a role in clinical practice, what remains clear as main indication for this technique is the post-operative stage, during follow-up, mainly in case of patients with aggressive histologies so to have a starting reference point or in chase of high or increasing Tg levels (Tg  $> 10$  ng/mL or doubling time of less than 1 year) with negative post-therapeutic I-131 whole-body scan [39]. A meta-analysis performed by Wan et al. [40] evaluated 17 studies with 571 patients who had recurrent or metastatic DTC and I-131 negative whole-body scan and determined that FDG-PET/CT a pooled sensitivity and specificity of 93.5% and 83.9%, respectively, with an overall diagnostic accuracy of 90.9%. Moreover, studies have shown that the positivity rate of FDG-PET/CT increases as Tg level rises, though there is lack of consensus on what the precise threshold level of Tg should be since positive findings have also been reported in 10–20% of DTC patients with Tg levels  $< 10$  ng/mL [41]. In this sense, becomes crucial the comparison of post-therapeutic I-131 whole-body scan with FDG-PET/CT because the latter could be helpful in the reduction of unnecessary second administration of high I-131 activities, which means direct implication on patients' clinical management [42]. In fact, the current guideline to define a radioactive iodine-refractory (RAIR) DTC is based on the clinical negative response to a cumulative I-131 dose of 600 mCi or more, which means at least 3 RAI therapies over a two-year period, taking in consideration a 6-month treatment interval [43]. This may lead to a therapeutic delay, i.e. to not receive an appropriate treatment at the earliest possibility [44]. FDG-PET/CT could be useful in this sense as an early response predictor, thus allowing the early implementation of alternate therapies such as Tyrosine Kinase Inhibitors (TKIs). Kang et al. recently studied this problem by evaluating 54 patients with metastatic DTC who underwent both RAI therapy scan and FDG PET/CT during the same period in order to predict the response rate of RAI itself. Of 54 patients, only 22 had a therapeutic response to RAI with a 43% rate of concordance between the two techniques and with significant negative correlation between FDG avidity of metastatic lesions and response rate. Therefore, they concluded that the patient group with FDG-avid metastasis showed poor response to RAI therapy regardless of the degree of RAI uptake at I-131 whole-body scan [45].

### **BRAF<sup>V600E</sup> and FDG PET/CT**

Recent clinical studies demonstrated the relationship between BRAF<sup>V600E</sup> mutation and FDG uptake, showing that BRAF<sup>V600E</sup> mutation is associated with downregulation of the NIS symporter, loss of RAI avidity and increased glucose transporter (GLUT-1) expression in both primary and metastatic PTCs, thus determining poorer

prognosis, including events such as increased incidence of recurrence, extrathyroidal invasion and distant metastases [46]. More in particular, in BRAF<sup>V600E</sup>-positive PTCs, several studies demonstrated that at mitochondrial level there is a reduction of O<sub>2</sub> consumption and increased glucose uptake, thus favoring an anaerobic glycolytic shift in cancer cells by targeting at transcriptional level both hypoxia inducible factor (HIF)-1 that acts on GLUT1, GLUT3 and hexokinase II, which play an important role in trapping FDG inside cancer cells and the M2 isoform of pyruvate kinase (the rate-limiting step of glycolysis) which showed significantly higher levels compared to BRAF wild-type PTCs [47]. Therefore, the association between BRAF<sup>V600E</sup> mutation and FDG uptake could be explained with the induction of MAPK transduction pathway and the subsequent activation of HIF-1 resulting in increased glycolysis and loss of RAI avidity [48]. In this sense, as a recent study reported, BRAF<sup>V600E</sup> mutations were present in 62% of RAI recurrent/metastatic TCs; analogously, all patients with RAI PTCs and FDG-PET/CT positive scan were BRAF<sup>V600E</sup>-positive, compared to 45% of positive PET/CT scans in PTCs in general [49]. In a recent meta-analysis, Santhanam and colleagues not only show the significant correlation in DTC patients between BRAF<sup>V600E</sup>-positiveness and the higher odds of having FDG-PET/CT avid lesions (OR = 2.12) but they also demonstrated that these patients tend to have relatively higher mean SUV values (although SUV values may vary greatly across institutions and the measurement itself depends on multiple factors), thus concluding that BRAF<sup>V600E</sup> mutation, when present, should prompt the treating clinician to consider FDG-PET/CT as a useful diagnostic test to localize residual disease [46]. Nagarajah et al. [50] specifically evaluated the differences in terms of glucose metabolism of the BRAF<sup>V600E</sup> versus BRAF<sup>WT</sup> in patients with DTC and poorly differentiated TCs. While in the first cohort median SUV<sub>max</sub> was significantly higher in the mutated group versus wild-type (median SUV<sub>max</sub> 6.3 versus 4.7), in the latter FDG uptake was not significantly different between the two groups.

A very interesting study design instead, was carried out by Choi et al. that retrospectively reviewed 106 patients with PTC who underwent FDG PET/CT scan before undergoing total thyroidectomy, scans that were subsequently compared with clinicopathological data collected from surgical specimens, such as primary tumor size, capsular invasion, metastases and BRAF<sup>V600E</sup> mutation among the others.

Reported SUV<sub>max</sub> was significantly higher in primary tumors of size greater than 1 cm (SUV<sub>max</sub> 6.6 vs 3.4), in PTCs with extra-thyroid extension of the tumor (SUV<sub>max</sub> 5.8 vs 3.7) and in PTCs with BRAF<sup>V600E</sup> mutation (SUV<sub>max</sub> 5.7 vs 3.0), whereas at a multivariate analysis only tumor size and BRAF<sup>V600E</sup> were significantly associated with the SUV<sub>max</sub> of the primary tumor, as extra-thyroid extension and thyroid capsular invasion had no statistically significant association. Therefore, they concluded that FDG PET/CT may play an important role and yield additional information on tumor aggressiveness when associated to molecular biomarkers such as BRAF<sup>V600E</sup> mutation [51].

## Conclusions

Differentiated thyroid cancers are the most common histological types of thyroid cancer which are characterized by a favorable prognosis thanks to surgical removal of the tumor and radioiodine

ablation therapy, with an overall 5-year survival rate higher than 90%. However, in some patients we can have a more aggressive behavior that often becomes the cause of mortality due to tumor recurrence and RAI refractoriness. Neck US still represents the first-line imaging technique to stage DTCs before thyroidectomy and is the best methodology for preoperative assessment of nodal status; however, new possible scenarios of application seem to be possible when this PET/CT is associated with the presence of molecular biomarkers, such as BRAF<sup>V600E</sup> mutation. FDG PET/CT has already been used in clinical practice in cases of elevated serum thyroglobulin and negative I-131 whole-body scintigraphy, mainly to locate recurrent disease and for its prognostic role. Unfortunately, despite these promising reports, the relationship between F-18 FDG uptake and the BRAF<sup>V600E</sup> mutation for a possible pre-operative application is still poorly recognized as it will need further validation in consideration also of the genetic heterogeneity that has been reported (between different primary tumors and regional lymph node metastases), which requires that all lesions within the patient harbor the same genetic defect.

## References

1. Kitahara CM, Sosa JA. The changing incidence of thyroid cancer. *Nat Rev Endocrinol.* 2016; 12(11): 646–653, doi: [10.1038/nrendo.2016.110](https://doi.org/10.1038/nrendo.2016.110), indexed in Pubmed: [27418023](https://pubmed.ncbi.nlm.nih.gov/27418023/).
2. Roman BR, Morris LG, Davies L. The thyroid cancer epidemic, 2017 perspective. *Curr Opin Endocrinol Diabetes Obes.* 2017; 24(5): 332–336, doi: [10.1097/MED.0000000000000359](https://doi.org/10.1097/MED.0000000000000359), indexed in Pubmed: [28692457](https://pubmed.ncbi.nlm.nih.gov/28692457/).
3. Bauer AJ. Thyroid nodules and differentiated thyroid cancer. *Endocr Dev.* 2014; 26: 183–201, doi: [10.1159/000363164](https://doi.org/10.1159/000363164), indexed in Pubmed: [25231453](https://pubmed.ncbi.nlm.nih.gov/25231453/).
4. Nabhan F, Ringel MD. Thyroid nodules and cancer management guidelines: comparisons and controversies. *Endocr Relat Cancer.* 2017; 24(2): R13–R26, doi: [10.1530/ERC-16-0432](https://doi.org/10.1530/ERC-16-0432), indexed in Pubmed: [27965276](https://pubmed.ncbi.nlm.nih.gov/27965276/).
5. Song JS, Dmytriw AA, Yu E, et al. Investigation of thyroid nodules: A practical algorithm and review of guidelines. *Head Neck.* 2018; 40(8): 1861–1873, doi: [10.1002/hed.25160](https://doi.org/10.1002/hed.25160), indexed in Pubmed: [29607563](https://pubmed.ncbi.nlm.nih.gov/29607563/).
6. Mansi L, Moncayo R, Cuccurullo V, et al. Nuclear medicine in diagnosis, staging and follow-up of thyroid cancer. *Q J Nucl Med Mol Imaging.* 2004; 48(2): 82–95, indexed in Pubmed: [15243406](https://pubmed.ncbi.nlm.nih.gov/15243406/).
7. Haugen BR, Haugen BR, Alexander EK, et al. 2015 American Thyroid Association Management Guidelines for Adult Patients with Thyroid Nodules and Differentiated Thyroid Cancer: The American Thyroid Association Guidelines Task Force on Thyroid Nodules and Differentiated Thyroid Cancer. *Thyroid.* 2016; 26(1): 1–133, doi: [10.1089/thy.2015.0020](https://doi.org/10.1089/thy.2015.0020), indexed in Pubmed: [26462967](https://pubmed.ncbi.nlm.nih.gov/26462967/).
8. Boufraqueh M, Patel D, Xiong Y, et al. Diagnosis of thyroid cancer: state of art. *Expert Opin Med Diagn.* 2013; 7(4): 331–342, doi: [10.1517/17530059.2013.800481](https://doi.org/10.1517/17530059.2013.800481), indexed in Pubmed: [23701167](https://pubmed.ncbi.nlm.nih.gov/23701167/).
9. Krátký J, Vítková H, Bartáková J, et al. Thyroid nodules: pathophysiological insight on oncogenesis and novel diagnostic techniques. *Physiol Res.* 2014; 63 Suppl 2: S263–S275, indexed in Pubmed: [24908232](https://pubmed.ncbi.nlm.nih.gov/24908232/).
10. Fnais N, Soobiah C, Al-Qahtani K, et al. Diagnostic value of fine needle aspiration BRAF(V600E) mutation analysis in papillary thyroid cancer: a systematic review and meta-analysis. *Hum Pathol.* 2015; 46(10): 1443–1454, doi: [10.1016/j.humpath.2015.06.001](https://doi.org/10.1016/j.humpath.2015.06.001), indexed in Pubmed: [26232865](https://pubmed.ncbi.nlm.nih.gov/26232865/).
11. Kunavisarut T. Diagnostic biomarkers of differentiated thyroid cancer. *Endocrine.* 2013; 44(3): 616–622, doi: [10.1007/s12020-013-9974-2](https://doi.org/10.1007/s12020-013-9974-2), indexed in Pubmed: [23645523](https://pubmed.ncbi.nlm.nih.gov/23645523/).
12. Bauer AJ. Molecular Genetics of Thyroid Cancer in Children and Adolescents. *Endocrinol Metab Clin North Am.* 2017; 46(2): 389–403, doi: [10.1016/j.ecl.2017.01.014](https://doi.org/10.1016/j.ecl.2017.01.014), indexed in Pubmed: [28476228](https://pubmed.ncbi.nlm.nih.gov/28476228/).

13. Ravera S, Reyna-Neyra A, Ferrandino G, et al. The Sodium/Iodide Symporter (NIS): Molecular Physiology and Preclinical and Clinical Applications. *Annu Rev Physiol*. 2017; 79: 261–289, doi: [10.1146/annurev-physiol-022516-034125](https://doi.org/10.1146/annurev-physiol-022516-034125), indexed in Pubmed: [28192058](https://pubmed.ncbi.nlm.nih.gov/28192058/).
14. Haroon Al Rasheed MR, Xu B. Molecular Alterations in Thyroid Carcinoma. *Surg Pathol Clin*. 2019; 12(4): 921–930, doi: [10.1016/j.path.2019.08.002](https://doi.org/10.1016/j.path.2019.08.002), indexed in Pubmed: [31672298](https://pubmed.ncbi.nlm.nih.gov/31672298/).
15. Duan H, Liu X, Ren X, et al. Mutation profiles of follicular thyroid tumors by targeted sequencing. *Diagn Pathol*. 2019; 14(1): 39, doi: [10.1186/s13000-019-0817-1](https://doi.org/10.1186/s13000-019-0817-1), indexed in Pubmed: [31077238](https://pubmed.ncbi.nlm.nih.gov/31077238/).
16. Xia F, Jiang Bo, Chen Y, et al. Prediction of novel target genes and pathways involved in tall cell variant papillary thyroid carcinoma. *Medicine (Baltimore)*. 2018; 97(51): e13802, doi: [10.1097/MD.00000000000013802](https://doi.org/10.1097/MD.00000000000013802), indexed in Pubmed: [30572540](https://pubmed.ncbi.nlm.nih.gov/30572540/).
17. Iva J, Filip G, Martin B, et al. The Significance of BRAFV600E Mutation in Thyroid Cancer in Terms of Novel Targeted Therapies - Overview of Current Knowledge and Studies. *Klin Onkol*. 2018; 31(5): 339–344, doi: [10.14735/amko2018339](https://doi.org/10.14735/amko2018339), indexed in Pubmed: [30541319](https://pubmed.ncbi.nlm.nih.gov/30541319/).
18. Cuccurullo V, Di Stasio GD, Cascini GL, et al. The Molecular Effects of Ionizing Radiations on Brain Cells: Radiation Necrosis vs. Tumor Recurrence. *Diagnostics (Basel)*. 2019; 9(4), doi: [10.3390/diagnostics9040127](https://doi.org/10.3390/diagnostics9040127), indexed in Pubmed: [31554255](https://pubmed.ncbi.nlm.nih.gov/31554255/).
19. Colella G, Giudice A, Rambaldi P, et al. Parotid function after selective deep lobe parotidectomy. *Br J Oral Maxillofac Surg*. 2007; 45(2): 108–111, doi: [10.1016/j.bjoms.2006.04.006](https://doi.org/10.1016/j.bjoms.2006.04.006), indexed in Pubmed: [16782244](https://pubmed.ncbi.nlm.nih.gov/16782244/).
20. Larg MI, Barbus E, Gabor K, et al. 18F-FDG PET/CT IN DIFFERENTIATED THYROID CARCINOMA. *Acta Endocrinol (Buchar)*. 2019; 15(2): 203–208, doi: [10.4183/aeb.2019.203](https://doi.org/10.4183/aeb.2019.203), indexed in Pubmed: [31508177](https://pubmed.ncbi.nlm.nih.gov/31508177/).
21. Choudhury PS, Gupta M. Differentiated thyroid cancer theranostics: radioiodine and beyond. *Br J Radiol*. 2018; 91(1091): 20180136, doi: [10.1259/bjr.20180136](https://doi.org/10.1259/bjr.20180136), indexed in Pubmed: [30260232](https://pubmed.ncbi.nlm.nih.gov/30260232/).
22. Liu H, Wang X, Yang R, et al. Recent Development of Nuclear Molecular Imaging in Thyroid Cancer. *Biomed Res Int*. 2018; 2018: 2149532, doi: [10.1155/2018/2149532](https://doi.org/10.1155/2018/2149532), indexed in Pubmed: [29951528](https://pubmed.ncbi.nlm.nih.gov/29951528/).
23. Yip L, Sosa JA. Molecular-Directed Treatment of Differentiated Thyroid Cancer: Advances in Diagnosis and Treatment. *JAMA Surg*. 2016; 151(7): 663–670, doi: [10.1001/jamasurg.2016.0825](https://doi.org/10.1001/jamasurg.2016.0825), indexed in Pubmed: [27223483](https://pubmed.ncbi.nlm.nih.gov/27223483/).
24. Li X, Li E, Du J, et al. BRAF mutation analysis by ARMS-PCR refines thyroid nodule management. *Clin Endocrinol (Oxf)*. 2019; 91(6): 834–841, doi: [10.1111/cen.14079](https://doi.org/10.1111/cen.14079), indexed in Pubmed: [31441082](https://pubmed.ncbi.nlm.nih.gov/31441082/).
25. Crispo F, Notarangelo T, Pietrafesa M, et al. BRAF Inhibitors in Thyroid Cancer: Clinical Impact, Mechanisms of Resistance and Future Perspectives. *Cancers (Basel)*. 2019; 11(9), doi: [10.3390/cancers11091388](https://doi.org/10.3390/cancers11091388), indexed in Pubmed: [31540406](https://pubmed.ncbi.nlm.nih.gov/31540406/).
26. Piccardo A, Trimboli P, Foppiani L, et al. PET/CT in thyroid nodule and differentiated thyroid cancer patients. The evidence-based state of the art. *Rev Endocr Metab Disord*. 2019; 20(1): 47–64, doi: [10.1007/s11154-019-09491-2](https://doi.org/10.1007/s11154-019-09491-2), indexed in Pubmed: [30900067](https://pubmed.ncbi.nlm.nih.gov/30900067/).
27. Cuccurullo V, Di Stasio GD, Evangelista L, et al. Biochemical and Pathophysiological Premises to Positron Emission Tomography With Choline Radiotracers. *J Cell Physiol*. 2017; 232(2): 270–275, doi: [10.1002/jcp.25478](https://doi.org/10.1002/jcp.25478), indexed in Pubmed: [27381438](https://pubmed.ncbi.nlm.nih.gov/27381438/).
28. de Ko, de GeO, Dekkers OM, et al. Diagnostic Utility of Molecular and Imaging Biomarkers in Cytological Indeterminate Thyroid Nodules. *Endocr Rev*. 2018; 39(2): 154–191.
29. Giovannella L, Treglia G, Iakovou I, et al. EANM practice guideline for PET/CT imaging in medullary thyroid carcinoma. *Eur J Nucl Med Mol Imaging*. 2019; 47(1): 61–77, doi: [10.1007/s00259-019-04458-6](https://doi.org/10.1007/s00259-019-04458-6).
30. Pak K, Kim SJ, Kim InJ, et al. The role of 18F-fluorodeoxyglucose positron emission tomography in differentiated thyroid cancer before surgery. *Endocr Relat Cancer*. 2013; 20(4): R203–R213, doi: [10.1530/ERC-13-0088](https://doi.org/10.1530/ERC-13-0088), indexed in Pubmed: [23722225](https://pubmed.ncbi.nlm.nih.gov/23722225/).
31. Parangi S, Suh H. The role of genetic markers in the evaluation and management of thyroid nodules. *Surg Clin North Am*. 2014; 94(3): 515–528, doi: [10.1016/j.suc.2014.03.001](https://doi.org/10.1016/j.suc.2014.03.001), indexed in Pubmed: [24857574](https://pubmed.ncbi.nlm.nih.gov/24857574/).
32. Doubleday A, Sippel RS. Surgical options for thyroid cancer and post-surgical management. *Expert Rev Endocrinol Metab*. 2018; 13(3): 137–148, doi: [10.1080/17446651.2018.1464910](https://doi.org/10.1080/17446651.2018.1464910), indexed in Pubmed: [30058897](https://pubmed.ncbi.nlm.nih.gov/30058897/).
33. Soelberg KK, Bonnema SJ, Brix TH, et al. Risk of malignancy in thyroid incidentalomas detected by 18F-fluorodeoxyglucose positron emission tomography: a systematic review. *Thyroid*. 2012; 22(9): 918–925, doi: [10.1089/thy.2012.0005](https://doi.org/10.1089/thy.2012.0005), indexed in Pubmed: [22827552](https://pubmed.ncbi.nlm.nih.gov/22827552/).
34. Trimboli P, Piccardo A, Alevizaki M, et al. Dedicated neck F-FDG PET/CT: An additional tool for risk assessment in thyroid nodules at ultrasound intermediate risk. *Clin Endocrinol (Oxf)*. 2019; 90(5): 737–743, doi: [10.1111/cen.13949](https://doi.org/10.1111/cen.13949), indexed in Pubmed: [30740757](https://pubmed.ncbi.nlm.nih.gov/30740757/).
35. Schmidbauer B, Menhart K, Hellwig D, et al. Differentiated Thyroid Cancer-Treatment: State of the Art. *Int J Mol Sci*. 2017; 18(6), doi: [10.3390/ijms18061292](https://doi.org/10.3390/ijms18061292), indexed in Pubmed: [28629126](https://pubmed.ncbi.nlm.nih.gov/28629126/).
36. Agate L, Bianchi F, Giorgetti A, et al. Detection of metastases from differentiated thyroid cancer by different imaging techniques (neck ultrasound, computed tomography and [18F]-FDG positron emission tomography) in patients with negative post-therapeutic <sup>131</sup>I whole-body scan and detectable serum thyroglobulin levels. *J Endocrinol Invest*. 2014; 37(10): 967–972, doi: [10.1007/s40618-014-0134-1](https://doi.org/10.1007/s40618-014-0134-1), indexed in Pubmed: [25070043](https://pubmed.ncbi.nlm.nih.gov/25070043/).
37. Bae MiR, Roh JL, Kim JS, et al. F-FDG PET/CT versus CT/MR imaging for detection of neck lymph node metastasis in palpably node-negative oral cavity cancer. *J Cancer Res Clin Oncol*. 2020; 146(1): 237–244, doi: [10.1007/s00432-019-03054-3](https://doi.org/10.1007/s00432-019-03054-3), indexed in Pubmed: [31606761](https://pubmed.ncbi.nlm.nih.gov/31606761/).
38. Nakajo M, Jinguji M, Shinaji T, et al. F-FDG-PET/CT features of primary tumours for predicting the risk of recurrence in thyroid cancer after total thyroidectomy: potential usefulness of combination of the SUV-related, volumetric, and heterogeneous texture parameters. *Br J Radiol*. 2019; 92(1094): 20180620, doi: [10.1259/bjr.20180620](https://doi.org/10.1259/bjr.20180620), indexed in Pubmed: [30273012](https://pubmed.ncbi.nlm.nih.gov/30273012/).
39. Parmeggiani D, Gambardella C, Patrone R, et al. Radioguided thyroidectomy for follicular tumors: Multicentric experience. *Int J Surg*. 2017; 41 Suppl 1: S75–S81, doi: [10.1016/j.ijso.2017.03.081](https://doi.org/10.1016/j.ijso.2017.03.081), indexed in Pubmed: [28506419](https://pubmed.ncbi.nlm.nih.gov/28506419/).
40. Qichang W, Lin B, Gege Z, et al. Diagnostic performance of 18F-FDG-PET/CT in DTC patients with thyroglobulin elevation and negative iodine scintigraphy: a meta-analysis. *Eur J Endocrinol*. 2019; 181(2): 93–102, doi: [10.1530/EJE-19-0261](https://doi.org/10.1530/EJE-19-0261), indexed in Pubmed: [31117054](https://pubmed.ncbi.nlm.nih.gov/31117054/).
41. Schütz F, Lautenschläger C, Lorenz K, et al. Positron Emission Tomography (PET) and PET/CT in Thyroid Cancer: A Systematic Review and Meta-Analysis. *Eur Thyroid J*. 2018; 7(1): 13–20, doi: [10.1159/000481707](https://doi.org/10.1159/000481707), indexed in Pubmed: [29594049](https://pubmed.ncbi.nlm.nih.gov/29594049/).
42. Kim SJ, Lee SW, Pak K, et al. Diagnostic performance of PET in thyroid cancer with elevated anti-Tg Ab. *Endocr Relat Cancer*. 2018; 25(6): 643–652, doi: [10.1530/ERC-17-0341](https://doi.org/10.1530/ERC-17-0341), indexed in Pubmed: [29559552](https://pubmed.ncbi.nlm.nih.gov/29559552/).
43. Smallridge RC, Diehl N, Bernet V. Practice trends in patients with persistent detectable thyroglobulin and negative diagnostic radioiodine whole body scans: a survey of American Thyroid Association members. *Thyroid*. 2014; 24(10): 1501–1507, doi: [10.1089/thy.2014.0043](https://doi.org/10.1089/thy.2014.0043), indexed in Pubmed: [25058708](https://pubmed.ncbi.nlm.nih.gov/25058708/).
44. Cuccurullo V, Di Stasio GD, Mansi L. Radioguided surgery with radiolabeled somatostatin analogs: not only in GEP-NETs. *Nucl Med Rev Cent East Eur*. 2017; 20(1): 49–56, doi: [10.5603/NMR.2017.0003](https://doi.org/10.5603/NMR.2017.0003), indexed in Pubmed: [28218348](https://pubmed.ncbi.nlm.nih.gov/28218348/).
45. Kang SY, Bang JI, Kang KW, et al. FDG PET/CT for the early prediction of RAI therapy response in patients with metastatic differentiated thyroid carcinoma. *PLoS One*. 2019; 14(6): e0218416, doi: [10.1371/journal.pone.0218416](https://doi.org/10.1371/journal.pone.0218416), indexed in Pubmed: [31237886](https://pubmed.ncbi.nlm.nih.gov/31237886/).
46. Santhanam P, Khthir R, Solnes LB, et al. THE RELATIONSHIP OF BRAF MUTATION STATUS TO FDG PET/CT AVIDITY IN THYROID CANCER: A REVIEW AND META-ANALYSIS. *Endocr Pract*. 2018; 24(1): 21–26, doi: [10.4158/EP-2017-0080](https://doi.org/10.4158/EP-2017-0080), indexed in Pubmed: [29144823](https://pubmed.ncbi.nlm.nih.gov/29144823/).

47. Lee SH, Han S, Lee HS, et al. Association Between (18)F-FDG Avidity and the BRAF Mutation in Papillary Thyroid Carcinoma. *Nucl Med Mol Imaging*. 2016; 50(1): 38–45, doi: [10.1007/s13139-015-0367-8](https://doi.org/10.1007/s13139-015-0367-8), indexed in Pubmed: [26941858](https://pubmed.ncbi.nlm.nih.gov/26941858/).
48. Yoon M, Jung SJ, Kim TH, et al. Relationships between transporter expression and the status of BRAF V600E mutation and F-18 FDG uptake in papillary thyroid carcinomas. *Endocr Res*. 2016; 41(1): 64–69, doi: [10.3109/07435800.2015.1066803](https://doi.org/10.3109/07435800.2015.1066803), indexed in Pubmed: [26513490](https://pubmed.ncbi.nlm.nih.gov/26513490/).
49. Yoon S, An YS, Lee SuJ, et al. Relation Between F-18 FDG Uptake of PET/CT and BRAFV600E Mutation in Papillary Thyroid Cancer. *Medicine (Baltimore)*. 2015; 94(48): e2063, doi: [10.1097/MD.0000000000002063](https://doi.org/10.1097/MD.0000000000002063), indexed in Pubmed: [26632889](https://pubmed.ncbi.nlm.nih.gov/26632889/).
50. Nagarajah J, Ho AL, Tuttle RM, et al. Correlation of BRAFV600E Mutation and Glucose Metabolism in Thyroid Cancer Patients: An <sup>18</sup>F-FDG PET Study. *J Nucl Med*. 2015; 56(5): 662–667, doi: [10.2967/jnumed.114.150607](https://doi.org/10.2967/jnumed.114.150607), indexed in Pubmed: [25814520](https://pubmed.ncbi.nlm.nih.gov/25814520/).
51. Choi EK, Chong A, Ha JM, et al. Clinicopathological characteristics including BRAF V600E mutation status and PET/CT findings in papillary thyroid carcinoma. *Clin Endocrinol (Oxf)*. 2017; 87(1): 73–79, doi: [10.1111/cen.13335](https://doi.org/10.1111/cen.13335), indexed in Pubmed: [28329426](https://pubmed.ncbi.nlm.nih.gov/28329426/).

# Catheter malposition during a direct radionuclide cystography — case report

Shirin Shahlaei, Farnaz Nesari Javan, Atena Aghaee, Ramin Sadeghi 

Nuclear Medicine Research Center, School of Medicine, Mashhad University of Medical Sciences, Mashhad, Iran

[Received 1 XII 2019; Accepted 18 VI 2020]

## Abstract

We reported a 15-year-old girl with a history of mild left vesicoureteral reflux who underwent direct radionuclide cystography in our department. Bladder catheterization was mistakenly placed in the vagina. The filling phase showed vagina and uterine cavity which was similar to vesicoureteral reflux. The procedure was repeated with correct catheterization of the bladder and no vesicoureteral reflux was noted.

**KEY words:** vesicoureteral reflux; direct radionuclide cystography; vagina

Nucl Med Rev 2020; 23, 2: 103–104

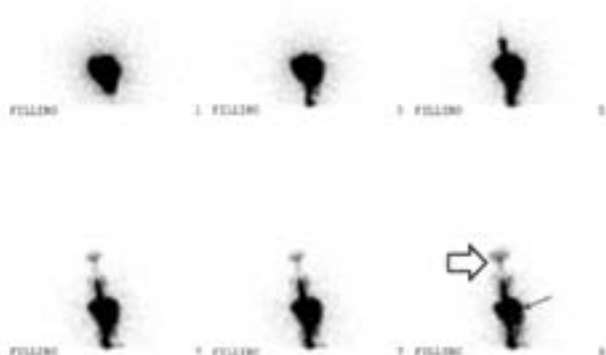


**Figure 1.** A 15-year-old girl with a previously diagnosed mild left vesicoureteral reflux (VUR) in childhood with history of follow up during previous years without any episode of urinary tract infection, was referred to our nuclear medicine center for direct radionuclide cystography (DRC). She was catheterized under the aseptic conditions using a urinary catheter appropriate for her age then one mCi of  $^{99m}\text{Tc}$  — pertechnetate was injected directly into the catheter and normal saline solution was used to fill the urinary bladder. The patient lied in supine position, and dynamic images were obtained (5 seconds per frame using a dual-head variable angle gamma camera and  $128 \times 128$  matrix equipped with low-energy high-resolution collimator) from the posterior view. The images showed a reverse pear shape of tracer accumulation with two abnormal linear tracer uptakes in the midline similar to vesicoureteral reflux. We checked the catheter and it was mistakenly placed in the vagina and unusual distribution of the tracer was due to tracer flow to the vagina (arrow) and uterine cavity (arrow head)

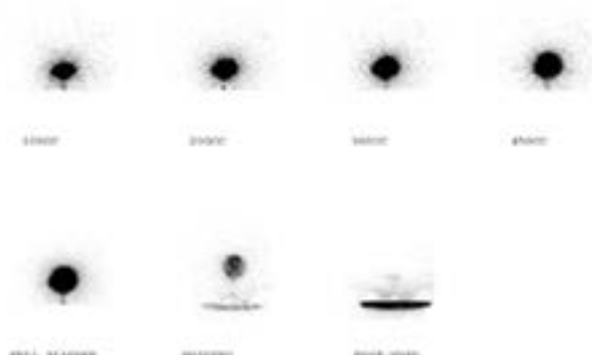


**Figure 2.** The catheter was removed and the correct catheterization was done. Filling phase and voiding imaging were done with a similar protocol. No VUR was shown in images

A major health problem in childhood is vesicoureteral reflux (VUR) [1]. Since VUR may have negative effects on kidneys it is important to detect the VUR as soon as possible [2]. In this regard voiding cystourethrography (VCUG) and direct radionuclide cystography (DRC) are common methods to diagnose and follow VUR [1, 3]. Voiding cystourethrography (VCUG) have some disadvantages *i.e.* high gonadal radiation compared with DRC [4]. Instead, direct radionuclide cystography (DRC) has been proposed to detect VUR with better detection of intermittent reflux. However, this method is suffering from the lack of enough anatomical details [5–7]. Our case report showed the importance of careful attention to correct catheterization (Fig. 1 and 2). Catheter

Correspondence to: Ramin Sadeghi  
 Nuclear Medicine Research Center, School of Medicine, Mashhad University of Medical Sciences, Mashhad, Iran  
 e-mail: sadeghir@mums.ac.ir

insertion in the vagina has been reported before during VCUG and this pitfall should always be borne in mind in case of DRC procedure especially in those with an unusual pattern of tracer distribution.

## References

1. Joaquim AI, de Godoy MF, Burdmann EA. Cyclic Direct Radionuclide Cystography in the Diagnosis and Characterization of Vesicoureteral Reflux in Children and Adults. *Clin Nucl Med.* 2015; 40(8): 627–631, doi: [10.1097/RLU.0000000000000799](https://doi.org/10.1097/RLU.0000000000000799), indexed in Pubmed: [26018721](https://pubmed.ncbi.nlm.nih.gov/26018721/).
2. Lebowitz RL, Lebowitz RL. The detection of vesicoureteral reflux in the child. *Invest Radiol.* 1986; 21(7): 519–531, doi: [10.1097/00004424-198607000-00003](https://doi.org/10.1097/00004424-198607000-00003), indexed in Pubmed: [3015828](https://pubmed.ncbi.nlm.nih.gov/3015828/).
3. Massoudi T, Shayegani H, Sadeghi R. Radiotracer Injection Into the Catheter Balloon: A Subtle Pitfall Which Can Be Overlooked in Direct Radionuclide Cystography. *Clin Nucl Med.* 2017; 42(4): 289–292, doi: [10.1097/RLU.0000000000001539](https://doi.org/10.1097/RLU.0000000000001539), indexed in Pubmed: [28121664](https://pubmed.ncbi.nlm.nih.gov/28121664/).
4. Zerlin JM, Lebowitz RL. Catheter malposition during cystography: a cause of diagnostic errors. *AJR Am J Roentgenol.* 1989; 153(2): 363–367, doi: [10.2214/ajr.153.2.363](https://doi.org/10.2214/ajr.153.2.363), indexed in Pubmed: [2750622](https://pubmed.ncbi.nlm.nih.gov/2750622/).
5. Fettich J, Colarinha P, Fischer S, et al. Empfehlungen zur Durchführung der direkten Radionuklid-Zystographie bei Kindern - Richtlinie übernommen vom Paediatric Committee der European Association of Nuclear Medicine (EANM). *Der Nuklearmediziner.* 2002; 25(2): 106–111, doi: [10.1055/s-2002-33278](https://doi.org/10.1055/s-2002-33278).
6. Mandell GA, Eggl DF, Gilday DL, et al. Procedure guideline for radionuclide cystography in children. *Society of Nuclear Medicine. J Nucl Med.* 1997; 38(10): 1650–1654, indexed in Pubmed: [9379209](https://pubmed.ncbi.nlm.nih.gov/9379209/).
7. Polito C, Moggio G, La Manna A, et al. Cyclic voiding cystourethrography in the diagnosis of occult vesicoureteric reflux. *Pediatr Nephrol.* 2000; 14(1): 39–41, doi: [10.1007/s004670050010](https://doi.org/10.1007/s004670050010), indexed in Pubmed: [10654329](https://pubmed.ncbi.nlm.nih.gov/10654329/).

# Primary nasal-ethmoid choriocarcinoma detected by 18F-FDG PET/CT: a rare tumor with complete remission

Maria Gazzilli<sup>1</sup> , Domenico Albano<sup>1</sup> , Laura Ardighieri<sup>2</sup> , Francesco Bertagna<sup>1</sup>, Raffaele Giubbini<sup>1</sup>

<sup>1</sup>Nuclear Medicine, University of Brescia, Spedali Civili Brescia, Brescia, Italy

<sup>2</sup>Department of Pathology ASST Spedali Civili, Brescia, Italy

[Received 09 IX 2020; Accepted 22 V 2020]

## Abstract

Choriocarcinoma is a highly malignant and rare tumor characterized by secretion of the beta-subunit-of-human-choriogonadotropin ( $\beta$ -HCG).

We report a case of primary nasal choriocarcinoma with good response to chemotherapy.

A 36-years-old woman gravida 0 and with history of 4 spontaneous abortion, in December 2018 referred to Otorhinolaryngology Department for repeated episodes of epistaxis. Cervical Magnetic Resonance Imaging (MRI) revealed a tumor mass involving right nasal cavity, right ethmoid, sphenoidal and maxillary sinuses.

For a differential diagnosis between metastatic gestational choriocarcinoma and primary choriocarcinoma in January 2019 she underwent 18Fluorine-Fluorodeoxyglucose Positron Emission Tomography/Computed Tomography (18F-FDG-PET/CT) scan that demonstrated intense uptake only in the nasal-ethmoid tumor mass showed by MRI. This was suggestive of primary nasal-ethmoid choriocarcinoma she received 3 courses of BEP – regimen and after  $\beta$ -HCG was reduced to 500 mIU/mL and 18F-FDG-PET/CT scan showed a decreased uptake in tumor mass but the appearance of a new uptake in cervical lymph node which was analysed and reported as metastatic localization of choriocarcinoma. Therefore she was treated with 2 cycles of TIP-regimen. Subsequents 18F-FDG-PET/CT and MRI showed a complete tumor remission.

This case proved the fundamental role of PET/CT to make diagnosis of primitive choriocarcinoma and to exclude the hypothesis of distant metastasis.

**KEY words:** choriocarcinoma; nasal-ethmoidal; PET/CT

Nucl Med Rev 2020; 23, 2: 105–107

Choriocarcinoma is a highly malignant and rare tumor characterized by secretion of the beta-subunit-of-human-choriogonadotropin ( $\beta$ -HCG). In women, can distinguish two types of choriocarcinoma: gestational and non-gestational primary choriocarcinoma, which is extremely rare, arising from germ cells. We report a case of primary nasal choriocarcinoma with good response to chemotherapy [1, 2].

A 36-year-old woman gravida 0 and with history of 4 spontaneous abortion, in December 2018 referred to Otorhinolaryngology Department for repeated episodes of epistaxis. Cervical Magnetic Resonance Imaging (MRI) revealed a tumor mass involving right nasal cavity, right ethmoid, sphenoidal and maxillary sinuses. At histological examination, the tumor was composed of cohesive

sheets of highly atypical mononucleate epithelioid tumor cells, minor component of plurinucleate cells referable to syncytiotrophoblast cells and areas of hemorrhage and necrosis. At immunohistochemical analysis tumor cells were positive for SALL4, GATA3, cytokeratin AE1/AE3, CK7, Glypican3 and  $\beta$ -HCG and negative for CD30, CD117, CX20 and S100. Ki67 proliferation index was > 90%. The final diagnosis was choriocarcinoma.

For a differential diagnosis between metastatic gestational choriocarcinoma and primary choriocarcinoma in January 2019 she underwent 18Fluorine-Fluorodeoxyglucose Positron Emission Tomography/Computed Tomography (18F-FDG-PET/CT) scan that demonstrated intense uptake only in the nasal-ethmoid tumor mass showed by MRI. This was suggestive of primary nasal-ethmoid choriocarcinoma [3, 4]. The serum levels of  $\beta$ -HCG were 3839 mIU/mL while serum  $\alpha$ -fetoprotein levels were normal.

Treatment of choriocarcinoma includes tumor resection and chemotherapy with EMA/CO (etoposide, methotrexate, actinomycin D, cisplatin), DCF (docetaxel, cisplatin, 5-FU) and BEP

Correspondence to: Maria Gazzilli  
 Nuclear Medicine, University of Brescia, Spedali Civili Brescia, Brescia, Italy  
 e-mail: marinagazzilli@msn.com

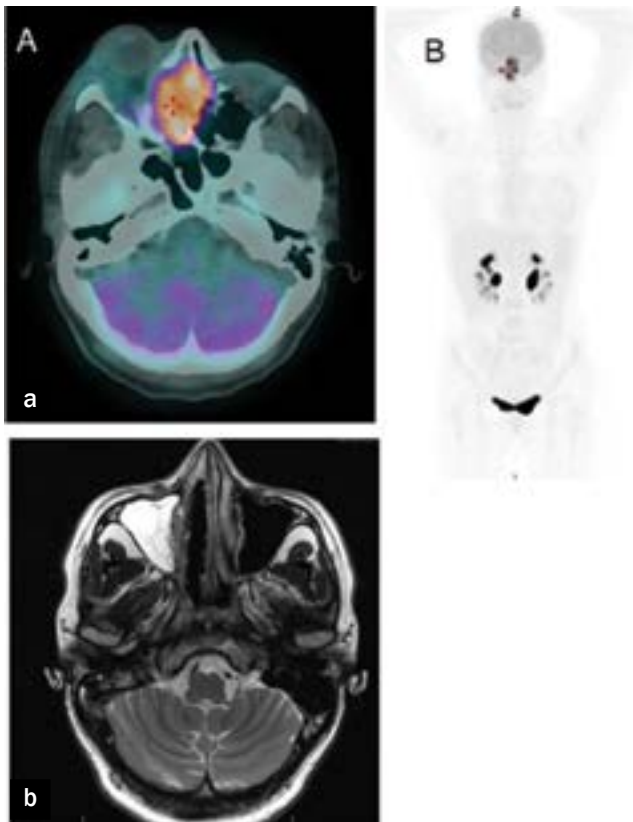


**Figure 1.** A. Staging PET/CT showed intense uptake in nasal-ethmoidal mass; a. Fused image; b. MIP image; B. Staging Cervical MRI showed large tumor mass involving right nasal cavity, right ethmoid, sphenoidal and maxillary sinuses

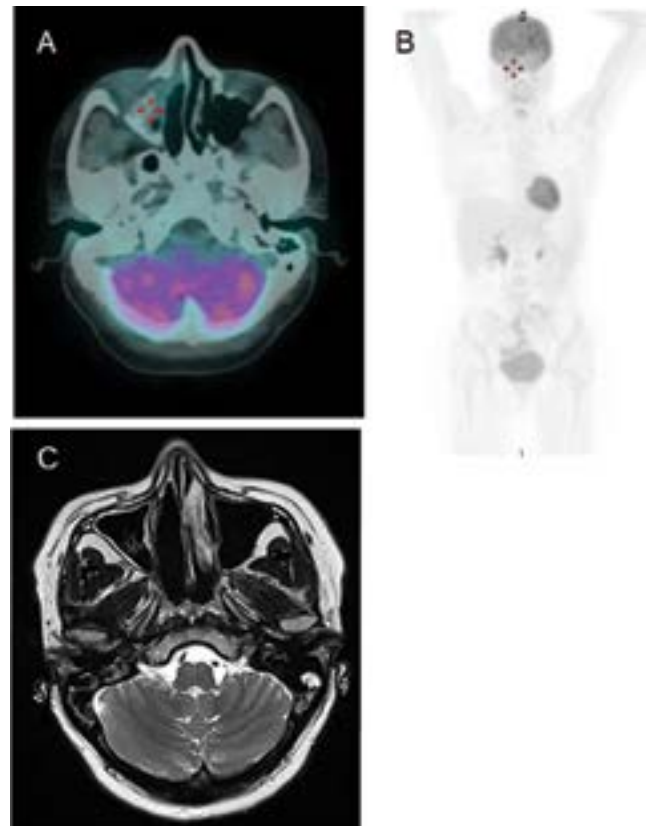


**Figure 2.** End-of-treatment images: A. PET/CT; B. Cervical MRI; both showed complete remission of nasal-ethmoidal mass

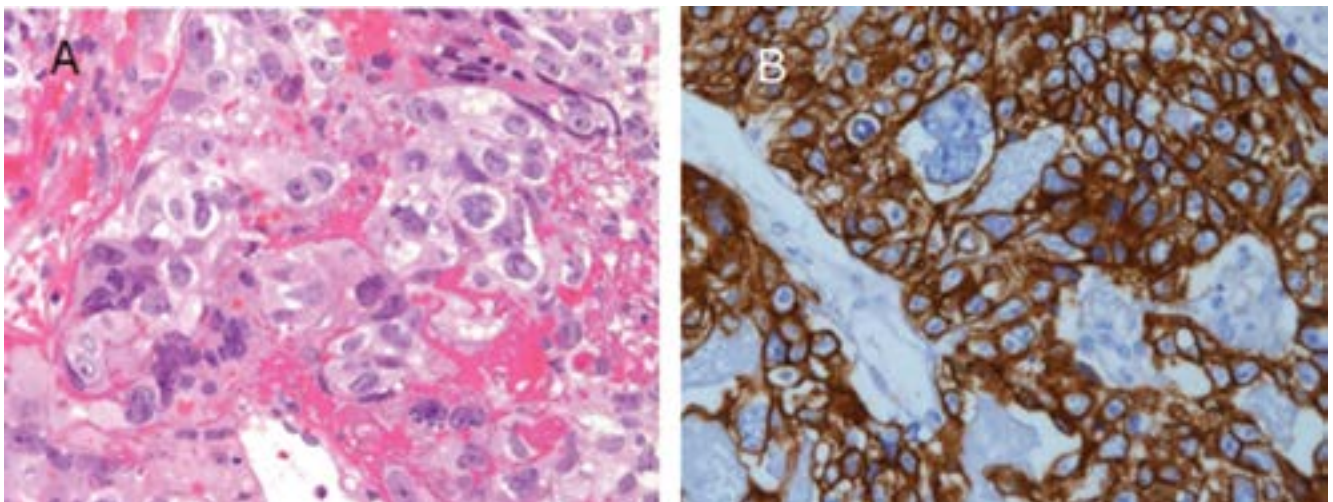


**Figure 3.** A. Hematoxylin and eosin stain showing mononucleated and plurinucleate tumor cells with striking cytologic atypia and central hemorrhage (200× magnification); B. Tumor cells positive for cytokeratin AE1/AE3 (200× magnification)

(bleomycin, etoposide and cisplatin), but patients who relapse after initial treatment or patients who didn't respond completely to chemotherapy have a poor prognosis [5, 6]. Motzer et al. [7, 8] showed in a study that it is possible to obtain promising results with

a combination of paclitaxel, ifosfamide and cisplatin (TIP) as a salvage therapy.

According to literature, she received 3 courses of BEP regimen and after that  $\beta$ -HCG was reduced to 500 mIU/mL and

18F-FDG-PET/CT scan showed a decreased uptake in tumor mass, but the appearance of a new uptake in cervical lymph node which was analyzed and reported as metastatic localization of choriocarcinoma. Therefore she was treated with 2 cycles of TIP regimen. Subsequent 18F-FDG-PET/CT and MRI showed a complete tumor remission.

Due to aggressive and malignant biology of the disease, a correct identification of this tumor is important to start an effective therapy to improve the poor prognosis of choriocarcinoma. This case proved the fundamental role of PET/CT in establishing diagnosis of primitive choriocarcinoma and excluding the hypothesis of distant metastasis.

## References

1. Zhou HY, Nguyen JK, Ganesan S, et al. Choriocarcinoma of the adrenal gland: A case report. *Int J Surg Case Rep.* 2015; 6C: 92–94, doi: [10.1016/j.ijscr.2014.12.018](https://doi.org/10.1016/j.ijscr.2014.12.018), indexed in Pubmed: [25528034](https://pubmed.ncbi.nlm.nih.gov/25528034/).
2. Gurzu S, Copotoiu C, Tugui A, et al. Primary gastric choriocarcinoma - a rare and aggressive tumor with multilineage differentiation: A case report. *World J Clin Cases.* 2019; 7(14): 1837–1843, doi: [10.12998/wjcc.v7.i14.1837](https://doi.org/10.12998/wjcc.v7.i14.1837), indexed in Pubmed: [31417929](https://pubmed.ncbi.nlm.nih.gov/31417929/).
3. Bell DM, Porras G, Tortoledo ME, et al. Primary sinonasal choriocarcinoma. *Ann Diagn Pathol.* 2009; 13(2): 96–100, doi: [10.1016/j.anndiag-path.2008.12.008](https://doi.org/10.1016/j.anndiag-path.2008.12.008), indexed in Pubmed: [19302957](https://pubmed.ncbi.nlm.nih.gov/19302957/).
4. Tariq M, Kalan A. Metastatic choriocarcinoma of the nasal cavity-presenting as intractable epistaxis. *Indian J Otolaryngol Head Neck Surg.* 2004; 56(3): 220–222, doi: [10.1007/BF02974356](https://doi.org/10.1007/BF02974356), indexed in Pubmed: [23120080](https://pubmed.ncbi.nlm.nih.gov/23120080/).
5. Stockton L, Green E, Kaur B, et al. Non-Gestational Choriocarcinoma with Widespread Metastases Presenting with Type 1 Respiratory Failure in a 39-Year-Old Female: Case Report and Review of the Literature. *Case Rep Oncol.* 2018; 11(1): 151–158, doi: [10.1159/000486639](https://doi.org/10.1159/000486639), indexed in Pubmed: [29681814](https://pubmed.ncbi.nlm.nih.gov/29681814/).
6. Sato S, Yamamoto E, Niimi K, et al. The efficacy and toxicity of 4-day chemotherapy with methotrexate, etoposide and actinomycin D in patients with choriocarcinoma and high-risk gestational trophoblastic neoplasia. *Int J Clin Oncol.* 2019.
7. Kurobe M, Kawai K, Oikawa T, et al. Paclitaxel, ifosfamide, and cisplatin (TIP) as salvage and consolidation chemotherapy for advanced germ cell tumor. *J Cancer Res Clin Oncol.* 2015; 141(1): 127–133, doi: [10.1007/s00432-014-1760-x](https://doi.org/10.1007/s00432-014-1760-x), indexed in Pubmed: [25062721](https://pubmed.ncbi.nlm.nih.gov/25062721/).
8. Motzer RJ, Sheinfeld J, Mazumdar M, et al. Paclitaxel, ifosfamide, and cisplatin second-line therapy for patients with relapsed testicular germ cell cancer. *J Clin Oncol.* 2000; 18(12): 2413–2418, doi: [10.1200/JCO.2000.18.12.2413](https://doi.org/10.1200/JCO.2000.18.12.2413), indexed in Pubmed: [10856101](https://pubmed.ncbi.nlm.nih.gov/10856101/).

# Primary skeletal muscle lymphoma with unusual soft tissue metastases in the stomach and pancreas detected by <sup>18</sup>F-FDG PET/CT

Fatemeh Farahmandfar<sup>1</sup>, Sara Shakeri<sup>1</sup> , Sadegh Moradian<sup>2</sup>, Shirin Shahlaei<sup>1</sup>, Ramin Sadeghi<sup>1</sup> 

<sup>1</sup>Nuclear Medicine Research Center, Mashhad University of Medical Sciences, Mashhad, Iran

<sup>2</sup>Department of Radiology, Amiralam Hospital, Tehran University of Medical Sciences, Tehran, Iran

[Received 20 II 2020; Accepted 8 VII 2020]

## Abstract

A 69 y/o woman with a history of primary diffuse large B cell lymphoma in the right thigh muscle was referred for recurrence evaluation with <sup>18</sup>F-FDG PET/CT. After routine courses of chemoradiation, MRI was done in order to evaluate treatment response with inconclusive findings. <sup>18</sup>FDG PET/CT revealed abnormal uptake in the primary site of the disease as well as secondary involvement of stomach, pancreas, pelvic lymph nodes, and both tibiae. Our case showed the importance of <sup>18</sup>F-FDG PET/CT in the detection of unusual soft tissue extension of lymphoma.

**KEY words:** Diffuse large B-cell lymphoma; non-Hodgkin's lymphoma; <sup>18</sup>F-FDG PET/CT

Nucl Med Rev 2020; 23, 2: 108–109

## Introduction

Diffuse large B cell lymphoma (DLBCL) is the most common subtype of non-Hodgkin's lymphomas (NHL) [1], which usually arises from lymph nodes. It can also have an extra-nodal origin in approximately 30–40% of the cases [2]. The most common extra-nodal sites are testis, skin, lung, bone, central nervous system, respiratory and gastrointestinal tracts [3]. Primary skeletal muscle involvement is very rare [1–3]. It has also been reported that upper extremities and gluteal muscle involvements are more predominantly affected [1]. In muscular lymphoma which usually is FDG avid, diffuse enlargement or focal intramuscular mass are seen [4]. Bone involvement is not common [5] and secondary involvement of the pancreas is very rare [6]. In the present case report, we described an unusual pattern of primary skeletal muscle NHL detected by whole body <sup>18</sup>F-FDG PET/CT.

## Case report

A 69-year-old woman with a history of DLBCL within the right thigh muscles had been treated with chemoradiation. She

experienced no pain in the involved region. The patient underwent MRI for response evaluation. MRI results were inconclusive and couldn't differentiate between post-radiation changes and residual disease. She was referred for more assessment with <sup>18</sup>F-FDG PET/CT. Whole body MIP image revealed multiple foci of increased FDG uptake in the right thigh, stomach, pancreas, pelvic lymph nodes and both tibiae (Fig. 1A). The axial images demonstrated increased FDG uptake throughout the right thigh muscles (Fig. 1B–D). Also, abnormal FDG uptake was noted in the thickened stomach wall (Fig. 1E–G) with SUVmax of 16.91 and pancreatic body and tail (Fig. 1H–J) with SUVmax of 17.79 which were in favor of secondary extranodal involvement. No further follow up scan was acquired.

## Discussion

Although the secondary extranodal disease is common in lymphoma, it rarely occurs as a primary site of lymphoma [9]. Primary skeletal muscle involvement occurs in only 0.1% of all lymphomas [7]. In addition, the pancreas is rarely involved by lymphoma [6]. Although the stomach is the most common site of involvement as the primary extra-nodal site or secondary to disseminated nodal disease [7], majority of secondary gastric NHL couldn't be detected by conventional diagnostic methods [8]. <sup>18</sup>F-FDG PET/CT is a valuable diagnostic test for identifying extranodal sites involvement in lymphoma staging, treatment response or recurrence evaluation [8, 9] and it is more sensitive

Correspondence to: Ramin Sadeghi  
Nuclear Medicine Research Center, Mashhad University of Medical Sciences, Mashhad, Iran  
e-mail: sadeghir@mums.ac.ir

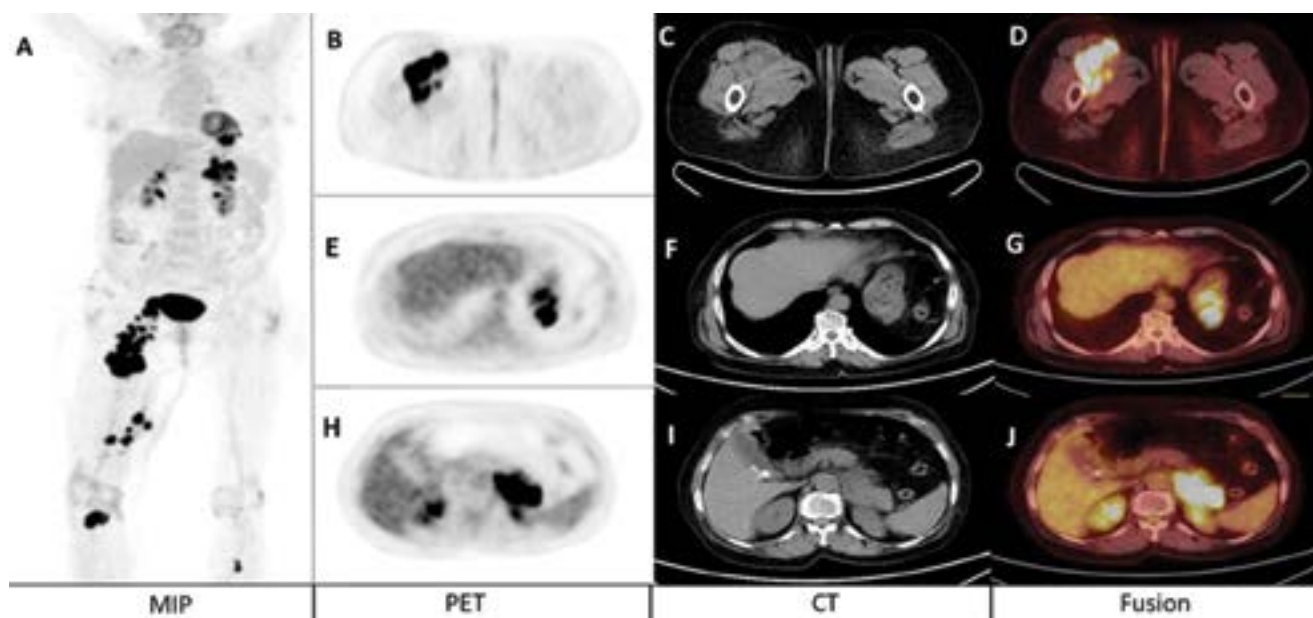


**Figure 1.** The Whole body MIP image showed multiple foci of increased FDG uptake in the right thigh, stomach, pancreas, pelvic lymph nodes and both tibiae (A); The axial images demonstrated increased FDG uptake throughout the right thigh muscles (B–D); stomach wall (E–G) and pancreatic body and tail (H–J)

and specific than conventional imaging for assessment of disease extension [10, 11]. Here, we showed an unusual pattern of NHL by emphasizing the role of  $^{18}\text{F}$ -FDG PET/CT in the differentiation of recurrence from post-radiation changes, as well as showing the extension of the disease.

## References

- Fujikawa T, Kawachi Y. Diffuse large B-cell lymphoma in the psoas muscle. *BMJ Case Rep.* 2015; 2015, doi: [10.1136/bcr-2015-209898](https://doi.org/10.1136/bcr-2015-209898), indexed in Pubmed: [25939975](https://pubmed.ncbi.nlm.nih.gov/25939975/).
- Bourdeanu L, Menon R, Somlo G. Diffuse large B-cell lymphoma with calf muscle localization. *Case Rep Hematol.* 2011; 2011: 292494, doi: [10.1155/2011/292494](https://doi.org/10.1155/2011/292494), indexed in Pubmed: [22937305](https://pubmed.ncbi.nlm.nih.gov/22937305/).
- Zhang L, Lin Q, Zhang L, et al. Primary skeletal muscle diffuse large B cell lymphoma: A case report and review of the literature. *Oncol Lett.* 2015; 10(4): 2156–2160, doi: [10.3892/ol.2015.3505](https://doi.org/10.3892/ol.2015.3505), indexed in Pubmed: [26622811](https://pubmed.ncbi.nlm.nih.gov/26622811/).
- Surov A, Surov A, Behrmann C. Diffusion-weighted imaging of skeletal muscle lymphoma. *Skeletal Radiol.* 2014; 43(7): 899–903, doi: [10.1007/s00256-014-1850-5](https://doi.org/10.1007/s00256-014-1850-5), indexed in Pubmed: [24638123](https://pubmed.ncbi.nlm.nih.gov/24638123/).
- Lehners N, Krämer I, Saadati M, et al. Analysis of clinical characteristics and outcome of patients with previously untreated diffuse large B-cell lymphoma and renal involvement in the rituximab era. *Leuk Lymphoma.* 2016; 57(11): 2619–2625, doi: [10.3109/10428194.2016.1157869](https://doi.org/10.3109/10428194.2016.1157869), indexed in Pubmed: [26999040](https://pubmed.ncbi.nlm.nih.gov/26999040/).
- Saif MW, Khubchandani S, Walczak M. Secondary pancreatic involvement by a diffuse large B-cell lymphoma presenting as acute pancreatitis. *World J Gastroenterol.* 2007; 13(36): 4909–4911, doi: [10.3748/wjg.v13.i36.4909](https://doi.org/10.3748/wjg.v13.i36.4909), indexed in Pubmed: [17828824](https://pubmed.ncbi.nlm.nih.gov/17828824/).
- Alekshun TJ, Reznia D, Ayala E, et al. Skeletal muscle peripheral T-cell lymphoma. *J Clin Oncol.* 2008; 26(3): 501–503, doi: [10.1200/JCO.2007.14.2794](https://doi.org/10.1200/JCO.2007.14.2794), indexed in Pubmed: [18202425](https://pubmed.ncbi.nlm.nih.gov/18202425/).
- Sin KM, Ho SK, Wong BY, et al. Beyond the lymph nodes: FDG-PET/CT in primary extranodal lymphoma. *Clin Imaging.* 2017; 42: 25–33, doi: [10.1016/j.clinimag.2016.11.006](https://doi.org/10.1016/j.clinimag.2016.11.006), indexed in Pubmed: [27875758](https://pubmed.ncbi.nlm.nih.gov/27875758/).
- Ding JJ, Chen YL, Zhou SH, et al. Positron emission tomography/computed tomography in the diagnosis, staging, and prognostic evaluation of natural killer/T-cell lymphoma. *J Int Med Res.* 2018; 46(12): 4920–4929, doi: [10.1177/0300060518804375](https://doi.org/10.1177/0300060518804375), indexed in Pubmed: [30328364](https://pubmed.ncbi.nlm.nih.gov/30328364/).
- Gallamini A, Zwarthoed C, Borra A. Positron Emission Tomography (PET) in Oncology. *Cancers (Basel).* 2014; 6(4): 1821–1889, doi: [10.3390/cancers6041821](https://doi.org/10.3390/cancers6041821), indexed in Pubmed: [25268160](https://pubmed.ncbi.nlm.nih.gov/25268160/).
- Hutchings M, Loft A, Hansen M, et al. Positron emission tomography with or without computed tomography in the primary staging of Hodgkin's lymphoma. *Haematologica.* 2006; 91(4): 482–489, indexed in Pubmed: [16585015](https://pubmed.ncbi.nlm.nih.gov/16585015/).

# Unusual <sup>18</sup>F-FDG PET-CT finding of paraneoplastic polymyositis in a patient with lung epidermoid carcinoma

Salah Nabih Oueriagli, Yassir Benameur, Omar Ait Sahel, Abdelhamid Biyi, Abderrahim Doudouh  
Department of Nuclear Medicine, Mohammed V Military Teaching Hospital, Mohamed V University Souissi, Rabat, Morocco

[Received 28 III 2020; Accepted 8 VII 2020]

We report the case of a 67 years old male patient, followed for epidermoid carcinoma of the right lung, and hyper-eosinophilia on peripheral blood exploration. <sup>18</sup>F-FDG positron emission tomography-computed tomography (<sup>18</sup>F-FDG PET-CT) performed

for initial extension assessment showed, in addition to the intense hypermetabolism in the right upper pulmonary lobe related to the primary tumor and the mediastinal lymph node involvement (Fig. 1A), an unusually intense muscular hypermatbolism

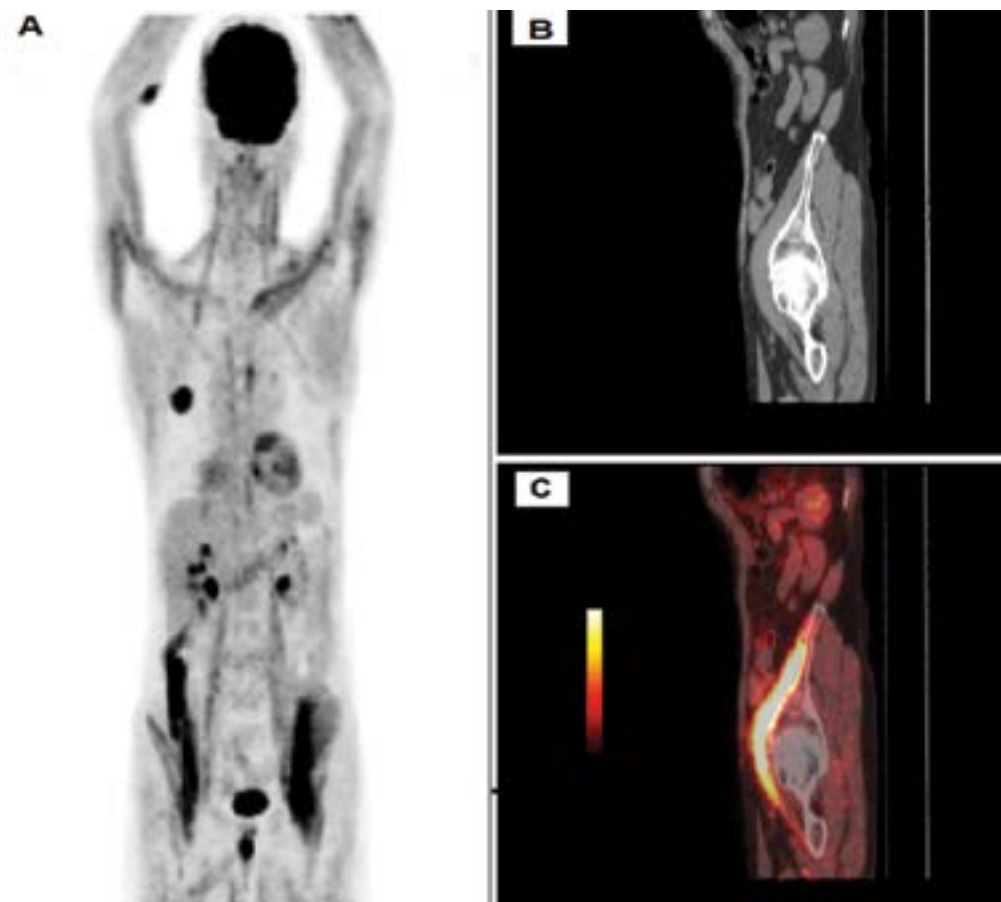


**Figure 1.** A. Maximum intensity projection PET image revealing intense hypermetabolism in the right upper pulmonary lobe related to the primary tumor associated to mediastinal lymph node involvement with unusual intense hypermatbolism interesting long muscles of the neck, sterno-cleido-mastoid muscles, para-vertebral, iliac and ilio-psoas muscles. B. Whole body CT image and (C) <sup>18</sup>F-FDG PET-CT fusion image in sagittal sections showing intense and symmetric hypermetabolism in ilio-psoas muscles

Correspondence to: Oueriagli Nabih Salah, Department of Nuclear Medicine, Mohammed V Military Teaching Hospital, BP 1018, Rabat, Morocco  
phone: +212662101402  
e-mail: salah.nabihoueriagli@gmail.com

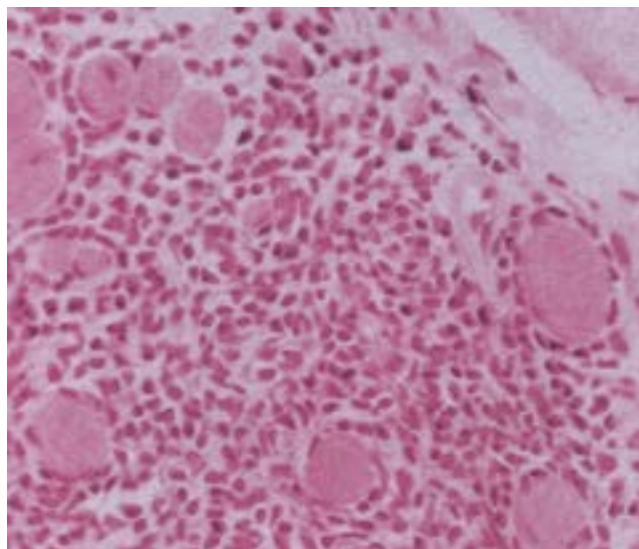


**Figure 2:** Biopsy of the right ilio-psoas muscle showing myofiber degeneration with predominant inflammatory cell (CD8+ T lymphocyte) compatible with polymyositis

interesting bilaterally and symmetrically long muscles of the neck, sterno-cleido-mastoid muscles, para-vertebral, iliac and ilio-psoas muscles (Fig. 1B and 1C).

Biopsy of the right ilio-psoas muscle reveals evidence of myofiber degeneration and regeneration with lymphocytes invading non-necrotic myofibers, predominant inflammatory cell (CD8+ T

lymphocyte) compatible with paraneoplastic polymyositis (Fig. 2). Serum CK (creatine kinase), aldolase and sedimentation rate levels were abnormally very high.

Our patient was put under corticotherapy with good clinical, biological and radiological evolution, even on 18F-FDG PET-CT.

In our knowledge, a link between paraneoplastic polymyositis and cancer has never been clearly defined [1–2], and its clinical expression does not differ from idiopathic polymyositis [3]. Clinicopathologic diagnosis is based on histology, electromyographic data, high-level serum of muscular enzymes (creatine kinase, aldolase), and also an elevated sedimentation rate [4]. This group of patients can be treated by corticotherapy or immunomodulators, and also by physiotherapy [5].

## References

1. Brown H, Steven M. Myositis and malignancy: is there a true association? *Hosp Med.* 1999; 60(1): 51–53, doi: [10.12968/hosp.1999.60.1.1026](https://doi.org/10.12968/hosp.1999.60.1.1026), indexed in Pubmed: [10197100](https://pubmed.ncbi.nlm.nih.gov/10197100/).
2. Hill CL, Zhang Y, Sigurgeirsson B, et al. Frequency of specific cancer types in dermatomyositis and polymyositis: a population-based study. *Lancet.* 2001; 357(9250): 96–100, doi: [10.1016/S0140-6736\(00\)03540-6](https://doi.org/10.1016/S0140-6736(00)03540-6), indexed in Pubmed: [11197446](https://pubmed.ncbi.nlm.nih.gov/11197446/).
3. Dubas F. Syndromes paranéoplasiques. Ed techniques. *Encycl Med Chir.* 1985; 17162(A): 10.
4. Troyanov Y, Targoff IN, Tremblay JL, et al. Novel classification of idiopathic inflammatory myopathies based on overlap syndrome features and autoantibodies: analysis of 100 French Canadian patients. *Medicine (Baltimore).* 2005; 84(4): 231–249, doi: [10.1097/01.md.0000173991.74008.b0](https://doi.org/10.1097/01.md.0000173991.74008.b0), indexed in Pubmed: [16010208](https://pubmed.ncbi.nlm.nih.gov/16010208/).
5. Dalakas MC. Polymyositis and dermatomyositis. *Lancet.* 2003; 362: 971–82.

# Technetium pertechnetate uptake in parathyroid adenoma

Ali Sellem , Wassim Elajmi , Hatem Hammami 

Military Hospital of Tunis, Montfleury, Tunis

[Received 16 I 2020; Accepted 20 VII 2020]

We report the case of a 37-year-old woman newly diagnosed primary hyperparathyroidism with hypercalcemia 16.1 mg/dL (Ref range 8.5–10.1) and an increased parathyroid hormone level 110 pg/mL (reference range 10.0–70.0). She was referred to our department for scintigraphic localization of a parathyroid adenoma. The Tc-99m scintigraphy (Fig. 1) revealed a normal thyroid uptake associated with one focal uptake below the left lobe of the thyroid. A Tc-99m sestamibi parathyroid scan (Fig. 2) was performed showing an accumulation of the tracer in the

same localization of Tc-99m focal uptake. It was a dilemma: is it an eccentric thyroid tissue that fixes the two radiotracers or a parathyroid adenoma fixing the  $^{99m}\text{Tc}$ . Since we do not have the iodine 123 we realized an image (Fig. 3) with a tracer dose of iodine 131 showing no uptake below the left lobe of thyroid which allowed us to conclude to a parathyroid adenoma. The patient subsequently underwent minimally invasive cervicotomy with the resection of this lesion which was histologically diagnosed as a parathyroid adenoma.



**Figure 1.** Tc-99m scintigraphy showing one focal uptake below the left lobe of thyroid



**Figure 2.** Sestamibi parathyroid scan showing an accumulation of the tracer in the same localization of Tc-99m focal uptake



**Figure 3.** Iodine 131 scintigraphy showing no uptake below the left lobe of thyroid

Correspondence to: Ali Sellem, Military Hospital of Tunis,  
Montfleury, 1009 Tunis  
e-mail: sellem\_ali@yahoo.fr